Analog Programmable-Photonic Computation

Andrés Macho-Ortiz[1,*], Daniel Pérez-López[1,2], José Azaña[3] and José Capmany[1,2,*]

[1]ITEAM Research Institute, Universitat Politècnica de València, Valencia 46022, Spain
[2]iPronics, Programmable Photonics, S.L, Camino de Vera s/n, Valencia 46022, Spain
[3]Institut National de la Recherche Scientifique – Énergie, Matériaux, et Télécommunications (INRS-EMT), Montréal, QC, Canada

*corresponding author: amachor@iteam.upv.es, jcapmany@iteam.upv.es

Abstract

Digital electronics is a technological cornerstone in our modern society which has covered the increasing demand in computing power during the last decades thanks to a periodic doubling of transistor density and power efficiency in integrated circuits. Currently, such scaling laws are reaching their fundamental limits, leading to the emergence of a large gamut of applications that cannot be supported by digital electronics, specifically, those that involve real-time *analog* multi-data processing, e.g., medical diagnostic imaging, robotic control and remote sensing, among others. In this scenario, an analog computing approach implemented in a reconfigurable non-electronic hardware such as programmable integrated photonics (PIP) can be more efficient than digital electronics to perform these emerging applications. However, actual analog computing models such as quantum and neuromorphic computation were not conceived to extract the benefits of PIP technology (and integrated photonics in general). In this work, we present the foundations of a new computation theory, termed *Analog Programmable-Photonic Computation* (APC), explicitly designed to unleash the full potential of PIP. Interestingly, APC enables overcoming some of the basic theoretical and technological limitations of existing computational models, can be implemented in other technologies (e.g. in electronics, acoustics or using metamaterials) and, consequently, exhibits the potential to spark a ground-breaking impact on our information society.

Introduction

Over the last decades, digital electronic technology has supported the increasing demand in signal processing and computing power thanks to an exponential performance scaling in microelectronics. In particular, this progress is embodied in Moore's and Dennard's laws by which the density of transistors, power efficiency and clock frequency in microprocessors has approximately doubled every 18-24 months [1, 2]. Nevertheless, as seen in Fig. 1a, these scaling laws are reaching their fundamental limits. As a result, there is currently a wide range of emerging real-time signal processing and computing applications (including medical diagnostic imaging, robotic control, remote sensing, smart homes, and autonomous driving, among others) which may not be efficiently dealt with using the dominant digital electronic paradigm [1–6].

Despite the fact that the electronic industry has proposed to circumvent the end of Moore's and Dennard's laws by introducing multi-core technology, there is a limit in the number of cores that can simultaneously be powered on with a fixed power budget and a constant heat extraction rate (Amdahl's law) [2, 3]. Moreover, as the bandwidth limitations of silicon electronics and printed metallic tracks are reached, the time and power consumed in data transport in an electrical circuit cannot be further reduced [2, 4]. These physical bottlenecks − in combination with the fact that conventional computational models are conceived as serialized and centralized processing architectures (von Neumann machines) implementing the nonlinear Boolean algebra − severely limit the performance of digital electronic computers [1,2,7–9]. In general, such schemes are inefficient to perform multi-linear analog operations and computational architectures that are distributed, parallel and adaptive (Fig. 1b); for instance, those used to perform real-time matrix operations, requiring low latency, high bandwidth, low energy consumption and high reconfigurability (such as the applications mentioned above) [5, 6].

Although from the Church-Turing thesis can be inferred that any class of computational problem (or computable function) can be solved by a digital electronic computer [2, 10], this does not imply that digital computation (DC) [9] and electronic technology always lead to the most suitable marriage between a mathematical computing theory and a hardware platform. Other non-digital computing approaches implemented in alternative system-on-chip technologies can be mathematically more efficient than DC to solve the aforementioned computational scenarios and may provide hardware advantages over electronics in basic performance parameters (latency, bandwidth, parallelism, power consumption, or reconfigurability) [1, 5, 6, 10, 11]. Specifically, technologies that are inherently capable of performing analog operations offering complementary hardware requirements to those of electronics and being CMOS-compatible are a priority [4, 12, 13].

In this context, programmable integrated photonics (PIP) is the ideal technology to explore an analog computation paradigm since it is a hardware platform with complementary features to electronics (providing lower latency, higher bandwidth, massive parallelism via wavelength-division multiplexing (WDM), lower power consumption and higher reconfigurability) and which may be integrated into existing microelectronic processors by exploiting its CMOS compatibility via silicon photonic platforms (Fig. 1c) [12–14]. Furthermore, PIP benefits from the scalable fabrication methods of integrated circuits and its manufacturing could achieve economies of scale comparable with microelectronic industry in the next decades [12].

So far, in the same vein as other optical computing platforms [4–7, 11, 15–19], PIP has essentially been explored as a hardware acceleration solution for existing computational models such as DC [9], quantum computation (QC) [10] and neuromorphic computation (NC) [20] implemented in electronic circuits. Here, PIP only carries out analog signal processing tasks (i.e. wave transformations) which involve a high degree of complexity in electronics (in particular, multi-dimensional wave transformations via vector-by-matrix multiplications [12–14]), but does not perform true computational tasks (i.e. operations among units of information, e.g., among digital bits). In fact, at present, there is no specific computation theory available explicitly designed for PIP (and integrated photonics in general) that allows us to exploit this technology to implement true optical computing, in the same way as DC sparked a paradigm shift in commercial electronics. Moreover, DC, QC and NC were not conceived to extract the benefits of PIP since these models were originally built without considering the complexity of their implementation in integrated optics [4, 6, 11, 16, 21, 22].

Being PIP a hardware technology that naturally performs analog matrix transformations on optical signals, and whose building block may be designed by using a mathematical framework similar to QC [23], one could ask whether a classical version of QC might be proposed within the realm of classical wave-optics. Different works have been reported revolving around this idea in order to [24–30]: (*i*) simulate a quantum computer with a classical computer and (*ii*) dig into the fundamental differences between quantum and classical systems. However, to our knowledge, the QC formalism has never been extrapolated to a classical scenario to construct an analog computing landscape, based on deterministic physical laws, which allows us to overcome some of the main theoretical and technological limitations of QC [10, 25, 31, 32] (e.g., the need to operate with extreme low temperatures, the practical difficulties to scale the capabilities of a quantum computer to a large number of quantum bits (qubits), the wave function collapse in data measurement, and the impossibility of performing cloning, summation, feedback and non-unitary operations) and being explicitly designed to harness the full potential of PIP technology.

To this end, here we present the foundations of an entire new class of computation theory, termed as Analog Programmable-Photonic Computation (APC). To achieve this overall aim, we will follow the steps sketched in Fig. 1d. Firstly, we will propose a unit of information named as analog bit (or anbit) and defined as a two-dimensional (2D) analog function (similar to the qubit, but with essential differences, as detailed below). Secondly, we will introduce the basic operations (i.e. gates) among anbits formalising the underlying algebra. Thirdly, we will design the circuit implementations of these gates using PIP technology and, fourthly, we will specify a roadmap to further develop the APC in future works. Finally, a qualitative comparison among the main properties of APC, DC, QC and NC is discussed, assessing the unique potential and versatility offered by this computing paradigm.

Results

Unit of information: the analog bit

APC emerges around the concept of performing analog operations on a new unit of information, the anbit, which must be easily implementable using PIP technology. In this vein, considering that the building block of PIP is usually an optical circuit carrying out 2×2 matrix transformations [12–14, 23], we define an anbit as a 2D vector function $\boldsymbol{\psi}(t) = \psi_0(t)\,\hat{\mathbf{e}}_0 + \psi_1(t)\,\hat{\mathbf{e}}_1$, where

$\psi_{0,1}$ are scalar complex functions referred to as the anbit amplitudes and $\hat{\mathbf{e}}_{0,1}$ are constant orthonormal vectors. The user information is encoded in the moduli and phases of $\psi_{0,1}$, which may be directly implementable in PIP using two classical optical wave packets propagated in the fundamental modes of two parallel uncoupled waveguides, a technique termed as space-encoding modulation (see Fig. 2a and Methods). In this work, for the sake of simplicity, the temporal shape of the wave packets are assumed rectangular (quasi-rectangular in practice, e.g., using super-Gaussian pulses). In this fashion, the anbit amplitudes can be regarded as time-invariant functions (complex numbers) within the time intervals where $\psi_{0,1}$ are defined. Thus, in contrast to the discrete 1D nature of the bit used in DC (whose value may be 0 or 1), $\psi_{0,1}$ can actually take on a continuous range of complex values. Alternative physical implementations of an anbit can be proposed by generating diverse shapes of the wave packets in the space, mode, polarisation, frequency and time domains, giving rise to different anbit modulation formats (Supplementary Note 1). Moreover, the following noteworthy features of an anbit should be highlighted:

- *Hilbert space.* The single-anbit vector space $\mathscr{E}_1 = \text{span}\{\hat{\mathbf{e}}_0, \hat{\mathbf{e}}_1\}$ in combination with the standard complex inner product $\langle\cdot|\cdot\rangle$ lead to a Hilbert space with a finite norm ($0 \leq \|\boldsymbol{\psi}\| < \infty$) whose square provides information about the optical power ($\mathcal{P}$) propagated by the waveguides depicted in Fig. 2a: $\mathcal{P} \equiv \|\boldsymbol{\psi}\|^2 = \langle\boldsymbol{\psi}|\boldsymbol{\psi}\rangle = |\psi_0|^2 + |\psi_1|^2$ (see Methods).

- *Dimension.* Although, in general, we will work in a Hilbert space with dimension $d = 2$, we have the possibility of defining the unit of information in a Hilbert space with $d \geq 1$, leading to different versions of APC termed as d-APC (the usual case with $d = 2$ will be referred to as APC for short). In Supplementary Note 4, we discuss how to construct the theory with $d \neq 2$.

- *Anbit period.* $\boldsymbol{\psi}$ is defined in a time interval T_{ANBIT}, termed as the anbit period, encompassing from the beginning of ψ_0 or ψ_1 to the end of ψ_0 and ψ_1 (Fig. 2a). The anbit amplitudes are defined in different time intervals T_0 and T_1 (with the possibility of setting $T_0 = T_1$ or $T_0 \neq T_1$), and the time delay ΔT between $\psi_0 = |\psi_0|\, e^{i\angle_0}$ and $\psi_1 = |\psi_1|\, e^{i\angle_1}$ establishes a differential phase $\angle_1 - \angle_0 = \omega_{\text{c}}\Delta T$, where ω_{c} is the angular frequency of the optical carrier.

- *Measurement and degrees of freedom.* The recovering of the user information at the receiver will be referred to as the anbit measurement and can be carried out via two different ways: (*i*) a coherent measurement, implementable using coherent detection, or (*ii*) a differential measurement, associated to a direct detection scheme (Fig. 2b). The former retrieves the moduli and phases of $\psi_{0,1}$ (4 real degrees of freedom) and the latter only provides information about $|\psi_{0,1}|^2$ and $\angle_1 - \angle_0$ (3 real degrees of freedom, in this case the global phase of $\psi_{0,1}$ cannot be recovered, see Supplementary Note 1). Hence, the number of effective degrees of freedom (EDFs) where the user information can be encoded depends solely on the kind of anbit measurement employed at the receiver. Although a differential measurement provides the lowest number of EDFs, it is the most economical anbit measurement strategy in PIP.

- *Geometric representations.* An anbit with 4 EDFs (coherent measurement) can be geometrically represented by using a polar diagram illustrating the moduli and phases of $\psi_{0,1}$ (Fig. 2c). An anbit with 3 EDFs (differential measurement) may be represented in the generalised Bloch sphere (GBS), with a radius different from 1 (Fig. 2d).

- *Multiple anbits.* A multi-anbit gate will require to operate in a Hilbert space 'higher' than $\mathscr{E}_1$. The construction of such a Hilbert space can be carried out in APC by using the tensor product [33] or the Cartesian product [34]. The former will allow us to extrapolate multi-anbit gates from QC (e.g. controlled gates). The latter will be of great benefit to construct multi-anbit linear operations which otherwise would exhibit a nonlinear nature using the tensor product (e.g. the fan-in and fan-out gates, see below). In Supplementary Note 1, we detail the main properties of the tensor and Cartesian products within the framework of APC.

Despite the fact that the anbit is similar to the qubit (and to its classical counterpart, the cebit [24]), the following fundamental differences should be highlighted: (*i*) the anbit norm may be different from 1 and can be modified using a non-unitary operation, (*ii*) the vector superposition of $\hat{\mathbf{e}}_0$ and $\hat{\mathbf{e}}_1$ is preserved after an anbit measurement (Fig. 2b), (*iii*) an anbit has 1 or 2 more EDFs than the qubit, (*iv*) multiple anbits can be composed by using not only the tensor product but also the Cartesian product, (*v*) an anbit may be defined in a one-dimensional Hilbert space (the qubit cannot be restricted to one dimension given that a global phase is not observable [10]). However, in contrast to QC, in APC we will not be able to perform instantaneous non-local operations among different anbits (i.e., the entanglement of multiple units of information) because the underlying physical laws are deterministic [35].

Furthermore, taking into account the vector formalism required to describe an anbit and its mathematical similitude with a qubit (but with the essential differences discussed above), let us introduce at this point the use of Dirac's notation in order to: (*i*) simplify the mathematical calculations when designing complex APC computing architectures and (*ii*) extrapolate diverse analysis and design strategies from QC, preserving the same notation between both computation theories. Therefore, from now on, let us express the anbit as $\big|\psi\big\rangle = \psi_0\big|0\big\rangle + \psi_1\big|1\big\rangle$, with $\boldsymbol{\psi} \equiv \big|\psi\big\rangle$, $\hat{\mathbf{e}}_0 \equiv \big|0\big\rangle$ and $\hat{\mathbf{e}}_1 \equiv \big|1\big\rangle$.

Fundamentals of combinational design: basic anbit gates

The second natural step to construct the computation theory is to introduce the basic anbit operations (or gates), see Fig. 3. The simplest operation that can be built in APC is a gate of a single anbit: a non-feedback (or combinational) system carrying out a transformation between two different anbits, the input anbit $\big|\psi\big\rangle = \psi_0\big|0\big\rangle + \psi_1\big|1\big\rangle$ and the output anbit $\big|\varphi\big\rangle = \varphi_0\big|0\big\rangle + \varphi_1\big|1\big\rangle$ (Fig. 3a). Mathematically, the gate is described via an arbitrary mapping (or operator) $\widehat{\mathrm{F}} : \mathscr{E}_1 \to \mathscr{E}_1$, which will be assumed to be a holomorphic function for convenience. In this way, such a mapping can be written as a power series $\widehat{\mathrm{F}} = \widehat{\mathrm{F}}^{(1)} + \widehat{\mathrm{F}}^{(2)} + \widehat{\mathrm{F}}^{(3)} + \ldots$, with $\widehat{\mathrm{F}}^{(k)}$ accounting for the linear ($k = 1$) and nonlinear ($k > 1$) responses of the gate. Considering that the PIP circuits are typically linear systems [12–14], we will focus our attention on the case $\widehat{\mathrm{F}} \equiv \widehat{\mathrm{F}}^{(1)}$, that is, in linear gates. Nonetheless, it is worth mentioning that APC may also be constructed by using nonlinear gates (see Methods).

Specifically, a single-anbit linear gate is described by a linear operator (or endomorphism) $\widehat{\mathrm{F}}$ exhibiting the following general properties:

- *Uniqueness.* The input and output anbits are always related by a unique endomorphism $\widehat{\mathrm{F}}$. This property directly follows from the uniqueness of a linear transformation between vector spaces [36].

- *Matrix representation.* Given an orthonormal vector basis $\mathcal{B}_1 = \{|0\rangle, |1\rangle\}$, the matrix representation of $\widehat{\mathrm{F}}$ is unique and is given by the expression (Supplementary Note 2):

$$F = \begin{pmatrix} \langle 0|\widehat{\mathrm{F}}|0\rangle & \langle 0|\widehat{\mathrm{F}}|1\rangle \\ \langle 1|\widehat{\mathrm{F}}|0\rangle & \langle 1|\widehat{\mathrm{F}}|1\rangle \end{pmatrix}. \tag{1}$$

  Hence, the gate can equivalently be described by the matrix F and the input-output relation $|\varphi\rangle = \widehat{\mathrm{F}}|\psi\rangle$ can be expressed as $\left[|\varphi\rangle\right]_{\mathcal{B}_1} = F\left[|\psi\rangle\right]_{\mathcal{B}_1}$, where $\left[|\varphi\rangle\right]_{\mathcal{B}_1} = \begin{pmatrix} \varphi_0 & \varphi_1 \end{pmatrix}^T$ and $\left[|\psi\rangle\right]_{\mathcal{B}_1} = \begin{pmatrix} \psi_0 & \psi_1 \end{pmatrix}^T$ (T denotes the transpose matrix).

- *Reversibility.* By definition, a gate is reversible when $\widehat{\mathrm{F}}$ is a bijective mapping (automorphism). In such circumstances, $\det(F) \neq 0$ and the input anbit can be recovered from the output anbit by applying the inverse mapping $\widehat{\mathrm{F}}^{-1}$, whose matrix representation is F^{-1}. Contrariwise, a gate is irreversible when $\det(F) = 0$ and the input anbit cannot be retrieved from the output anbit given that $\nexists \widehat{\mathrm{F}}^{-1}$.

- *Non-locality.* The input-output relation $|\varphi\rangle = \widehat{\mathrm{F}}|\psi\rangle$ is non-local and causal. The input and output anbits are respectively encoded by two different electric fields $\boldsymbol{\mathcal{E}}(\mathbf{r}_1, t_1)$ and $\boldsymbol{\mathcal{E}}(\mathbf{r}_2, t_2)$ with $\mathbf{r}_1 \neq \mathbf{r}_2$ and $t_1 < t_2$ (see Methods).

- *Classes of linear gates.* Since a linear gate can be described by a matrix, we will use a terminology based on matrix theory [37] to define different classes of operations: unitary gates (U-gates), general linear gates (G-gates) and general matrix gates (M-gates). Concretely, the U-gates will account for the linear reversible mappings that preserve the norm of the input anbit (conservative operations) via a unitary matrix transformation. Contrariwise, the G- and M-gates will describe non-conservative linear operations. While, by definition, a G-gate is always reversible, an M-gate may be reversible or irreversible, encompassing both possibilities. Hence, a G-gate will be described by a general linear (i.e. non-singular) matrix, whereas an M-gate will be associated to a general complex matrix (singular or non-singular).

- *Geometric representation.* Using differential measurement (that will be the case in most scenarios of APC), a single-anbit gate may be geometrically interpreted as a trajectory between two different points in the GBS (Fig. 3a). Specifically, the kind of trajectory depends on the class of the gate, see Supplementary Note 2 for more details.

- *Algebraic structure and universal matrices.* The U- and G-gates belong to the $\mathrm{U}(2)$ and $\mathrm{GL}(2, \mathbb{C})$ Lie groups, respectively, while an M-gate belongs to the $\mathfrak{gl}(2, \mathbb{C})$ Lie algebra [37]. Using the fundamentals of these algebraic structures [10, 23, 37, 38], it is straightforward to find a universal (or arbitrary) matrix in each class of gate, which must be able to describe all the possible 2×2 matrix transformations associated to the class

when varying the value of its entries, encoded by parameters. In particular, a universal matrix of a U-gate reads as follows [10, 23]:

$$U = e^{i\delta} R_{\hat{\mathbf{n}}}(\alpha) = e^{i\delta} \begin{pmatrix} \cos\frac{\alpha}{2} - in_z \sin\frac{\alpha}{2} & -(n_y + in_x)\sin\frac{\alpha}{2} \\ (n_y - in_x)\sin\frac{\alpha}{2} & \cos\frac{\alpha}{2} + in_z \sin\frac{\alpha}{2} \end{pmatrix}, \tag{2}$$

where $\delta \in [0, 2\pi)$ is a global phase shifting and $R_{\hat{\mathbf{n}}}(\alpha)$ is a rotation matrix accounting for a rotation of an angle $\alpha \in [0, 2\pi]$ around an arbitrary unit vector $\hat{\mathbf{n}} = n_x\hat{\mathbf{x}} + n_y\hat{\mathbf{y}} + n_z\hat{\mathbf{z}}$ ($n_{x,y,z} \in [-1, 1]$) in the GBS (Fig. 3b). In addition, a possible universal matrix of a G- or M-gate is a parametric matrix (denoted as G or M, respectively) with the four entries described by four independent complex numbers [37, 38]. Nevertheless, in the former case (G-gate), the condition $\det(G) \neq 0$ must be fulfilled.

- *PIP implementation.* The optical implementation (or circuit architecture) of a U-, G- or M-gate must be able to perform the 2×2 matrix transformation described by its universal matrix by utilising basic PIP devices: phase shifters (PSs), resonators, attenuators, amplifiers, and beam splitters (combiners) such as directional couplers (DICs) and multi-mode interferometers (MMIs). Since a universal matrix may be implementable by different equivalent circuit architectures, we should introduce here the concept of *minimal circuit architecture* (MCA), defined as the PIP implementation encompassing the minimum number of basic devices. Furthermore, since any PIP circuit is fully characterized by analysing the Lorentz reciprocity and the forward-backward (FB) symmetry [13], we include an extended discussion about these properties within the context of APC in Supplementary Note 2.

Uncovering the MCA of the U-, G-, and M-gates requires to explore diverse matrix factorization techniques that allow us to implement the universal matrix of each class of operation by utilising PIP technology. After a thorough examination of the matrix theory literature [10, 34, 36–42], two different factorization techniques should be taken into consideration in our discussions: Euler's rotation theorem and the singular value decomposition (SVD).

As reported in ref. [23], a 2×2 universal unitary matrix of the form given by Eq. (2) cannot be directly implemented by using mainstream PIP devices because of the arbitrary nature of $\hat{\mathbf{n}}$. Here, we can take advantage of Euler's rotation theorem to factorize the U matrix as a concatenation of three rotations around two Cartesian axes of the GBS, which are implementable via PSs, MMIs and DICs. In addition, taking into account that a U-gate can be regarded as a 2×2 universal unitary signal processor, then the MCA of a U-gate (Fig. 3b) must be the same as the MCA of a 2×2 universal unitary signal PIP processor, shown in Fig. 4a of ref. [23] and based on the Euler factorization $U = e^{i\delta} R_{\hat{\mathbf{n}}}(\alpha) \equiv e^{i\delta} R_{\hat{\mathbf{z}}}(\alpha_3) R_{\hat{\mathbf{x}}}(\alpha_2) R_{\hat{\mathbf{z}}}(\alpha_1)$. The matrices $R_{\hat{\mathbf{z}}}(\alpha_{1,3})$ can be implemented by PSs integrated in parallel uncoupled waveguides and the matrix $R_{\hat{\mathbf{x}}}(\alpha_2)$ may be generated by a synchronous DIC with tunable mode-coupling coefficient $\kappa = \alpha_2/(2L)$, where L is the length of its arms. This MCA preserves the Lorentz reciprocity but breaks the FB symmetry (provided that $\alpha_1 \neq \alpha_3$). Equivalent circuit architectures of a U-gate may be explored by selecting different rotation vectors when using Euler's rotation theorem. As an example, in Supplementary Note 2 it is shown a scheme built from fixed couplers, based on the factorization $U = e^{i\delta} R_{\hat{\mathbf{z}}}(\alpha_3) R_{\hat{\mathbf{y}}}(\alpha_2) R_{\hat{\mathbf{z}}}(\alpha_1)$.

While a U-gate is a conservative transformation (given that it preserves the norm of the input anbit or, equivalently, the power of the 2D wave that encodes the anbit), both G- and M-gates are non-conservative transformations. This implies that their MCAs will require to include attenuators and amplifiers. Remarkably, a common MCA for both kind of gates is found from the SVD [34, 36, 39], which factorizes the universal matrices of these gates as a function of two U-gates along with a 2×2 diagonal matrix with positive real entries, implementable by using tunable optical attenuators and amplifiers (Fig. 3c). The reciprocal (non-reciprocal) nature of such devices preserves (breaks) the Lorentz reciprocity in the MCA. Likewise, note that the FB symmetry is broken in the MCA when using the circuit of Fig. 3b to implement the U-gates.

Although equivalent circuit architectures of the U-, G- and M-gates can be proposed by using matrix factorizations different from Euler's rotation theorem and the SVD, all of them lead to optical schemes integrating a higher number of basic PIP devices than the structures depicted in Fig. 3 (see Supplementary Note 2).

So far, we have presented the basic operations of a single anbit. Nonetheless, bearing in mind that PIP is a reconfigurable hardware [12–14], the design of complex combinational architectures requires to introduce an additional fundamental piece: a *controlled gate*. In APC, such a kind of gate may be defined in the same way as in QC [10]. By convention, a controlled anbit gate performs a transformation $\widehat{\mathrm{F}}$ on the target anbits when the control anbits are equal to $\left|1\right\rangle$. Otherwise, the target anbits remain invariant at the output. Figure 4a illustrates the functionality of a controlled gate with a single target anbit $\left|t\right\rangle$ and a single control anbit $\left|c\right\rangle$. Using the tensor product, the mathematical formalisation and properties of a controlled gate in APC can be directly extrapolated from QC (Supplementary Note 2), with the essential difference that a controlled gate may be constructed from a non-unitary $\widehat{\mathrm{F}}$ mapping in APC.

An additional crucial difference between a controlled gate in APC and QC emerges when analysing its implementation using PIP technology. Since the reconfigurability of a PIP circuit is realised by utilising classical electrical control signals [12–14], the implementation of a controlled anbit gate does not require the intricate design strategies and architectures employed in optical QC [10, 21, 43, 44] (however, these schemes could be extrapolated to APC, if desired). As seen in Fig. 4b, the simplest implementation of a controlled anbit gate arises from an electro-optic design, where the control anbit is encoded by the electrical control signals of the PIP platform and the target anbit is encoded by a 2D optical wave (alternatively, both control and target anbits can be encoded by optical waves, giving rise to an all-optical architecture requiring a higher footprint than that of the electro-optic design, see Fig. 4c). In this fashion, the same MCAs as those of the U-, G-, and M-gates (Fig. 3) may be employed to perform controlled operations of each kind of gate. Therefore, the electro-optic architecture only entails the definition of a mapping between the control anbit and the electrical control signals of the PIP circuit (e.g. via software [45]).

As an illustrative example, the electro-optic implementation of the controlled-NOT (CNOT) gate is sketched in Fig. 4d. Any suitable mapping between the control anbit and the electrical control signals must guarantee that the 2×2 unitary matrix transformations $F = iR_{\hat{\mathbf{x}}}(\pi)$ (the Pauli matrix σ_x) and $F = I$ (the identity matrix) are induced on the amplitudes of $\left|t\right\rangle$ when $\left|c\right\rangle = \left|1\right\rangle$ and $\left|c\right\rangle = \left|0\right\rangle$, respectively. It is worthy to note that, in contrast to the seminal optical implementation of the quantum CNOT gate reported in ref. [43], in APC the implementation of this gate integrates a lower number of basic devices and does not require to use extra (ancilla or garbage) units of information.

Interestingly, the concept of controlled gates can be easily extended to the case of multiple control anbits without requiring extra devices in the optical circuits. Accordingly, multi-controlled operations such as the Toffoli gate (an indispensable tool to implement Boolean functions) can be carried out in APC using the same circuit as that of Fig. 4d by encoding an additional control anbit in the electrical control signals, see Supplementary Note 2.

Fundamentals of sequential design: taming prohibited operations in QC

In a combinational system such as the U-, G-, and M-gates, the outputs depend solely on the inputs. Nevertheless, in a sequential system, the outputs can be connected with the inputs allowing feedback operations. Since sequential architectures are of paramount importance in DC (e.g. to construct digital memories [8, 9]), we wonder about the possibility of exploiting such a kind of systems within the context of APC.

Remarkably, in contrast to QC, feedback schemes will be allowed in APC thanks to the feasibility of performing summation (fan-in) and cloning (fan-out) of anbits using PIP circuits. These are prohibited operations within the realm of QC that will however play a fundamental role to construct any sequential architecture in APC. Concretely, both fan-in and fan-out anbit gates can be implemented via the PIP circuit depicted in Fig. 5a, which preserves the Lorentz reciprocity and the FB symmetry (provided that the amplifiers have a reciprocal and FB symmetric behaviour). This scheme transforms the input anbits $|\psi\rangle$ and $|\varphi\rangle$ into the output anbits $|\psi+\varphi\rangle = (\psi_0+\varphi_0)|0\rangle + (\psi_1+\varphi_1)|1\rangle$ and $|\psi-\varphi\rangle = (\psi_0-\varphi_0)|0\rangle + (\psi_1-\varphi_1)|1\rangle$. Thus, setting $|\varphi\rangle = |\mathbf{0}\rangle = 0|0\rangle + 0|1\rangle$ (the null vector of $\mathscr{E}_1$) we will carry out a fan-out operation of the anbit $|\psi\rangle$ (a perfect cloning) and taking $|\varphi\rangle \neq |\mathbf{0}\rangle$ we will perform a fan-in operation of the anbits $|\psi\rangle$ and $|\varphi\rangle$. Moreover, in order to guarantee a linear behaviour, both fan-in and fan-out gates should be defined by using the Cartesian product, which allows us to independently transform the anbit amplitudes ψ_0, ψ_1, φ_0 and φ_1 (conversely, the tensor product leads to multi-anbit nonlinear operations, see Supplementary Note 3, including a more in-depth discussion about the mathematical properties and optical implementation of these gates).

Figure 5b shows the simplest sequential architecture that can be built in APC, integrated by both fan-in and fan-out gates along with two M-gates ($\widehat{\mathrm{M}}_1$ and $\widehat{\mathrm{M}}_2$) to complete the feedback loop. The analysis of the input-output relation $|\varphi\rangle = \widehat{\mathrm{M}}_{\mathrm{eq}}|\psi\rangle$ indicates that this sequential scheme is equivalent to a combinational M-gate described by the matrix representation $M_{\mathrm{eq}} = \big(I - M_1M_2\big)^{-1}M_1$. Hence, the existence of M_{eq} is closely linked to the condition $\det\big(I - M_1M_2\big) \neq 0$. Contrariwise, the loop cannot be built because the matrix $I - M_1M_2$ is singular. In Supplementary Note 3, we provide further information about the analysis and properties of this structure.

Although the same single-anbit operation $\widehat{\mathrm{M}}_{\mathrm{eq}}$ can be implemented via the MCA of an M-gate (Fig. 3c), the potential of this basic sequential scheme relies on the fact that it establishes the fundamental strategies to analyse and design more complex sequential architectures in APC. For instance, the intricate multi-anbit combinational scheme shown in Fig. 5c can elegantly be simplified with the equivalent sequential architecture depicted in Fig. 5d, composed by a lower number of gates. Surprisingly, both systems have the same input-output relation (see Supplementary Note 3).

Discussion

These results lay the theoretical foundations of APC, a new computing paradigm conceived to exploit the full potential of PIP technology and, consequently, leading to the emergence of an entire field of research within computational science and photonics. In addition, APC can be regarded as a new optical design toolbox which blazes a trail for manufacturing advanced photonic computing architectures that can team-up with digital electronic processors to unlock in the near- and middle-term the serious limitations imposed by the demise of Moore's and Dennard's laws.

Bearing in mind that this work is completely devoted to establishing the fundamentals of APC, a roadmap must be specified to further develop this computation theory in forthcoming works (Fig. 1d). Firstly, the fundamentals of combinational design should be extended to the case of multiple anbits for both U- , G-, and M-gates. We may expect that the MCA of these multi-anbit gates can also be employed to implement controlled gates with multiple target anbits (encoding the control anbits in the electrical control signals of the PIP platform). Secondly, the fundamentals of sequential design should be further developed to the case of multiple anbits, embracing the research of fan-in, fan-out and feedback operations. Given that a digital memory is built from a multi-bit sequential architecture in DC [9], the study of multi-anbit feedback schemes could be of paramount importance to revisit the concept of memory within the scope of APC. Outstandingly, the capacity to scale both combinational and sequential architectures to multiple anbits is inherently related to the feasibility to scale the PIP circuits integrating multiple waveguides [12–14] in combination with the exploitation of WDM technique [19] to perform massive parallel computing of anbits. Thirdly, APC must be completed by conceiving a specific gamut of analog search algorithms to speed up the solution of a representative set of deterministic polynomial time (P) and non-deterministic polynomial time (NP) computational problems (here, it is not possible to rigorously specify such a set of problems because it previously requires to completely develop the multi-anbit operations. In any case, as an example, two possible P and NP problems that could be evaluated are the maximum cardinality matching [46] and the integer factorization problem [47], respectively). The time, resources and energy required in APC to solve these computational problems must be compared with the time, resources and energy required in DC, QC and NC using the general methodologies of computational science [10, 48].

Compared with these existing computational models, APC relaxes some of their theoretical and technological limitations, see Table 1. While in APC we have the possibility of defining both linear and nonlinear gates, DC and QC can only be constructed from nonlinear and linear gates, respectively [9, 10]. Moreover, NC embraces both linear and nonlinear operations, but the global transformation induced on the units of information in a neural network is nonlinear [49]. In contrast, in APC there exists the possibility of exclusively performing linear or nonlinear operations (or a combination of both). A similar remark applies to the reversible and irreversible nature of the operations. Both design possibilities can be found in APC via the U-, G- and M-gates, a feature that is not shared by the other computation theories (in DC reversible operations are not efficient since ancilla and garbage bits are required [50], in QC all operations are reversible, and in NC the multi-dimensional transformation of a neural network is irreversible, inherited from its nonlinear nature).

On the other hand, an essential difference between DC and APC relies on the fact that a combinational APC architecture can take advantage of both forward and backward propagations of light to compute the double of units of information (the same (a different) multi-anbit transformation will be induced in each propagation direction when the circuit preserves (breaks) the FB symmetry). This property also applies to QC and NC when implementing the corresponding computational architectures via PIP technology [6, 44].

The additional properties shown in Table 1 highlight common differences of APC, DC and NC with QC. Although QC provides the outstanding feature of performing instantaneous non-local operations (via the entanglement of qubits, a characteristic that is not shared by the other computation theories), APC can be readily implemented by current PIP technology operating at room temperature. Along this line, it is worth mentioning that APC can also be implemented in any technological platform enabling analog signal processing based on matrix transformations (e.g. optical metamaterials [17, 18], electronics [27, 51, 52] and acoustics [53]).

Likewise, being APC a computation theory using classical waves, we may expect that this new computing paradigm has more tolerance to external noise than QC. This subsequently implies that we will require a lower number of extra units of information than in QC to detect and correct the data errors, simplifying the scalability of APC architectures to a large number of anbits.

An additional intriguing feature of APC arises from the general nature of its mathematical framework, inherited from the versatile properties of the anbit and the basic gates, allowing to implement (at least partially) other computing paradigms using APC architectures (see Supplementary Note 5).

Given that any computation theory has associated an information theory, APC also leads to an additional field of research: the *Analog Programmable-Photonic Information* (API). Concretely, API will be focus on the study of anbit modulation formats (Supplementary Note 1), analysis of noise, error detection and correction strategies, entropy analysis, data compression, and cryptography techniques. Both APC and API have the potential to spark a crucial impact on fundamental and applied research, as well as on our information society.

Methods

Space-encoding modulation

The description of this modulation format (similar to the path-encoding strategy employed in optical QC [54]) can be done by specifying the electric field strength encoding the anbit of Fig. 2a. According to the usual features of the optical waveguides employed in PIP [13], we may assume that the parallel waveguides of Fig. 2a have a negligible inter-waveguide mode-coupling and operate in the paraxial and single-mode regimes. Hence, a space-encoded anbit is characterized by an electric field of the form:

$$\begin{aligned}\boldsymbol{\mathcal{E}}\left(\mathbf{r},t\right) &\simeq \sum_{k=0}^{1}\mathrm{Re}\left\{\psi_k\left(t-\beta_k^{(1)}r_{\parallel}\right)\hat{\mathbf{e}}_k\left(r_{\perp,1},r_{\perp,2},\omega_{\mathrm{c}}\right)e^{i\omega_{\mathrm{c}}t}e^{-i\beta_k^{(0)}r_{\parallel}}\right\}\\ &= \sum_{k=0}^{1}\left|\psi_k\left(t-\beta_k^{(1)}r_{\parallel}\right)\right|\hat{\mathbf{e}}_k\left(r_{\perp,1},r_{\perp,2},\omega_{\mathrm{c}}\right)\cos\left(\omega_{\mathrm{c}}t-\beta_k^{(0)}r_{\parallel}+\angle_k\right),\end{aligned} \tag{3}$$

where the anbit amplitudes $\psi_0 = |\psi_0| e^{i\angle_0}$ and $\psi_1 = |\psi_1| e^{i\angle_1}$ play the role of the optical wave packets (or complex envelopes), ω_{c} is the angular frequency of the optical carrier, $\mathbf{r} = r_{\perp,1}\hat{\mathbf{r}}_{\perp,1} + r_{\perp,2}\hat{\mathbf{r}}_{\perp,2} + r_{\parallel}\hat{\mathbf{r}}_{\parallel}$ is the vector position written as a function of its transverse $(r_{\perp,1},\ r_{\perp,2})$ and longitudinal $(r_{\parallel})$ components, and $\hat{\mathbf{e}}_k$ and $\beta_k(\omega) \simeq \beta_k^{(0)} + (\omega - \omega_{\mathrm{c}})\,\beta_k^{(1)}$ are respectively the normalised mode profile and the propagation constant of the fundamental mode in waveguide k (being $\beta_k^{(0)} = \beta_k(\omega = \omega_{\mathrm{c}})$, $\beta_k^{(1)} = \mathrm{d}\beta_k(\omega = \omega_{\mathrm{c}})/\mathrm{d}\omega$ and omitting the dispersive terms $\beta_k^{(n\geq 2)}$ in the Taylor series expansion of $\beta_k(\omega)$). In particular, $\hat{\mathbf{e}}_k$ must satisfy the condition [55]:

$$\iint_{-\infty}^{\infty} \hat{\mathbf{e}}_k \times \hat{\mathbf{h}}_k^* \cdot \hat{\mathbf{r}}_{\parallel} \mathrm{d}r_{\perp,1}\mathrm{d}r_{\perp,2} = 2, \tag{4}$$

being $\hat{\mathbf{h}}_k$ the normalised mode profile of the magnetic field strength. Equation (4) guarantees that the optical power propagated by the fundamental modes of both waveguides can be calculated as $\mathcal{P} = |\psi_0|^2 + |\psi_1|^2$.

Using Eq. (3), it is straightforward to describe the electric field strength at the input $\boldsymbol{\mathcal{E}}(\mathbf{r}_1, t_1)$ and at the output $\boldsymbol{\mathcal{E}}(\mathbf{r}_2, t_2)$ of the single-anbit gate depicted in Fig. 3a, which must be particularised at two different vector positions $\mathbf{r}_1 \neq \mathbf{r}_2$ and time instants $t_1 \neq t_2$. Taking into account the causal response of the materials employed in PIP [13], then it follows that $t_1 < t_2$. Hence, the input-output relation of the gate is non-local and causal.

Nonlinear anbit gates

Single-anbit nonlinear gates can be implemented in PIP, e.g., by means of the Pockels and Kerr effects, which allow to carry out second- and third-order nonlinear anbit transformations, respectively. For instance, stimulating the self-phase modulation effect in two parallel uncoupled waveguides (similar to those of depicted in Fig. 2a), a nonlinear anbit operation of the form $\widehat{\mathrm{F}}|\psi\rangle = \psi_0 \exp\big(-i\gamma|\psi_0|^2 L_{\mathrm{eff}}\big)|0\rangle + \psi_1 \exp\big(-i\gamma|\psi_1|^2 L_{\mathrm{eff}}\big)|1\rangle$ may be obtained (γ and L_{eff} are nonlinear parameters of the waveguides [56]). In the same vein, optical devices such as nonlinear directional couplers [57] and ring resonators [58] can also be employed to exploit third-order nonlinearities in silicon platforms.

The most general definition of a single-anbit gate (including both linear and nonlinear contributions) is given by the expression $\widehat{\mathrm{F}}|\psi\rangle := f_0\big(\psi_0, \psi_1\big)|0\rangle + f_1\big(\psi_0, \psi_1\big)|1\rangle$, with f_0 and f_1 belonging to $\mathcal{F}\big(\mathbb{C}^2, \mathbb{C}\big)$. Thus, $\widehat{\mathrm{F}}$ will induce a nonlinear transformation on the input anbit when the functions $f_{0,1}$ have a nonlinear behaviour. Therefore, using holomorphic $f_{0,1}$ functions in a neighbourhood of a reference point $\big(\psi_{0,\mathrm{ref}}, \psi_{1,\mathrm{ref}}\big) \in \mathbb{C}^2$, we will be able to build a nonlinear response of the desired order.

The main drawback of operating with nonlinear anbit gates relies on the fact that we cannot deal with a matrix formalism. Nevertheless, the mathematical description of the above nonlinear anbit operation can be simplified by performing a Taylor series expansion of $f_{0,1}$. To this end, let us introduce the vectors $\mathbf{z} := \psi_0\hat{\mathbf{z}}_0 + \psi_1\hat{\mathbf{z}}_1$ and $\mathbf{z}_{\mathrm{ref}} := \psi_{0,\mathrm{ref}}\hat{\mathbf{z}}_0 + \psi_{1,\mathrm{ref}}\hat{\mathbf{z}}_1$ belonging to the vector space $\mathcal{Z} = \mathrm{span}\{\hat{\mathbf{z}}_0, \hat{\mathbf{z}}_1\}$ (isomorphic to $\mathbb{C}^2$) and being $\hat{\mathbf{z}}_{0,1}$ complex orthonormal vectors. In this way, we can write $\widehat{\mathrm{F}} = \sum_{n=1}^{\infty} \widehat{\mathrm{F}}^{(n)}$ where:

$$\widehat{\mathrm{F}}^{(n)}|\psi\rangle = \frac{1}{n!}\mathrm{d}^n\, f_0\rfloor_{\mathbf{z}_{\mathrm{ref}}}(\mathbf{z})\,|0\rangle + \frac{1}{n!}\mathrm{d}^n\, f_1\rfloor_{\mathbf{z}_{\mathrm{ref}}}(\mathbf{z})\,|1\rangle, \tag{5}$$

is the n-th order nonlinear response of the gate with:

$$\mathrm{d}^n f_0\rfloor_{\mathbf{z}_{\mathrm{ref}}}(\mathbf{z}) = \sum_{i_1,\ldots,i_n\in\{0,1\}} \psi_{i_1}\cdots\psi_{i_n}\frac{\partial^n f_0\big(\mathbf{z}_{\mathrm{ref}}\big)}{\partial\hat{\mathbf{z}}_{i_1}\cdots\partial\hat{\mathbf{z}}_{i_n}}, \tag{6}$$

and similar for $\mathrm{d}^n f_1\rfloor_{\mathbf{z}_{\mathrm{ref}}}(\mathbf{z})$. Obviously, this nonlinear mathematical framework should be further extended in forthcoming contributions by defining diverse classes of nonlinear anbit gates, encompassing both combinational and sequential computational architectures.

Author contributions

A. Macho Ortiz originally conceived the idea of APC and API. A. Macho Ortiz and J. Capmany developed the theory. D. Pérez López, J. Azaña and J. Capmany supervised the work. All authors contributed to write the manuscript.

References

[1] Cavin, R. K., Lugli, P. & Zhirnov, V. V. Science and engineering beyond Moore's law. *Proceedings of the IEEE, Special Centennial Issue* **100**, 1720 (2012).

[2] Markov, I. L. Limits on fundamental limits to computation. *Nature* **512**, 147 (2014).

[3] Shalf, J. The future of computing beyond Moore's Law. *Phil. Trans. R. Soc. A* **378**, 20190061 (2020).

[4] Ferreira de Lima, T., Shastri, B. J., Tait, A. N., Nahmias, M. A. & Prucnal, P. R. Progress in neuromorphic photonics. *Nanophotonics* **6**, 577 (2017).

[5] Wetzstein, G. *et al.* Inference in artificial intelligence with deep optics and photonics. *Nature* **588**, 39 (2020).

[6] Shastri, B. J. *et al.* Photonics for artificial intelligence and neuromorphic computing. *Nature Photonics* **15**, 102 (2021).

[7] Shastri, B. J., Tait, A. N., Ferreira de Lima, T., Nahmias, M. A., Peng, H. T. & Prucnal, P. R. Principles of Neuromorphic Photonics. In *Encyclopedia of Complexity and Systems Science* (ed. Meyers, R.) (Springer, Berlin, 2018).

[8] Bartee, T. C. *Digital Computer Fundamentals.* (McGraw-Hill, New York, 1985).

[9] Wakerly, J. F. *Digital Design: Principles and Practices.* (Pearson, New Jersey, 2006).

[10] Nielsen, M. A. & Chuang, I. L. *Quantum Computation and Quantum Information.* (Cambridge University Press, Cambridge, 2016).

[11] Solli, D. R. & Jalali, B. Analog optical computing. *Nature Photonics* **9**, 704 (2015).

[12] Bogaerts, W. *et al.* Programmable photonic circuits. *Nature* **586**, 207 (2020).

[13] Capmany J. & Pérez, D. *Programmable Integrated Photonics.* (Oxford University Press, Oxford, 2020).

[14] Pérez, D., Gasulla, I., DasMahapatra, P. & Capmany, J. Principles, fundamentals and applications of programmable integrated photonics. *Advances in Optics and Photonics* **12**, 709 (2020).

[15] Shamir, J., Caulfield, H. J., Micelli, W. & Seymour, R. J. Optical computing and the Fredkin gates. *Applied Optics* **25**, 1604 (1986).

[16] Miller, D. A. B. Are optical transistors the logical next step?. *Nature Photonics* **4**, 3 (2010).

[17] Camacho, M., Edwards, B. & Engheta, N. A single inverse-designed photonic structure that performs parallel computing. Nature Communications 12, 1466 (2021).

[18] Zangeneh-Nejad, F., Sounas, D. L., Alù, A. & Fleury, R. Analogue computing with metamaterials. *Nature Reviews Materials* **6**, 207 (2021).

[19] Feldmann, J. *et al.* Parallel convolutional processing using an integrated photonic tensor core. *Nature* **589**, 52 (2021).

[20] Mohamed, K. S. *Neuromorphic Computing and Beyond.* (Springer, Cham, 2020).

[21] O'Brien, J. L. Optical quantum computing. *Science* **318**, 1567 (2007).

[22] De Leon, N. P. *et al.* Materials challenges and opportunities for quantum computing hardware. *Science* **372**, 6539 (2021).

[23] Macho, A., Pérez, D. & Capmany, J. Optical implementation of 2×2 universal unitary matrix transformations. *Laser & Photonics Reviews* **15**, 2000473 (2021).

[24] Spreeuw, R. J. C. Classical wave-optics analogy of quantum-information processing. *Physical Review A* **63**, 062302 (1998).

[25] Kish, L. B. Quantum computing with analog circuits: Hilbert space computing. *Proc. of SPIE 5055, Smart Structures and Materials 2003: Smart Electronics, MEMS, BioMEMS, and Nanotechnology*, 0277-786X (2003).

[26] Van den Nest, M. Classical simulation of quantum computation, the Gottesman-Knill theorem, and slightly beyond. Preprint at https://arxiv.org/abs/0811.0898 (2010).

[27] La Cour, B. R. & Ott, G. E. Signal-based classical emulation of a universal quantum computer. *New Journal of Physics* **17**, 053017 (2015).

[28] Wetterich, C. Quantum computing with classical bits. *Nuclear Physics B* **948**, 114776 (2019).

[29] Zhang, S., Li, P., Wang, B., Zeng, Q. & Zhang, X. Implementation of quantum permutation algorithm with classical light. *Journal of Physics Communications* **3**, 015008 (2019).

[30] Zhang, S., Zhang, Y., Sun, Y., Sun, H. & Zhang, X. Quantum-inspired microwave signal processing for implementing unitary transforms. *Optics Express* **27**, 436 (2019).

[31] Cirac, J. I. Quantum computing and simulation. *Nanophotonics* **10**, 453 (2021).

[32] Yang, C. H. *et al.* Operation of a silicon quantum processor unit cell above one kelvin. *Nature* **580**, 350 (2020).

[33] Cohen-Tannoudji, C., Diu, B. & Laloë, F. *Quantum Mechanics, Volume I: Basic Concepts, Tools, and Applications, Ch. 2.* (Wiley, Weinheim, 2020).

[34] Landi, G. & Zampini, A. *Linear Algebra and Analytic Geometry for Physical Sciences.* (Springer, Cham, 2018).

[35] Popescu, S. Nonlocality beyond quantum mechanics. *Nature Physics* **10**, 264 (2014).

[36] Roman, S. *Advanced Linear Algebra.* (Springer, New York, 2005).

[37] Hall, B. C. *Lie Groups, Lie Algebras, and Representations.* (Springer, New York, 2003).

[38] Kirillov, A. *An Introduction to Lie Groups and Lie Algebras.* (Cambridge University Press, Cambridge, 2008).

[39] Golub, G. H. & Van Loan, C. F. *Matrix Computations.* (The Johns Hopkins University Press, Baltimore, 2013).

[40] Hamada, M. The minimum number of rotations about two axes for constructing an arbitrarily fixed rotation. *Royal Society Open Science* **1**, 140145 (2014).

[41] De Vos, A. & De Baerdemacker, S. Block-ZXZ synthesis of an arbitrary quantum circuit. *Physical Review A* **94**, 052317 (2016).

[42] Führ, H. & Rzeszotnik, Z. A note on factoring unitary matrices. *Linear Algebra and its Applications* **547**, 32 (2018).

[43] Ralph, T. C., Langford, N. K., Bell, T. B. & White, A. G. Linear optical controlled-NOT gate in the coincidence basis. *Physical Review A* **65**, 062324 (2002).

[44] Wang, J., Sciarrino, F., Laing, A. & Thompson, M. G. Integrated photonic quantum technologies. *Nature Photonics* **14**, 273 (2020).

[45] Pérez, D., López, A., Dasmahapatra, P. & Capmany, J. Multipurpose self-configuration of programmable photonic circuits. *Nature Communications* **11**, 6359 (2020).

[46] West, D. B. *Introduction to Graph Theory.* (Pearson, New Jersey, 2018).

[47] Lenstra, H. W. & Pomerance, C. A rigorous time bound for factoring integers. *Journal of the American Mathematical Society* **5**, 483 (1992).

[48] Goldreich, O. *Computational Complexity: A Conceptual Perspective.* (Cambridge University Press, Cambridge, 2008).

[49] Cartlidge, E. Optical neural networks. *Optics & Photonics News* **6**, 34 (2020).

[50] Desurvire, E. *Classical and Quantum Information Theory: An Introduction for the Telecom Scientist.* (Cambridge University Press, Cambridge, 2009).

[51] Hubbard, W. *et al.* Electronic neural networks. *AIP Conference Proceedings* **151**, 227 (1986).

[52] Van Schaik, A. Building blocks for electronic spiking neural networks. *Neural Networks* **14**, 617 (2001).

[53] Andersson, G. *et al.* Squeezing and multimode entanglement of surface acoustic wave phonons. *PRX Quantum* **3**, 010312 (2022).

[54] Flamini, F., Spagnolo, N. & Sciarrino, F. Photonic quantum information processing: a review. *Reports on Progress in Physics* **82**, 016001 (2019).

[55] Jalas, D. *et al.* What is - and what is not - an optical isolator. *Nature Photonics* **7**, 579 (2013).

[56] Agrawal, G. P. *Nonlinear Fiber Optics*. (Elsevier, Oxford, 2013).

[57] Fraile-Peláez, F. J. & Assanto, G. Coupled-mode equations for nonlinear directional couplers. *Applied Optics* **29**, 2216 (1990).

[58] Li, A. & Bogaerts, W. Reconfigurable nonlinear nonreciprocal transmission in a silicon photonic integrated circuit. *Optica* **7**, 7 (2020).

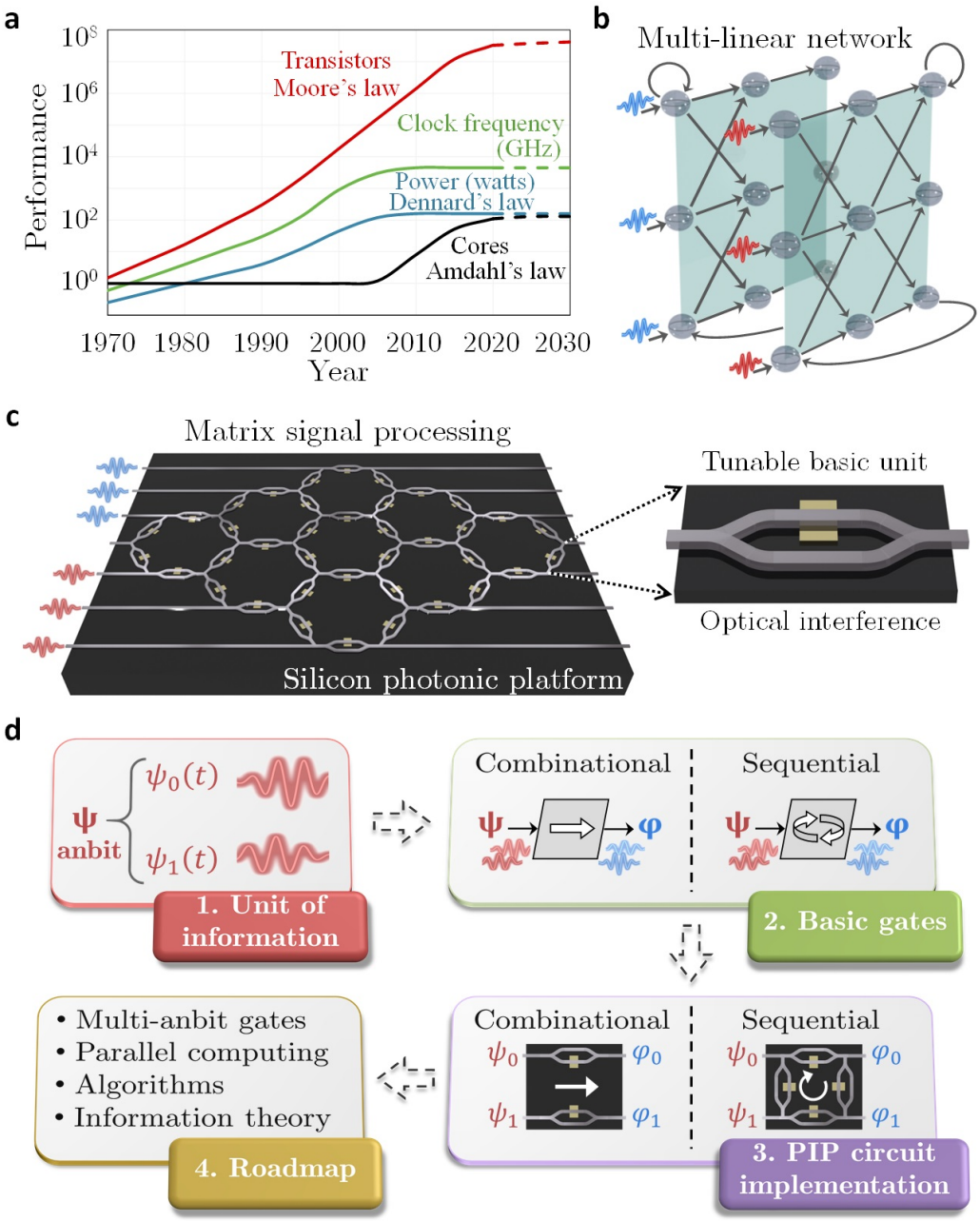

Fig. 1 Limitations of digital electronics and new computation theory proposed in this work. **a** Historical evolution and perspective of the main performance parameters of digital electronics [3]. **b** Distributed, parallel and adaptive network performing multi-linear analog operations via real-time matrix transformations of the input signals, a scenario where digital electronic paradigm shows significant mathematical and technological limitations [5, 6]. **c** Programmable integrated photonic (PIP) circuit integrated into a silicon photonic platform. This system-on-chip technology carries out parallel reconfigurable matrix transformations on the analog input signals using optical interference as a fundamental physical principle. **d** Flowchart of the steps required to construct the new computation theory, termed Analog Programmable-Photonic Computation (APC) and implementable with PIP technology. APC revolves around the idea of performing analog operations on a new unit of information, the analog bit (anbit), evolving the concept of optical signal processing shown in (**c**) into true optical computing.

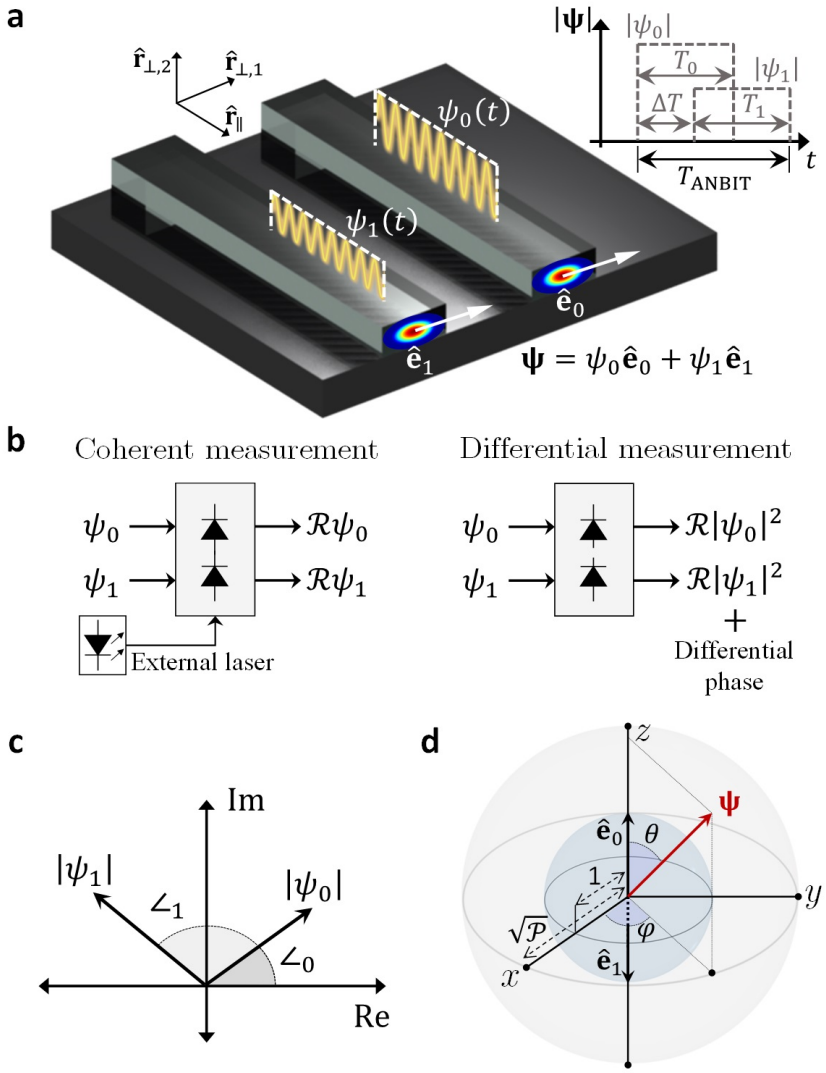

Fig. 2 The analog bit. **a** Physical implementation of an anbit $\boldsymbol{\psi}(t) = \psi_0(t)\,\hat{\mathbf{e}}_0 + \psi_1(t)\,\hat{\mathbf{e}}_1$ using PIP technology and a space-encoding modulation (see Methods). The anbit amplitudes $\psi_{0,1} = |\psi_{0,1}|\,e^{i\angle_{0,1}}$ are encoded by the optical wave packets propagated in the fundamental modes $\hat{\mathbf{e}}_{0,1}$ of two uncoupled waveguides. **b** Different classes of anbit measurement using coherent or direct detection at the optical receiver. In the former case, an anbit of the form $\mathcal{R}\psi_0\hat{\mathbf{e}}_0 + \mathcal{R}\psi_1\hat{\mathbf{e}}_1$ is measured, where $\mathcal{R}$ is the responsivity of the photodiodes. In the latter case, an anbit of the form $\mathcal{R}\,|\psi_0|^2\,\hat{\mathbf{e}}_0 + \mathcal{R}\,|\psi_1|^2\,e^{i(\angle_1-\angle_0)}\hat{\mathbf{e}}_1$ is retrieved (Supplementary Note 1). **c** Geometric representation of an anbit with 4 effective degrees of freedom (EDFs) using a polar diagram in the complex plane. **d** Geometric representation of an anbit with 3 EDFs in the generalised Bloch sphere (GBS). In such a situation, the anbit $\boldsymbol{\psi}$ can be rewritten as $\boldsymbol{\psi} = \sqrt{\mathcal{P}}\left[\cos(\theta/2)\hat{\mathbf{e}}_0 + e^{i\varphi}\sin(\theta/2)\hat{\mathbf{e}}_1\right]$, see Supplementary Note 1.

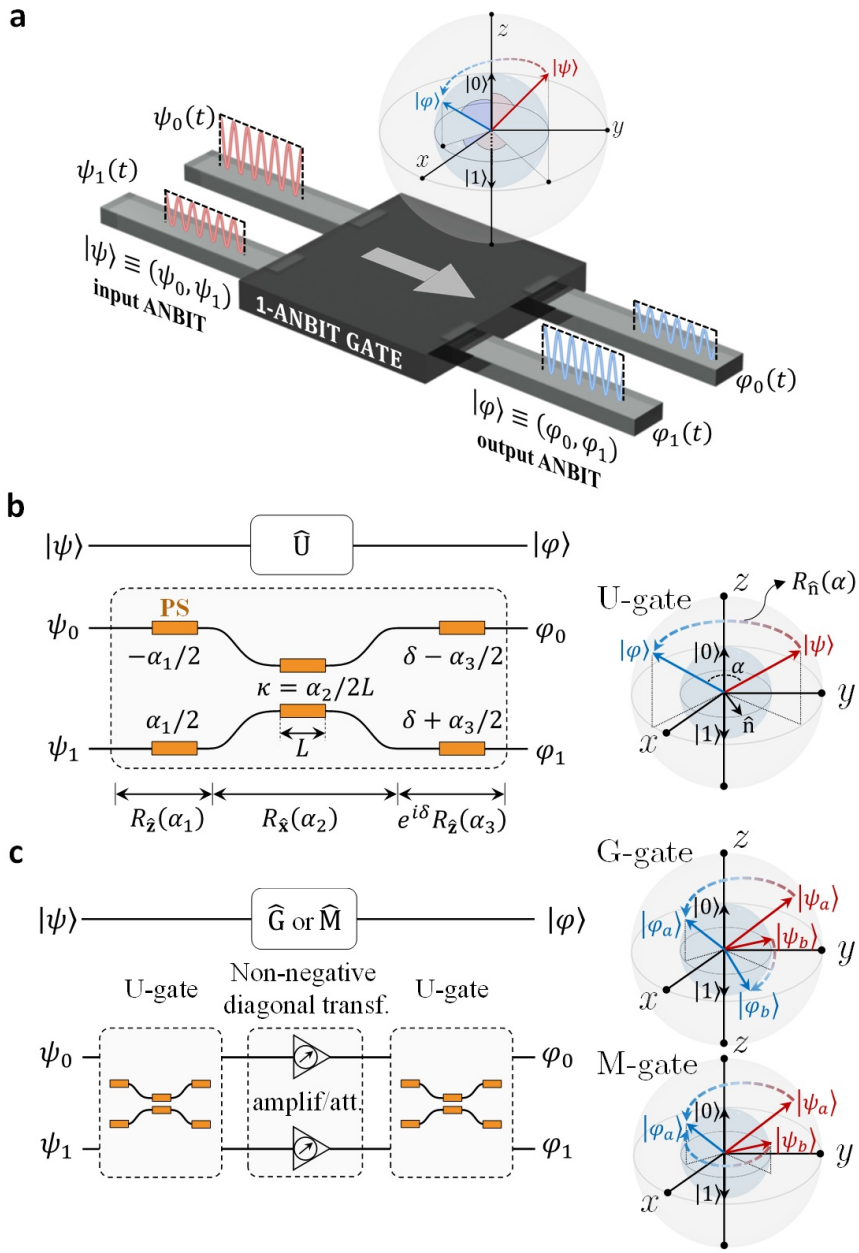

Fig. 3 Basic combinational anbit gates. **a** A combinational single-anbit gate is a non-feedback system performing a transformation between two different 2D vector functions: the input anbit $|\psi\rangle = \psi_0(t)|0\rangle + \psi_1(t)|1\rangle$ and the output anbit $|\varphi\rangle = \varphi_0(t)|0\rangle + \varphi_1(t)|1\rangle$. Using differential anbit measurement, the gate can be geometrically represented as a trajectory between two different points in the GBS. **b** Minimal circuit architecture (MCA) of a U-gate, implementing the universal unitary matrix of Eq. (2) via the Euler factorization $U = e^{i\delta} R_{\hat{\mathbf{n}}}(\alpha) \equiv e^{i\delta} R_{\hat{\mathbf{z}}}(\alpha_3) R_{\hat{\mathbf{x}}}(\alpha_2) R_{\hat{\mathbf{z}}}(\alpha_1)$. The U-gate generates a rotation around an arbitrary unit vector $\hat{\mathbf{n}}$ of the GBS, preserving the norm of the input anbit. **c** MCA of a G- and M-gate, based on the singular value decomposition. While a G-gate is a reversible operation (two different input anbits $|\psi_a\rangle$ and $|\psi_b\rangle$ are always transformed into two different output anbits $|\varphi_a\rangle$ and $|\varphi_b\rangle$), an M-gate may be an irreversible operation (two different input anbits $|\psi_a\rangle$ and $|\psi_b\rangle$ may generate the same output anbit $|\varphi_a\rangle$).

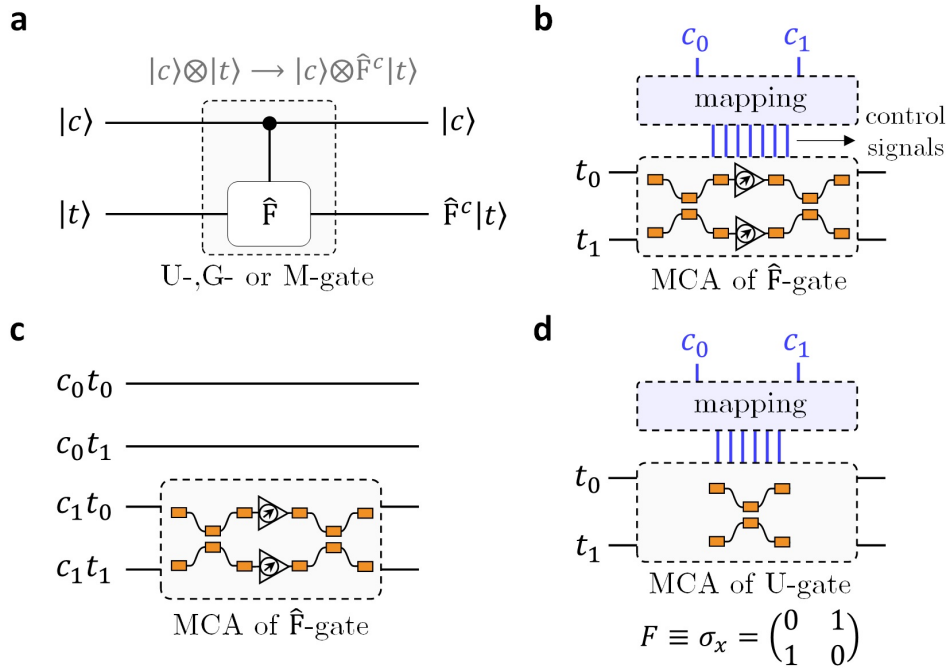

Fig. 4 Controlled anbit gates. a Functional scheme of a controlled gate with a single control anbit $|c\rangle \in \{|0\rangle, |1\rangle\}$ and a single target anbit $|t\rangle$. Inspired in a controlled quantum gate [10], the operation $\widehat{\mathrm{F}}$ (a U-, G-, or M-gate) is applied to $|t\rangle$ when $|c\rangle = |1\rangle$ or, otherwise, $|t\rangle$ remains invariant at the output. **b** Electro-optic design of a controlled gate. The PIP circuit must implement the MCA of the $\widehat{\mathrm{F}}$-gate (here we depict the MCA of an M-gate to cover the general case), whose basic devices are controlled by electrical signals (blue lines) mapped with the electrical amplitudes of $|c\rangle = c_0|0\rangle + c_1|1\rangle$, e.g., via software [45]. The optical inputs encode the amplitudes of $|t\rangle = t_0|0\rangle + t_1|1\rangle$ (black lines). **c** All-optical design of a controlled gate. The optical inputs encode the amplitudes of $|c\rangle \otimes |t\rangle$, where $\otimes$ is the tensor product. **d** Electro-optic implementation of the controlled-NOT anbit gate. The PIP circuit is the MCA of a U-gate since $F = \sigma_x$ is a unitary matrix.

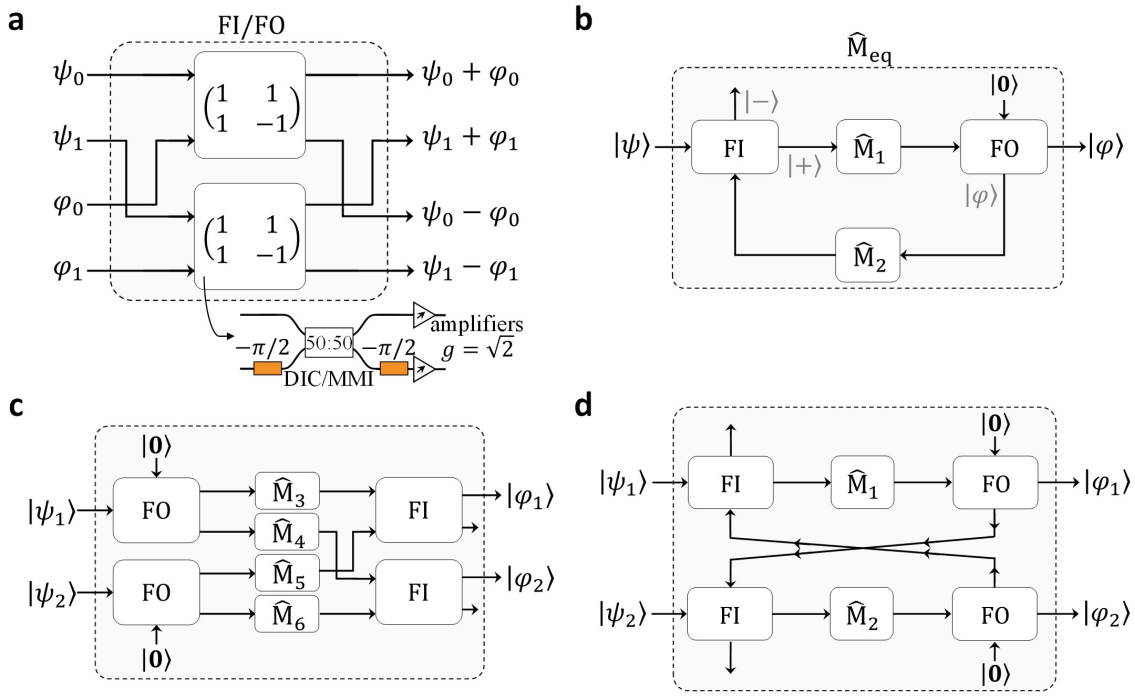

Fig. 5 Sequential anbit architectures. **a** Optical implementation using PIP technology of both fan-in (FI) and fan-out (FO) anbit gates. The FI operation maps the input $|\psi\rangle \times |\varphi\rangle$ into the output $|\psi + \varphi\rangle \times |\psi - \varphi\rangle$, where $\times$ is the Cartesian product. The FO operation performs a perfect cloning of $|\psi\rangle$ when $\varphi_0 = \varphi_1 = 0$, i.e., taking $|\varphi\rangle = |\mathbf{0}\rangle$, where $|\mathbf{0}\rangle = 0|0\rangle + 0|1\rangle$ is the null anbit. **b** Sequential computational architecture of a single anbit, composed by both FI and FO gates along with 2 single-anbit M-gates ($\widehat{\mathrm{M}}_1$ and $\widehat{\mathrm{M}}_2$). **c** Multi-anbit combinational architecture composed by 4 single-anbit M-gates, 2 FI gates and 2 FO gates. **d** Equivalent multi-anbit sequential architecture, integrating 2 single-anbit M-gates, 2 FI gates and 2 FO gates.

Properties	**DC**	**QC**	**NC**	**APC**
Linear computation	×	✓	×	✓
Nonlinear computation	✓	×	✓	✓
Reversible operations	×	✓	×	✓
Irreversible operations	✓	×	✓	✓
Forward-backward propagation	×	✓	✓	✓
Parallel computing	✓	✓	✓	✓
Summation, cloning and feedback	✓	×	✓	✓
Instantaneous non-locality	×	✓	×	×
Implementation with current technology	✓	×	✓	✓
Operation at room temperature	✓	×	✓	✓
Tolerance to external perturbations	✓	×	✓	✓

Table 1. Qualitative comparison of APC *vs* digital computation (DC), quantum computation (QC) and neuromorphic computation (NC).

Supplementary Information

Contents

Supplementary Note 1: the analog bit **25**
1.1 Anbit modulation formats . . . 25
1.2 Anbit measurement . . . 28
1.3 Geometric representation: the generalised Bloch Sphere (GBS) . . . 30
1.4 Anbit amplitudes: component isomorphism . . . 31
1.5 Multiple anbits: tensor product *vs* Cartesian product . . . 32

Supplementary Note 2: combinational design **36**
2.1 General properties of single-anbit linear gates . . . 36
2.2 Equivalent circuit architectures of single-anbit linear gates . . . 39
2.3 Controlled gates . . . 42
2.3.1 Single control anbit . . . 42
2.3.2 Multiple control anbits . . . 45

Supplementary Note 3: sequential design **49**
3.1 Fan-in and fan-out gates . . . 49
3.1.1 Fan-in: anbit addition . . . 49
3.1.2 Fan-out: anbit cloning . . . 52
3.1.3 PIP implementation: a common architecture . . . 54
3.2 First sequential system of the paper . . . 55
3.3 Second sequential system of the paper . . . 57

Supplementary Note 4: different versions of APC **60**
4.1 One-dimensional APC (1-APC) . . . 60
4.1.1 Unit of information: the analog dit . . . 60
4.1.2 Single-andit linear gates . . . 61
4.1.3 Dual-andit linear gates . . . 62
4.1.4 Controlled gates . . . 62
4.1.5 Sequential design . . . 62
4.1.6 Nonlinear andit gates . . . 63
4.2 Multi-dimensional APC (d-APC) . . . 63

Supplementary Note 5: implementing other computing theories **65**
5.1 Digital computation . . . 65
5.2 Neuromorphic computation . . . 66
5.3 Quantum computation . . . 67

Supplementary Note 1: the analog bit

In this section, we provide further information about the analog bit (or anbit for short) including supplementary notes about: the anbit modulation formats, the anbit measurement, the generalised Bloch sphere (GBS), the anbit amplitudes, and the mathematical properties of the tensor and Cartesian products within the context of Analog Programmable-Photonic Computation (APC).

1.1 Anbit modulation formats

The optical implementation of an anbit $\boldsymbol{\psi}(t) = \psi_0(t)\,\hat{\mathbf{e}}_0 + \psi_1(t)\,\hat{\mathbf{e}}_1$ can be carried out by exploiting the different degrees of freedom of light (space, mode, polarisation, frequency and time), unveiling a gamut of *anbit modulation formats*.

Space-encoding modulation (SEM). This modulation technique (described in Fig. 2a and Methods of the main text) is the simplest strategy to implement an anbit in programmable integrated photonics (PIP) using current technology.

Mode-encoding modulation (MEM). Instead of implementing $\boldsymbol{\psi}(t)$ by encoding $\hat{\mathbf{e}}_0$ and $\hat{\mathbf{e}}_1$ in the fundamental modes of two different single-mode waveguides, we can associate $\hat{\mathbf{e}}_0$ and $\hat{\mathbf{e}}_1$ to two different guided modes of a single waveguide operating in the multi-mode regime (Supplementary Figure 1a). Therefore, a mode-encoded anbit is characterized by an electric field strength of the form (paraxial regime is assumed):

$$\boldsymbol{\mathcal{E}}(\mathbf{r},t) \simeq \sum_{k=0}^{1} \mathrm{Re}\left\{\psi_k\left(t-\beta_k^{(1)} r_{\parallel}\right)\hat{\mathbf{e}}_k\left(r_{\perp,1},r_{\perp,2},\omega_{\mathrm{c}}\right)e^{i\omega_{\mathrm{c}}t}e^{-i\beta_k^{(0)}r_{\parallel}}\right\}, \tag{1}$$

where the anbit amplitudes ψ_0 and ψ_1 are encoded by the optical wave packets (or complex envelopes) propagated by the guided modes, ω_{c} is the angular frequency of the optical carrier, $\mathbf{r} = r_{\perp,1}\hat{\mathbf{r}}_{\perp,1} + r_{\perp,2}\hat{\mathbf{r}}_{\perp,2} + r_{\parallel}\hat{\mathbf{r}}_{\parallel}$ is the vector position written as a function of its transverse $(r_{\perp,1},\ r_{\perp,2})$ and longitudinal $(r_{\parallel})$ components, and $\hat{\mathbf{e}}_k$ and $\beta_k(\omega) \simeq \beta_k^{(0)} + (\omega-\omega_{\mathrm{c}})\,\beta_k^{(1)}$ are respectively the normalised mode profile and the propagation constant of the k-th guided mode (being $\beta_k^{(0)} = \beta_k(\omega=\omega_{\mathrm{c}})$, $\beta_k^{(1)} = \mathrm{d}\beta_k(\omega=\omega_{\mathrm{c}})/\mathrm{d}\omega$ and omitting the dispersive terms $\beta_k^{(n\geq 2)}$ in the Taylor series expansion of $\beta_k(\omega)$). This modulation format requires to use mode-division multiplexing devices and circuits to generate, transform and measure the anbits.

Polarisation-encoding modulation (PEM). While the above modulation formats only make use of a single transverse component of the electric field (in the $\hat{\mathbf{r}}_{\perp,1}$ direction), a polarisation-encoded anbit exploits the two transverse components $\hat{\mathbf{e}}_0$ and $\hat{\mathbf{e}}_1$ of the fundamental mode propagated by a single-mode waveguide (Supplementary Figure 1b). In this vein, the electric field strength propagating a polarisation-encoded anbit is found to be (paraxial conditions):

$$\boldsymbol{\mathcal{E}}(\mathbf{r},t) \simeq \sum_{k=0}^{1} \mathrm{Re}\left\{\psi_k\left(t-\beta^{(1)} r_{\parallel}\right)\hat{\mathbf{e}}_k\left(r_{\perp,1},r_{\perp,2},\omega_{\mathrm{c}}\right)e^{i\omega_{\mathrm{c}}t}e^{-i\beta^{(0)}r_{\parallel}}\right\}, \tag{2}$$

with the same propagation constant $\beta(\omega) \simeq \beta^{(0)} + (\omega - \omega_{\mathrm{c}})\beta^{(1)}$ for both transverse components of the fundamental mode considering a lowly-birefringent waveguide [1]. This modulation format entails the utilisation of polarisation devices and systems to generate, transform and measure the anbits.

Frequency-encoding modulation (FEM). The frequency domain can also be employed to implement $\boldsymbol{\psi}(t)$ by encoding $\hat{\mathbf{e}}_0$ and $\hat{\mathbf{e}}_1$ in the same fundamental mode of a given single-mode waveguide, but stimulated at two different angular frequencies ω_0 and ω_1. The spectral separation between both optical carriers must avoid the frequency overlapping between the Fourier transforms of $\psi_0(t)$ and $\psi_1(t)$, namely $\widetilde{\psi}_0(\omega)$ and $\widetilde{\psi}_1(\omega)$ (Supplementary Figure 1c). Specifically, the electric field strength associated to a frequency-encoded anbit is (paraxial regime):

$$\boldsymbol{\mathcal{E}}(\mathbf{r},t) \simeq \sum_{k=0}^{1} \mathrm{Re}\left\{\psi_k\left(t - \beta_k^{(1)} r_{\parallel}\right)\hat{\mathbf{e}}(r_{\perp,1}, r_{\perp,2}, \omega_k)\, e^{i\omega_k t} e^{-i\beta_k^{(0)} r_{\parallel}}\right\}, \tag{3}$$

with $\beta_k^{(0)} = \beta(\omega = \omega_k)$ and $\beta_k^{(1)} = \mathrm{d}\beta(\omega = \omega_k)/\mathrm{d}\omega$, being $\beta(\omega)$ the propagation constant of the fundamental mode. Note that the vector basis $\mathcal{B}_1 = \{\hat{\mathbf{e}}_0, \hat{\mathbf{e}}_1\}$ of the anbit is implemented with the normalised profile $\hat{\mathbf{e}}$ of the fundamental mode stimulated at the angular frequencies ω_0 and ω_1, respectively. The Fourier transform of $\boldsymbol{\mathcal{E}}$ takes the form:

$$\widetilde{\boldsymbol{\mathcal{E}}}(\mathbf{r},\omega) \simeq \sum_{k=0}^{1} \mathrm{Re}\left\{\widetilde{\psi}_k(\omega - \omega_k)\,\hat{\mathbf{e}}(r_{\perp,1}, r_{\perp,2}, \omega_k)\, e^{-i\beta_k^{(0)} r_{\parallel}} e^{-i(\omega-\omega_k)\beta_k^{(1)} r_{\parallel}}\right\}. \tag{4}$$

Here, wavelength-division multiplexing devices and circuits will be required to generate, transform and measure the anbits.

Time-encoding modulation (TEM). The time domain is an additional degree of freedom of light that can also be explored to implement an anbit in optics. The basic idea is to generate a complex envelope of the form $\mathcal{A}(t) = \psi_0(t - t_0) + \psi_1(t - t_1)$ that will be propagated by the fundamental mode of a single-mode waveguide. In particular, the time delay $\Delta\tau = |t_1 - t_0|$ must avoid the temporal overlapping between ψ_0 and ψ_1 (Supplementary Figure 1d). Here, the vector basis $\mathcal{B}_1 = \{\hat{\mathbf{e}}_0, \hat{\mathbf{e}}_1\}$ of the anbit is implemented with the normalised profile $\hat{\mathbf{e}}$ of the fundamental mode stimulated at $t = t_0$ and $t = t_1$, respectively. For sufficient short propagation distances where the chromatic dispersion of the waveguide can be neglected, the electric field strength of a time-encoded anbit can be approximated as (paraxial regime):

$$\begin{aligned}\boldsymbol{\mathcal{E}}(\mathbf{r},t) &\simeq \mathrm{Re}\left\{\mathcal{A}\left(t - \beta^{(1)} r_{\parallel}\right)\hat{\mathbf{e}}(r_{\perp,1}, r_{\perp,2}, \omega_{\mathrm{c}})\, e^{i\omega_{\mathrm{c}} t} e^{-i\beta^{(0)} r_{\parallel}}\right\} \\ &= \sum_{k=0}^{1} \mathrm{Re}\left\{\psi_k\left(t - t_k - \beta^{(1)} r_{\parallel}\right)\hat{\mathbf{e}}(r_{\perp,1}, r_{\perp,2}, \omega_{\mathrm{c}})\, e^{i\omega_{\mathrm{c}} t} e^{-i\beta^{(0)} r_{\parallel}}\right\}. \end{aligned} \tag{5}$$

However, for sufficient propagation distances, the chromatic dispersion will generate fluctuations in $\Delta\tau$ that could give rise to an undesirable temporal overlapping between ψ_0 and ψ_1. Consequently, this propagation impairment is the main drawback of this modulation format, which would require an external synchronization system to control the fluctuations of $\Delta\tau$ within the whole computational system.

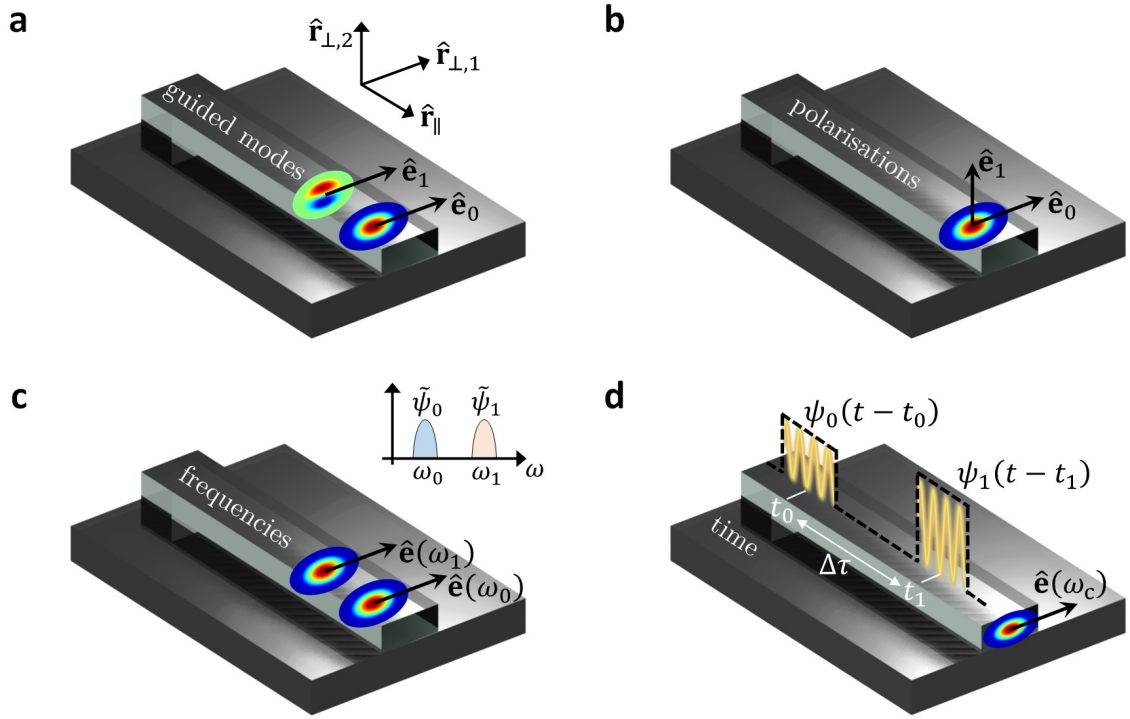

Supplementary Figure 1. Anbit modulation formats. **a** Mode-encoding modulation. **b** Polarisation-encoding modulation. **c** Frequency-encoding modulation. **d** Time-encoding modulation. Each modulation format exploits a different degree of freedom of light to encode an anbit.

Pulse shape. In a similar way to digital information theory [2, 3], we can engineer the temporal shape of the complex envelopes (encoding $\psi_0(t)$ and $\psi_1(t)$) to improve the tolerance of the above anbit modulation formats to the different propagation impairments within a PIP circuit (optical filtering, optical crosstalk, chromatic dispersion, polarisation-mode dispersion, and nonlinear Kerr effects, among others [4]). In particular, using rectangular or quasi-rectangular shapes in $\psi_0(t)$ and $\psi_1(t)$ (e.g., via super-Gaussian pulses), we may explore the introduction of a duty cycle (the ratio of pulse width of $|\psi_0(t)|$ and $|\psi_1(t)|$ over the total time intervals T_0 and T_1 where $\psi_0(t)$ and $\psi_1(t)$ are respectively defined) to study the pulse-to-pulse interaction between different anbits. In such a scenario, we should compare non-return-to-zero (NRZ) versus return-to-zero (RZ) pulse shapes (Supplementary Figure 2). This will lead to different versions of each modulation format (e.g., NRZ-SEM, 33%RZ-SEM, 50%RZ-SEM...). Likewise, arbitrary shapes of $\psi_0(t)$ and $\psi_1(t)$ (such as prolate spheroidal wave functions [5]) can also be investigated in each modulation format to improve the tolerance of the anbit to the aforementioned propagation impairments, although it is out of the scope of this work.

Other modulation formats. The implementation of APC in other technologies different from PIP (e.g., in electronics or acoustics) will require to develop new modulation formats that allow us to physically generate the anbit in the corresponding hardware platforms.

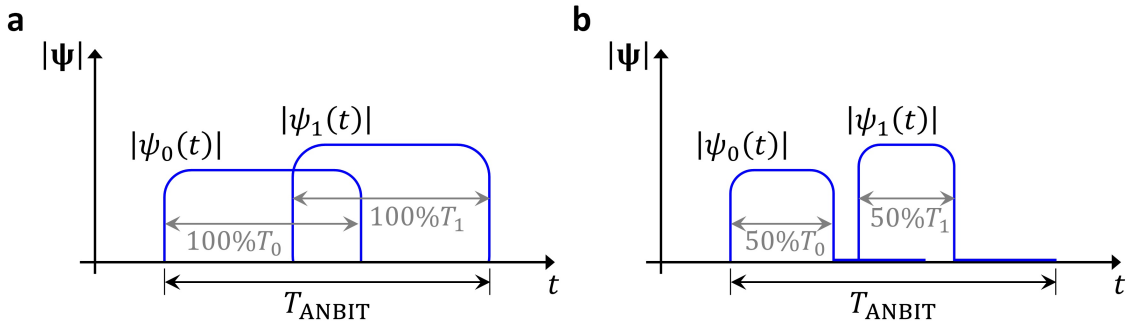

Supplementary Figure 2. Different temporal shapes of rectangular (or quasi-rectangular) anbit amplitudes. **a** Non-return-to-zero (NRZ), where the pulse width covers the whole duration of $|\psi_0(t)|$ and $|\psi_1(t)|$. **b** Return-to-zero (RZ), where the pulse width encompasses only a percentage (50% in this figure) of the time intervals T_0 and T_1 over which $|\psi_0(t)|$ and $|\psi_1(t)|$ are respectively defined.

1.2 Anbit measurement

Each modulation format requires a different optical architecture to perform a coherent or a differential anbit measurement. Here, we only discuss the architectures associated to both classes of anbit measurement within the context of a SEM, the simplest modulation format to implement APC using current PIP technology.

In general, any anbit measurement can be mathematically described as an anbit mapping $\boldsymbol{\psi} \to \boldsymbol{\varphi}$, which transforms the input (optical) anbit:

$$\boldsymbol{\psi} = \psi_0 \hat{\mathbf{e}}_0 + \psi_1 \hat{\mathbf{e}}_1 = |\psi_0| \, e^{i\angle_0} \hat{\mathbf{e}}_0 + |\psi_1| \, e^{i\angle_1} \hat{\mathbf{e}}_1, \tag{6}$$

into an output (electrical) anbit $\boldsymbol{\varphi} = \varphi_0 \hat{\mathbf{e}}_0 + \varphi_1 \hat{\mathbf{e}}_1$. The main difference between a coherent and a differential measurement is that each kind of measurement establishes a different mapping between $\boldsymbol{\psi}$ and $\boldsymbol{\varphi}$, as detailed below. In this context, for the sake of simplicity, we will assume that any (coherent or differential) anbit measurement will be carried out at the receiver by using the same orthonormal vector basis $\mathcal{B}_1 = \{\hat{\mathbf{e}}_0, \hat{\mathbf{e}}_1\}$ as that of the transmitter.

Coherent anbit measurement. Here, the 4 real degrees of freedom of $\boldsymbol{\psi}$ (the moduli and phases of $\psi_{0,1}$) can be completely recovered, leading to 4 *effective degrees of freedom* (EDFs) where the user information can be encoded and retrieved. Using a coherent optical receiver, e.g., combining two quadrature homodyne receivers (Supplementary Figure 3), the phase and quadrature photocurrents obtained are (see pp. 66-68 of ref. [6]):

$$I_{\mathrm{I},k} = \mathcal{R} \, |\psi_k| \cos \angle_k, \tag{7}$$

$$I_{\mathrm{Q},k} = \mathcal{R} \, |\psi_k| \sin \angle_k, \tag{8}$$

where $k \in \{0, 1\}$ and $\mathcal{R}$ is the responsivity of the photodiodes. Next, applying a simple signal processing routine to the above photocurrents using the expressions:

$$|\psi_k| = \frac{1}{\mathcal{R}} \sqrt{I_{\mathrm{I},k}^2 + I_{\mathrm{Q},k}^2}, \qquad \angle_k = \arctan \frac{I_{\mathrm{Q},k}}{I_{\mathrm{I},k}}, \tag{9}$$

we will be able to retrieve the moduli and phases of $\psi_{0,1}$. Consequently, we can safely assume that the output (electrical) anbit is of the form $\boldsymbol{\varphi} = \mathcal{R} \, |\psi_0| \, e^{i\angle_0} \hat{\mathbf{e}}_0 + \mathcal{R} \, |\psi_1| \, e^{i\angle_1} \hat{\mathbf{e}}_1 \equiv \mathcal{R} \boldsymbol{\psi}$.

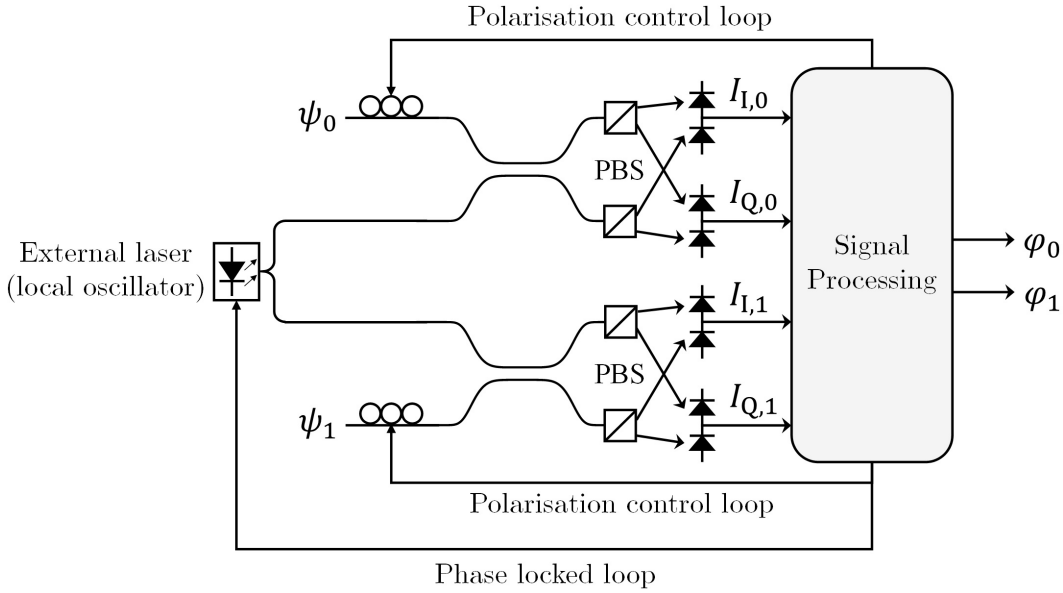

Supplementary Figure 3. Structure of the optical receiver proposed to perform a coherent anbit measurement. The system is composed by two quadrature homodyne receivers (PBS: polarisation beam splitter) [6].

Differential anbit measurement. Using two different photodiodes with the same responsivity $\mathcal{R}$ to measure ψ_0 and ψ_1 via direct detection (see Fig. 2b), we will obtain two independent photocurrents: $I_0 = \mathcal{R}\left|\psi_0\right|^2$ and $I_1 = \mathcal{R}\left|\psi_1\right|^2$. The time delay between both photocurrents will be the same as the time delay ΔT between $\psi_0\left(t\right)$ and $\psi_1\left(t\right)$ depicted in Fig. 2a. As mentioned in the main text, ΔT provides information about the differential phase between ψ_0 and ψ_1 via the relation $\angle_1 - \angle_0 = \omega_{\mathrm{c}}\Delta T$, where ω_{c} is the angular frequency of the optical carrier. Consequently, the output anbit is found to be $\boldsymbol{\varphi} = \mathcal{R}\left|\psi_0\right|^2\hat{\mathbf{e}}_0 + \mathcal{R}\left|\psi_1\right|^2 e^{i(\angle_1-\angle_0)}\hat{\mathbf{e}}_1$.

As seen, this anbit measurement technique only provides 3 EDFs where the user information can be encoded and retrieved: $|\psi_0|$, $|\psi_1|$ and $\angle_1 - \angle_0$. Here, the phase $\angle_0$ cannot be recovered. Consequently, this (global) phase term can be omitted to describe $\boldsymbol{\psi}$, which may be restated as:

$$\boldsymbol{\psi} = \left|\psi_0\right|\hat{\mathbf{e}}_0 + \left|\psi_1\right| e^{i(\angle_1-\angle_0)}\hat{\mathbf{e}}_1. \tag{10}$$

Note that Supplementary Equations 6 and 10 generate the same output anbit $\boldsymbol{\varphi}$ in a differential measurement. For this reason, both expressions are considered to be equivalent to describe the input anbit. Alternatively, the above equation can be rewritten as:

$$\boldsymbol{\psi} = \sqrt{\mathcal{P}}\left(\cos\frac{\theta}{2}\hat{\mathbf{e}}_0 + e^{i\varphi}\sin\frac{\theta}{2}\hat{\mathbf{e}}_1\right), \tag{11}$$

by identifying $\sqrt{\mathcal{P}}\cos\left(\theta/2\right) \equiv |\psi_0|$, $\sqrt{\mathcal{P}}\sin\left(\theta/2\right) \equiv |\psi_1|$, $\varphi \equiv \angle_1 - \angle_0$ and $\mathcal{P} \equiv |\psi_0|^2 + |\psi_1|^2$. In particular, Supplementary Equation 11 will allow us to geometrically represent an anbit with 3 EDFs in the generalised Bloch sphere (see below).

On the other hand, a particular scenario associated to a differential measurement should be mentioned. The case where the differential phase $\angle_1 - \angle_0$ is not encoded by a time delay ΔT between ψ_0 and ψ_1 at the transmitter. This can be done, for instance, modulating ψ_0

and ψ_1 with two different optical carriers having the same angular frequency ω_c but exhibiting a different phase $\angle_0 \neq \angle_1$ at $t = 0$. In such a situation, the differential phase $\angle_1 - \angle_0$ cannot be recovered with a differential anbit measurement because the time delay between the photocurrents is found to be null. Here, a differential measurement will only recover the information encoded by $|\psi_0|$ and $|\psi_1|$ (2 EDFs). This remark highlights the importance of the parameter ΔT depicted in Fig. 2a of the paper.

1.3 Geometric representation: the generalised Bloch Sphere (GBS)

The construction of the GBS is actually more complex than a mere analogy of Supplementary Equation 11 with the spherical coordinates $\left(\sqrt{\mathcal{P}}, \theta, \varphi\right)$ in the vector space $\mathbb{R}^3$. Specifically, the construction of the GBS can be regarded as a geometrical transformation of the hypersphere $S^2\left(\sqrt{\mathcal{P}}\right) \subset \mathbb{R}^3$ into the hypersphere $S^3\left(\sqrt{\mathcal{P}}\right) \subset \mathbb{C}^2$ [7, 8]. Supplementary Figure 4 illustrates such a transformation, summarised in the following steps:

1. Let us start from an anbit with 3 EDFs described by Supplementary Equation 10. Here, we can identify the 3-tuple $\left(|\psi_1| \cos\left(\angle_1 - \angle_0\right), |\psi_1| \sin\left(\angle_1 - \angle_0\right), |\psi_0|\right)$ with the Cartesian coordinates (x, y, z) of the hypersphere $S^2\left(\sqrt{\mathcal{P}}\right) \subset \mathbb{R}^3$ with $z > 0$ and radius:

$$\sqrt{x^2 + y^2 + z^2} = \sqrt{|\psi_0|^2 + |\psi_1|^2} = \sqrt{\mathcal{P}}, \tag{12}$$

see Supplementary Figure 4a. Hence, Supplementary Equation 10 can be rewritten as:

$$\boldsymbol{\psi} = z\hat{\mathbf{e}}_0 + (x + iy)\,\hat{\mathbf{e}}_1. \tag{13}$$

Here, note that $\hat{\mathbf{e}}_0 \equiv \hat{\mathbf{z}}$ and $\hat{\mathbf{e}}_1 \equiv \hat{\mathbf{x}}$. Moving from Cartesian to spherical coordinates $\left(\sqrt{\mathcal{P}}, \theta, \varphi\right)$ via the transformations:

$$x = \sqrt{\mathcal{P}} \sin\theta \cos\varphi, \tag{14}$$

$$y = \sqrt{\mathcal{P}} \sin\theta \sin\varphi, \tag{15}$$

$$z = \sqrt{\mathcal{P}} \cos\theta, \tag{16}$$

the anbit can equivalently be expressed as:

$$\boldsymbol{\psi} = \sqrt{\mathcal{P}} \left(\cos\theta \hat{\mathbf{e}}_0 + e^{i\varphi} \sin\theta \hat{\mathbf{e}}_1\right), \tag{17}$$

with $\theta \in [0, \pi/2]$ and $\varphi \in [0, 2\pi)$.

2. In order to extend the geometrical representation of $\boldsymbol{\psi}$ to the whole sphere (i.e. including the points with $z < 0$), we should perform the coordinate transformation $\theta' := 2\theta$, which maps the Cartesian coordinates (x, y, z) into the coordinates (x', y', z') depicted in Supplementary Figure 4b. Hence, Supplementary Equation 17 becomes:

$$\boldsymbol{\psi} = \sqrt{\mathcal{P}} \left(\cos\frac{\theta'}{2}\,\hat{\mathbf{e}}_0 + e^{i\varphi} \sin\frac{\theta'}{2}\,\hat{\mathbf{e}}_1\right), \tag{18}$$

with $\theta' \in [0, \pi]$ and $\varphi \in [0, 2\pi)$. However, note that a coordinate transformation cannot perform a geometrical transformation on its own.

3. In order to transform $S^2(\sqrt{\mathcal{P}}) \subset \mathbb{R}^3$ into $S^3(\sqrt{\mathcal{P}}) \subset \mathbb{C}^2$, we must carry out the relabelling $\theta' \to \theta$, which is equivalent to reinterpret the coordinates (x', y', z') as the original Cartesian coordinates (x, y, z). As a result, $\hat{\mathbf{e}}_1$ now appears located at the south pole of the new sphere: the GBS (Supplementary Figure 4c). Finally, applying this relabelling to Supplementary Equation 18, we obtain the sought Supplementary Equation 11.

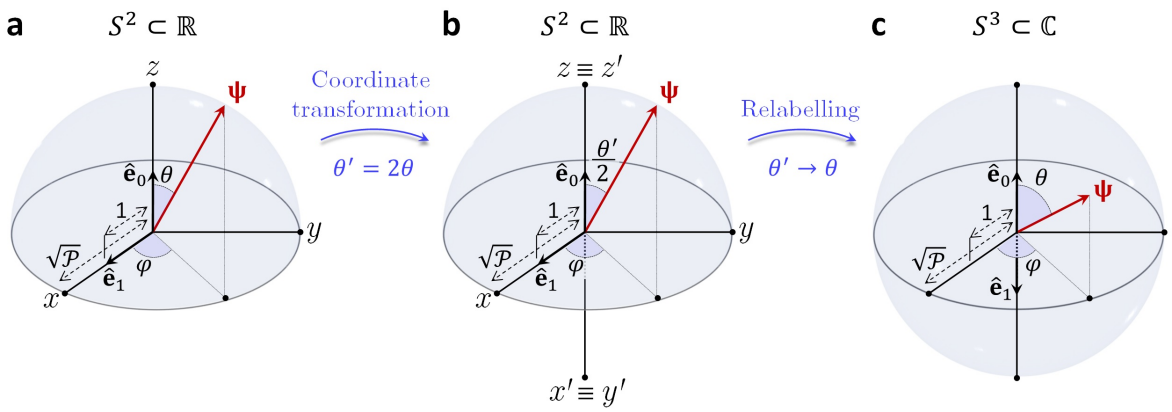

Supplementary Figure 4. Geometrical construction of the generalised Bloch sphere (GBS) to represent an anbit with 3 effective degrees of freedom (Supplementary Equation 11). **a**,**b** Transformation of the hypersphere $S^2(\sqrt{\mathcal{P}}) \subset \mathbb{R}^3$ into **c** the hypersphere $S^3(\sqrt{\mathcal{P}}) \subset \mathbb{C}^2$, the GBS.

Final remark: Dirac's notation. As seen from the GBS, it is clear the mathematical similitude between an anbit and a quantum bit (qubit), but with the basic differences discussed in the paper. In this sense and to be coherent with the main text at the end of subsection "*Unit of information: the analog bit*", let us introduce at this point the use of Dirac's notation from now on. Therefore, let us recast the anbit as $|\psi\rangle = \psi_0|0\rangle + \psi_1|1\rangle$ by performing the identifications $\boldsymbol{\psi} \equiv |\psi\rangle$, $\hat{\mathbf{e}}_0 \equiv |0\rangle$ and $\hat{\mathbf{e}}_1 \equiv |1\rangle$. As we will see through the next sections, Dirac's notation will allow us to simplify the mathematical framework of APC.

1.4 Anbit amplitudes: component isomorphism

Consider the single-anbit vector space $\mathscr{E}_1 = \text{span}(\mathcal{B}_1)$, where $\mathcal{B}_1 = \{|u\rangle, |w\rangle\}$ is a vector basis (that may be the canonical orthonormal basis $\{|0\rangle, |1\rangle\}$ or a different basis). For any anbit $|\psi\rangle \in \mathscr{E}_1$, $\exists(\psi_u, \psi_w) \in \mathbb{C}^2$ (referred to as the anbit amplitudes) satisfying that $|\psi\rangle = \psi_u|u\rangle + \psi_w|w\rangle$. Using an algebraic terminology, ψ_u and ψ_w are specifically the components of the vector $|\psi\rangle$ associated to the basis $\mathcal{B}_1$, which can be calculated using the inner product of $\mathscr{E}_1$ as follows [9]:

$$\psi_u = \text{proj}_{\text{span}\{|u\rangle\}}\left(|\psi\rangle\right) = \frac{\langle u|\psi\rangle}{\langle u|u\rangle}, \qquad \psi_w = \text{proj}_{\text{span}\{|w\rangle\}}\left(|\psi\rangle\right) = \frac{\langle w|\psi\rangle}{\langle w|w\rangle}. \tag{19}$$

In this context, a useful analytical tool that allows us to provide a matrix nature to the concept of component is the *component isomorphism*, defined as the mapping $[\cdot]_{\mathcal{B}_1} : \mathscr{E}_1 \to M_{2\times 1}(\mathbb{C})$:

$$[|\psi\rangle]_{\mathcal{B}_1} := \begin{pmatrix} \psi_u \\ \psi_w \end{pmatrix}. \tag{20}$$

In particular, this mapping is employed in APC to describe the input-output relation of the anbit gates using matrices instead of linear operators (see the description of equation 1 in the main text and Supplementary Note 2 on p. 36).

1.5 Multiple anbits: tensor product *vs* Cartesian product

In order to operate with multiple anbits, we must construct a vector space "higher" than the single-anbit vector space $\mathscr{E}_1$. This can be done by using the tensor product or the Cartesian product. In this subsection, we detail the main properties of both operations within the context of APC.

Tensor product. The definition and mathematical properties of the tensor product can be found rigorously detailed in Ch. 2 of ref. [10]. Here, we will only highlight the following remarks:

- The notation employed in APC will be the same as the notation used in quantum computing (QC) to describe a system with multiple qubits. The n-anbit vector space $\mathscr{E}_n$, constructed from $\mathscr{E}_1$ using the tensor product, is denoted as:

$$\mathscr{E}_n = \underbrace{\mathscr{E}_1 \otimes \mathscr{E}_1 \otimes \ldots \otimes \mathscr{E}_1}_{n-1 \text{ times}} \equiv \mathscr{E}_1^{\otimes(n-1)}. \tag{21}$$

- A vector belonging to $\mathscr{E}_n$ ($\mathscr{E}_1$) will usually be denoted by using an uppercase (lowercase) Greek letter, e.g., $\big|\Psi\big\rangle = \big|\psi_1\big\rangle \otimes \big|\psi_2\big\rangle \otimes \ldots \otimes \big|\psi_n\big\rangle$, with $\big|\Psi\big\rangle \in \mathscr{E}_n$ and $\big|\psi_k\big\rangle \in \mathscr{E}_1$, $\forall k \in \{1, \ldots, n\}$. Here, we can use a more economical notation by describing the above expression of the form $\big|\Psi\big\rangle = \big|\psi_1, \psi_2, \ldots, \psi_n\big\rangle$.

- The dimension of such a vector space is $\dim\big(\mathscr{E}_n\big) = \dim\big(\mathscr{E}_1\big)^n$.

- The scalar-vector product is ($\lambda \in \mathbb{C}$, $\big|\Psi\big\rangle \in \mathscr{E}_n$):

$$\begin{aligned} \lambda\big|\Psi\big\rangle &= \lambda\big|\psi_1\big\rangle \otimes \big|\psi_2\big\rangle \otimes \ldots \otimes \big|\psi_n\big\rangle \\ &= \big|\psi_1\big\rangle \otimes \lambda\big|\psi_2\big\rangle \otimes \ldots \otimes \big|\psi_n\big\rangle \\ &= \big|\psi_1\big\rangle \otimes \big|\psi_2\big\rangle \otimes \ldots \otimes \lambda\big|\psi_n\big\rangle. \end{aligned} \tag{22}$$

- The null vector of $\mathscr{E}_n$ is constructed by applying $n-1$ times the tensor product to the null vector $\big|\mathbf{0}\big\rangle := 0\big|0\big\rangle + 0\big|1\big\rangle$ of $\mathscr{E}_1$: $\big|\mathbf{0}\big\rangle^{\otimes(n-1)}$. For the sake of simplicity, we will also denote the null vector of $\mathscr{E}_n$ as $\big|\mathbf{0}\big\rangle$ and the context should avoid the confusion.

- The dual space of $\mathscr{E}_1$ is $\mathscr{L}\big(\mathscr{E}_1, \mathbb{C}\big)$: the set of homomorphisms $\big\langle\varphi\big|$ (described by a "bra") that transform an anbit (described by a "ket") $\big|\psi\big\rangle \in \mathscr{E}_1$ into the complex number $\big\langle\varphi|\psi\big\rangle$ by using the standard complex inner product of $\mathscr{E}_1$. Along this line, note that the dual space of $\mathscr{E}_n = \mathscr{E}_1^{\otimes(n-1)}$ is $\mathscr{L}\big(\mathscr{E}_1^{\otimes(n-1)}, \mathbb{C}\big) = \mathscr{L}\big(\mathscr{E}_1, \mathbb{C}\big)^{\otimes(n-1)}$, that is, the set of homomorphisms $\big\langle\Phi\big|$ constructed from the tensor product of n different homomorphisms $\big\langle\varphi_1\big|, \big\langle\varphi_2\big|, \ldots, \big\langle\varphi_n\big|$ belonging to $\mathscr{L}\big(\mathscr{E}_1, \mathbb{C}\big)$: $\big\langle\Phi\big| = \big\langle\varphi_1\big| \otimes \big\langle\varphi_2\big| \otimes \ldots \otimes \big\langle\varphi_n\big|$. Here, we can use a more economical notation rewriting the above expression as $\big\langle\Phi\big| = \big\langle\varphi_1, \varphi_2, \ldots, \varphi_n\big|$.

- The inner product of $\mathscr{E}_n$ is defined by combining the inner product of $\mathscr{E}_1$ along with the multiplication operation of $\mathbb{C}$. As an example, the inner product of $\big|\Psi\big\rangle = \big|\psi_1\big\rangle \otimes \big|\psi_2\big\rangle$ and $\big|\Phi\big\rangle = \big|\varphi_1\big\rangle \otimes \big|\varphi_2\big\rangle$ belonging to $\mathscr{E}_2$ is defined as:

$$\big\langle\Psi|\Phi\big\rangle := \big\langle\psi_1|\varphi_1\big\rangle \cdot \big\langle\psi_2|\varphi_2\big\rangle. \tag{23}$$

- The vector space $\mathscr{E}_n$ is a Hilbert space.

- The canonical vector basis of $\mathscr{E}_n$ is built by applying the tensor product to the canonical vector basis of $\mathscr{E}_1$. As an example, the canonical vector basis of $\mathscr{E}_2$ is:

$$\mathcal{B}_2 = \big\{\big|k\big\rangle \otimes \big|l\big\rangle\big\}_{k,l\in\{0,1\}} = \big\{\big|0,0\big\rangle, \big|0,1\big\rangle, \big|1,0\big\rangle, \big|1,1\big\rangle\big\}\,. \tag{24}$$

  Using the inner product given by Supplementary Equation 23, it follows that $\mathcal{B}_2$ is orthonormal.

- The components of a given ket $\big|\psi_1,\psi_2,\ldots,\psi_n\big\rangle$ belonging to $\mathscr{E}_n$ with vector basis $\mathcal{B}_n$ can be calculated from the components (or anbit amplitudes) of the individuals kets $\big|\psi_{1,\ldots,n}\big\rangle$ belonging to $\mathscr{E}_1$ with vector basis $\mathcal{B}_1$ by using the Kronecker product $\otimes_{\mathrm{K}}$:

$$\big[\big|\psi_1,\psi_2,\ldots,\psi_n\big\rangle\big]_{\mathcal{B}_n} = \big[\big|\psi_1\big\rangle\big]_{\mathcal{B}_1} \otimes_{\mathrm{K}} \big[\big|\psi_2\big\rangle\big]_{\mathcal{B}_1} \otimes_{\mathrm{K}} \ldots \otimes_{\mathrm{K}} \big[\big|\psi_n\big\rangle\big]_{\mathcal{B}_1}\,, \tag{25}$$

  where $[\cdot]_{\mathcal{B}_n}$ and $[\cdot]_{\mathcal{B}_1}$are the component isomorphisms associated to the bases $\mathcal{B}_n$ and $\mathcal{B}_1$, respectively (see p. 31). Supplementary Equation 25 applies to any basis $\mathcal{B}_n$ and $\mathcal{B}_1$ (not necessarily being the canonical bases). For instance, consider two different anbits $\big|\psi\big\rangle = \psi_0\big|0\big\rangle + \psi_1\big|1\big\rangle$ and $\big|\varphi\big\rangle = \varphi_0\big|0\big\rangle + \varphi_1\big|1\big\rangle$. The tensor product is:

$$\begin{aligned}\big|\psi\big\rangle \otimes \big|\varphi\big\rangle &= \big(\psi_0\big|0\big\rangle + \psi_1\big|1\big\rangle\big) \otimes \big(\varphi_0\big|0\big\rangle + \varphi_1\big|1\big\rangle\big)\\ &= \psi_0\varphi_0\big|0,0\big\rangle + \psi_0\varphi_1\big|0,1\big\rangle + \psi_1\varphi_0\big|1,0\big\rangle + \psi_1\varphi_1\big|1,1\big\rangle.\end{aligned} \tag{26}$$

  Therefore, the components of $\big|\psi\big\rangle\otimes\big|\varphi\big\rangle \in \mathscr{E}_2$ with vector basis $\mathcal{B}_2$ given by Supplementary Equation 24 can be calculated as:

$$\big[\big|\psi\big\rangle \otimes \big|\varphi\big\rangle\big]_{\mathcal{B}_2} = \begin{pmatrix}\psi_0\varphi_0\\ \psi_0\varphi_1\\ \psi_1\varphi_0\\ \psi_1\varphi_1\end{pmatrix} = \begin{pmatrix}\psi_0\\ \psi_1\end{pmatrix} \otimes_{\mathrm{K}} \begin{pmatrix}\varphi_0\\ \varphi_1\end{pmatrix} \equiv \big[\big|\psi\big\rangle\big]_{\mathcal{B}_1} \otimes_{\mathrm{K}} \big[\big|\varphi\big\rangle\big]_{\mathcal{B}_1}\,. \tag{27}$$

  Supplementary Equation 27 can be applied, e.g., to obtain the anbit amplitudes associated to the optical inputs depicted in Fig. 4c of the paper.

- The tensor product is non-commutative. The 1:1 correspondence between $\otimes$ and $\otimes_{\mathrm{K}}$ (emerged from the component isomorphism) allows us to infer that $\otimes$ inherits the non-commutative property from $\otimes_{\mathrm{K}}$. Using the above example, it is straightforward to verify that $\big|\psi\big\rangle \otimes \big|\varphi\big\rangle \neq \big|\varphi\big\rangle \otimes \big|\psi\big\rangle$ (when $\big|\psi\big\rangle \neq \big|\varphi\big\rangle$):

$$\begin{aligned}\big|\psi\big\rangle \otimes \big|\varphi\big\rangle \overset{1:1}{\longleftrightarrow} \big[\big|\psi\big\rangle \otimes \big|\varphi\big\rangle\big]_{\mathcal{B}_2} &= \big[\big|\psi\big\rangle\big]_{\mathcal{B}_1} \otimes_{\mathrm{K}} \big[\big|\varphi\big\rangle\big]_{\mathcal{B}_1}\\ &\neq \big[\big|\varphi\big\rangle\big]_{\mathcal{B}_1} \otimes_{\mathrm{K}} \big[\big|\psi\big\rangle\big]_{\mathcal{B}_1} = \big[\big|\varphi\big\rangle \otimes \big|\psi\big\rangle\big]_{\mathcal{B}_2} \overset{1:1}{\longleftrightarrow} \big|\varphi\big\rangle \otimes \big|\psi\big\rangle.\end{aligned} \tag{28}$$

Cartesian product. The definition and mathematical properties of the Cartesian product (equivalent to the direct sum when is applied to a finite number of vector spaces) are rigorously detailed in refs. [9, 11]. Here, we will only highlight the following remarks:

- The n-anbit vector space $\mathscr{E}_n$, constructed from $\mathscr{E}_1$ using the Cartesian product, is denoted as:

$$\mathscr{E}_n = \underbrace{\mathscr{E}_1 \times \mathscr{E}_1 \times \ldots \times \mathscr{E}_1}_{n-1 \text{ times}} \equiv \mathscr{E}_1^{\times(n-1)}. \tag{29}$$

- A vector belonging to $\mathscr{E}_n$ ($\mathscr{E}_1$) will usually be denoted by using an uppercase (lowercase) Greek letter, e.g., $\big|\Psi\big\rangle = \big|\psi_1\big\rangle \times \big|\psi_2\big\rangle \times \ldots \times \big|\psi_n\big\rangle$, with $\big|\Psi\big\rangle \in \mathscr{E}_n$ and $\big|\psi_k\big\rangle \in \mathscr{E}_1$, $\forall k \in \{1, \ldots, n\}$. Here, we can also use a classical notation by describing the above expression via an n-tuple $\big|\Psi\big\rangle = \big(\big|\psi_1\big\rangle, \big|\psi_2\big\rangle, \ldots, \big|\psi_n\big\rangle\big)$.

- The dimension of such a vector space is $\dim\big(\mathscr{E}_n\big) = n \dim\big(\mathscr{E}_1\big)$.

- The scalar-vector product is ($\lambda \in \mathbb{C}$, $\big|\Psi\big\rangle \in \mathscr{E}_n$):

$$\lambda\big|\Psi\big\rangle = \lambda\big|\psi_1\big\rangle \times \lambda\big|\psi_2\big\rangle \times \ldots \times \lambda\big|\psi_n\big\rangle \equiv \big(\lambda\big|\psi_1\big\rangle, \lambda\big|\psi_2\big\rangle, \ldots, \lambda\big|\psi_n\big\rangle\big). \tag{30}$$

- The null vector of $\mathscr{E}_n$ is constructed by applying $n-1$ times the Cartesian product to the null vector $\big|\mathbf{0}\big\rangle$ of $\mathscr{E}_1$: $\big|\mathbf{0}\big\rangle^{\times(n-1)}$. For the sake of simplicity, we will also denote the null vector of $\mathscr{E}_n$ with the ket $\big|\mathbf{0}\big\rangle$ and the context should avoid the confusion.

- The dual space of $\mathscr{E}_n = \mathscr{E}_1^{\times(n-1)}$ is $\mathscr{L}\big(\mathscr{E}_1^{\times(n-1)}, \mathbb{C}\big) = \mathscr{L}\big(\mathscr{E}_1, \mathbb{C}\big)^{\times(n-1)}$, that is, the set of homomorphisms $\big\langle\Phi\big|$ constructed from the Cartesian product of n different homomorphisms $\big\langle\varphi_1\big|, \big\langle\varphi_2\big|, \ldots, \big\langle\varphi_n\big|$ belonging to $\mathscr{L}\big(\mathscr{E}_1, \mathbb{C}\big)$: $\big\langle\Phi\big| = \big\langle\varphi_1\big| \times \big\langle\varphi_2\big| \times \ldots \times \big\langle\varphi_n\big| \equiv \big(\big\langle\varphi_1\big|, \big\langle\varphi_2\big|, \ldots, \big\langle\varphi_n\big|\big)$.

- The inner product of $\mathscr{E}_n$ is defined by combining the inner product of $\mathscr{E}_1$ along with the addition operation of $\mathbb{C}$. As an example, the inner product of $\big|\Psi\big\rangle = \big|\psi_1\big\rangle \times \big|\psi_2\big\rangle$ and $\big|\Phi\big\rangle = \big|\varphi_1\big\rangle \times \big|\varphi_2\big\rangle$ belonging to $\mathscr{E}_2$ is defined as:

$$\big\langle\Psi|\Phi\big\rangle := \big\langle\psi_1|\varphi_1\big\rangle + \big\langle\psi_2|\varphi_2\big\rangle. \tag{31}$$

- The vector space $\mathscr{E}_n$ is a Hilbert space.

- The canonical vector basis of $\mathscr{E}_n$ is built by combining the canonical vector basis of $\mathscr{E}_1$ along with the null anbit of $\mathscr{E}_1$. As an illustrative example, the canonical vector basis of $\mathscr{E}_2$ is found to be:

$$\mathcal{B}_2 = \big\{\big(\big|0\big\rangle, \big|\mathbf{0}\big\rangle\big), \big(\big|1\big\rangle, \big|\mathbf{0}\big\rangle\big), \big(\big|\mathbf{0}\big\rangle, \big|0\big\rangle\big), \big(\big|\mathbf{0}\big\rangle, \big|1\big\rangle\big)\big\}. \tag{32}$$

  Using the inner product given by Supplementary Equation 31, it follows that $\mathcal{B}_2$ is orthonormal.

- The components of a given ket $\big|\psi_1\big\rangle \times \big|\psi_2\big\rangle \times \ldots \times \big|\psi_n\big\rangle$ belonging to $\mathscr{E}_n$ with vector basis $\mathcal{B}_n$ can be calculated from the components (or anbit amplitudes) of the individuals kets $\big|\psi_{1,\ldots,n}\big\rangle$ belonging to $\mathscr{E}_1$ with vector basis $\mathcal{B}_1$ as follows:

$$\big[\big|\psi_1\big\rangle \times \big|\psi_2\big\rangle \times \ldots \times \big|\psi_n\big\rangle\big]_{\mathcal{B}_n} = \begin{pmatrix} \big[\big|\psi_1\big\rangle\big]_{\mathcal{B}_1} \\ \big[\big|\psi_2\big\rangle\big]_{\mathcal{B}_1} \\ \ldots \\ \big[\big|\psi_n\big\rangle\big]_{\mathcal{B}_1} \end{pmatrix}, \tag{33}$$

where $[\cdot]_{\mathcal{B}_n}$ and $[\cdot]_{\mathcal{B}_1}$are the component isomorphisms associated to the bases $\mathcal{B}_n$ and $\mathcal{B}_1$, respectively. Supplementary Equation 33 applies to any basis $\mathcal{B}_n$ and $\mathcal{B}_1$ (not necessarily being the canonical bases). For instance, consider two different anbits $\big|\psi\big\rangle = \psi_0\big|0\big\rangle + \psi_1\big|1\big\rangle$ and $\big|\varphi\big\rangle = \varphi_0\big|0\big\rangle + \varphi_1\big|1\big\rangle$. The Cartesian product is:

$$\begin{aligned} \big|\psi\big\rangle \times \big|\varphi\big\rangle \equiv \big(\big|\psi\big\rangle, \big|\varphi\big\rangle\big) &= \big(\sum_{k=0}^{1} \psi_k \big|k\big\rangle, \sum_{l=0}^{1} \varphi_l \big|l\big\rangle\big) \\ &= \sum_{k=0}^{1} \psi_k \big(\big|k\big\rangle, \big|\mathbf{0}\big\rangle\big) + \sum_{l=0}^{1} \varphi_l \big(\big|\mathbf{0}\big\rangle, \big|l\big\rangle\big). \end{aligned} \tag{34}$$

Therefore, the components of $\big|\psi\big\rangle \times \big|\varphi\big\rangle \in \mathscr{E}_2$ with vector basis $\mathcal{B}_2$ given by Supplementary Equation 32 can be calculated as:

$$\big[\big|\psi\big\rangle \times \big|\varphi\big\rangle\big]_{\mathcal{B}_2} = \begin{pmatrix} \psi_0 \\ \psi_1 \\ \varphi_0 \\ \varphi_1 \end{pmatrix} \equiv \begin{pmatrix} \big[\big|\psi\big\rangle\big]_{\mathcal{B}_1} \\ \big[\big|\varphi\big\rangle\big]_{\mathcal{B}_1} \end{pmatrix}. \tag{35}$$

Supplementary Equation 35 can be applied, e.g., to obtain the anbit amplitudes associated to the optical inputs shown in Fig. 5a of the paper.

- The Cartesian product is non-commutative: $\big|\psi\big\rangle \times \big|\varphi\big\rangle \neq \big|\varphi\big\rangle \times \big|\psi\big\rangle$ (when $\big|\psi\big\rangle \neq \big|\varphi\big\rangle$).

Final remarks. Consider two different anbits $\big|\psi\big\rangle = \psi_0\big|0\big\rangle + \psi_1\big|1\big\rangle$ and $\big|\varphi\big\rangle = \varphi_0\big|0\big\rangle + \varphi_1\big|1\big\rangle$. It is worthy to note that the tensor product mixes the information encoded by the anbit amplitudes (see Supplementary Equation 27). In contrast, the Cartesian product preserves this information (see Supplementary Equation 35) allowing us to independently transform the anbit amplitudes ψ_0, ψ_1, φ_0 and φ_1 in a multi-anbit gate (e.g. the fan-in gate, see Fig. 5a of the paper).

On the other hand, as commented in the main text, there are some specific multi-anbit gates (such as the fan-in and fan-out gates) that exhibit a linear (nonlinear) nature when using the Cartesian (tensor) product to construct them, see Supplementary Note 3 on p. 50 for more details.

Supplementary Note 2: combinational design

In this section, we include additional information about the fundamental pieces of combinational APC architectures: single-anbit linear gates and controlled gates.

2.1 General properties of single-anbit linear gates

A single-anbit linear gate is described by a linear operator (or endomorphism) $\widehat{\mathrm{F}} : \mathscr{E}_1 \to \mathscr{E}_1$ carrying out a transformation between two different anbits: the input anbit $\big|\psi\big\rangle = \psi_0\big|0\big\rangle + \psi_1\big|1\big\rangle$ and the output anbit $\big|\varphi\big\rangle = \varphi_0\big|0\big\rangle + \varphi_1\big|1\big\rangle$. In the next lines, we include supplementary notes about the general properties of $\widehat{\mathrm{F}}$ reported in the main text.

Matrix representation. Consider the canonical (orthonormal) vector basis $\mathcal{B}_1 = \{|0\rangle, |1\rangle\}$ of $\mathscr{E}_1$. Using the fundamentals of linear algebra [12], it is well-known that any *linear* mapping of $\mathscr{E}_1$ has associated the following (and unique) matrix representation:

$$F = M_{\mathcal{B}_1}^{\mathcal{B}_1}\big(\widehat{\mathrm{F}}\big) = \begin{pmatrix} \big[\widehat{\mathrm{F}}\big|0\big\rangle\big]_{\mathcal{B}_1} & \big[\widehat{\mathrm{F}}\big|1\big\rangle\big]_{\mathcal{B}_1} \end{pmatrix}, \tag{36}$$

where $[\cdot]_{\mathcal{B}_1}$ is the component isomorphism detailed on p. 31. Using Supplementary Equation 19 to calculate the components of $\widehat{\mathrm{F}}\,|0\rangle$ and $\widehat{\mathrm{F}}\,|1\rangle$ associated to the basis $\mathcal{B}_1$, we find that:

$$\big[\widehat{\mathrm{F}}\big|0\big\rangle\big]_{\mathcal{B}_1} = \begin{pmatrix} \big\langle 0\big|\widehat{\mathrm{F}}\big|0\big\rangle \\ \big\langle 1\big|\widehat{\mathrm{F}}\big|0\big\rangle \end{pmatrix}, \qquad \big[\widehat{\mathrm{F}}\big|1\big\rangle\big]_{\mathcal{B}_1} = \begin{pmatrix} \big\langle 0\big|\widehat{\mathrm{F}}\big|1\big\rangle \\ \big\langle 1\big|\widehat{\mathrm{F}}\big|1\big\rangle \end{pmatrix}. \tag{37}$$

Combining Supplementary Equations 36 and 37, we obtain equation 1 of the paper, reproduced here for clarity:

$$F = \begin{pmatrix} \big\langle 0\big|\widehat{\mathrm{F}}\big|0\big\rangle & \big\langle 0\big|\widehat{\mathrm{F}}\big|1\big\rangle \\ \big\langle 1\big|\widehat{\mathrm{F}}\big|0\big\rangle & \big\langle 1\big|\widehat{\mathrm{F}}\big|1\big\rangle \end{pmatrix}. \tag{38}$$

Moreover, applying the isomorphism $[\cdot]_{\mathcal{B}_1}$ to the input-output relation $\big|\varphi\big\rangle = \widehat{\mathrm{F}}\big|\psi\big\rangle$, we find that $\big[\big|\varphi\big\rangle\big]_{\mathcal{B}_1} = \big[\widehat{\mathrm{F}}\big|\psi\big\rangle\big]_{\mathcal{B}_1}$ where:

$$\big[\widehat{\mathrm{F}}\big|\psi\big\rangle\big]_{\mathcal{B}_1} = \begin{pmatrix} \big\langle 0\big|\widehat{\mathrm{F}}\big|\psi\big\rangle \\ \big\langle 1\big|\widehat{\mathrm{F}}\big|\psi\big\rangle \end{pmatrix} = \begin{pmatrix} \psi_0\big\langle 0\big|\widehat{\mathrm{F}}\big|0\big\rangle + \psi_1\big\langle 0\big|\widehat{\mathrm{F}}\big|1\big\rangle \\ \psi_0\big\langle 1\big|\widehat{\mathrm{F}}\big|0\big\rangle + \psi_1\big\langle 1\big|\widehat{\mathrm{F}}\big|1\big\rangle \end{pmatrix} = F \begin{pmatrix} \psi_0 \\ \psi_1 \end{pmatrix}. \tag{39}$$

Hence, $\big|\varphi\big\rangle = \widehat{\mathrm{F}}\big|\psi\big\rangle$ can equivalently be expressed via the matrix relation $\big[\big|\varphi\big\rangle\big]_{\mathcal{B}_1} = F\,\big[\big|\psi\big\rangle\big]_{\mathcal{B}_1}$, with $\big[\big|\varphi\big\rangle\big]_{\mathcal{B}_1} = \begin{pmatrix} \varphi_0 & \varphi_1 \end{pmatrix}^T$ and $\big[\big|\psi\big\rangle\big]_{\mathcal{B}_1} = \begin{pmatrix} \psi_0 & \psi_1 \end{pmatrix}^T$ (T denotes the transpose matrix). As commented above on p. 31, the component isomorphism allows us to describe the input-output relation of the anbit gates using matrices instead of linear operators.

Ket-bra representation. Keeping in mind that $M_{\mathcal{B}_1}^{\mathcal{B}_1}(\cdot)$ is an isomorphism [12], it should be noted that we can always recover the input from the output in Supplementary Equation 36. In this vein, the linear operator $\widehat{\mathrm{F}}$ can be calculated from the matrix F as follows:

$$\widehat{\mathrm{F}} = \sum_{n,m} F_{nm}\big|n\big\rangle\big\langle m\big|, \tag{40}$$

where $n, m \in \{0, 1\}$ and F_{nm} is the entry of F located at the $(n+1)$-th row and $(m+1)$-th column. Supplementary Equation 40 will be referred to as the *ket-bra representation* of the gate. This equation may be derived from Supplementary Equation 38, which can be recast of the form $F_{nm} = \langle n|\widehat{\mathrm{F}}|m\rangle$. Using this expression, we infer that $F_{nm}|n\rangle\langle m| = |n\rangle\langle n|\widehat{\mathrm{F}}|m\rangle\langle m|$. Applying the double summation $\sum_{n,m}$ at both sides and taking into account that the vector basis $\mathcal{B}_1$ satisfies the closure relation $\sum_n |n\rangle\langle n| = \widehat{1}$ (where $\widehat{1}$ is the identity operator) [10], then it directly follows Supplementary Equation 40.

Geometric representation. Using differential measurement, the input anbit $|\psi\rangle$ and the output anbit $|\varphi\rangle$ can be geometrically represented in the GBS as two different points (Fig. 3a). If the anbit transformation $\widehat{\mathrm{F}}$ is a U-gate, both points are connected by a trajectory describing a rotation of an angle α around an arbitrary unit vector $\hat{\mathbf{n}}$ (Fig. 3b). Such a trajectory preserves the radius in the GBS. However, if $\widehat{\mathrm{F}}$ is a G- or M-gate, there is no specific *kind* of trajectory connecting both points. This can be inferred from the singular value decomposition (SVD), which factorizes F as a function of two U-gates (U_1 and U_2) along with a 2×2 diagonal matrix D with non-negative real entries [9, 12, 13]: $F = U_2 D U_1$. The matrices U_1 and U_2 can be respectively described by two different rotations of angles α_1 and α_2 around two arbitrary unit vectors $\hat{\mathbf{n}}_1$ and $\hat{\mathbf{n}}_2$: $U_1 = e^{i\delta_1} R_{\hat{\mathbf{n}}_1}(\alpha_1)$ and $U_2 = e^{i\delta_2} R_{\hat{\mathbf{n}}_1}(\alpha_2)$ (the global phases δ_1 and δ_2 are not observable in the GBS). The diagonal matrix:

$$D = \begin{pmatrix} d_1 & 0 \\ 0 & d_2 \end{pmatrix}, \tag{41}$$

with $d_1 \geq d_2 \geq 0$, modifies $|\psi_0|$ and $|\psi_1|$ but, unfortunately, this parametric matrix cannot be associated to a specific class of trajectory. As an example, taking $d_2 = 0$, D projects $|\psi\rangle$ onto the positive z-axis of the GBS annihilating the anbit amplitude ψ_1. However, if $d_1 = d_2 = 1$, then D preserves the location of $|\psi\rangle$. Consequently, a G- or M-gate cannot be represented by a universal kind of trajectory. Each numerical case leads to a different trajectory in the GBS.

Lorentz reciprocity and forward-backward (FB) symmetry. By definition, an optical circuit is said to be reciprocal if and only if the Lorentz reciprocity theorem is satisfied in such a system [4, 14, 15]. By definition, an optical circuit is said to be symmetric (or, equivalently, it is said that preserves the FB symmetry) if and only if the system has the same transfer matrices associated to the forward and backward light propagation directions [4]. Specifically, the reciprocity and FB symmetry of an optical circuit may be theoretically analysed via the scattering and transfer matrices [4, 16].

In the following, let us discuss some remarks and logical implications between the F matrix of a single-anbit linear gate and the scattering and transfer matrices associated with an optical implementation of such a gate (for the sake of clarity, the reader should know the definition and basic properties of the scattering matrix (S), the forward and backward transfer matrices (T_{f}, T_{b}), and the reduced forward and backward transfer matrices ($\widetilde{T}_{\mathrm{f}}$, $\widetilde{T}_{\mathrm{b}}$) of an optical circuit, see Ch. 2 of ref. [4] for more details):

1. The Lorentz reciprocity and the FB symmetry are not properties of a gate. These are optical properties exclusively associated with a specific PIP implementation of a gate. Therefore, a gate could be implemented by different PIP circuits performing the same F matrix transformation, but exhibiting opposite optical properties.

2. An optical circuit preserving (breaking) the FB symmetry will induce the same (a different) anbit transformation in each propagation direction.

3. If an optical circuit of a gate preserves the FB symmetry ($T_{\mathrm{f}} = T_{\mathrm{b}}$), then the circuit is reciprocal ($S = S^T$). The converse is not true [4, 15].

4. The scattering matrix of a 2×2 *non-reflective* optical system is found to be [4]:

$$S = \left(\begin{array}{c|c} 0 & \widetilde{T}_{\mathrm{b}} \\ \hline \widetilde{T}_{\mathrm{f}} & 0 \end{array} \right) \in M_4(\mathbb{C}), \tag{42}$$

with $\widetilde{T}_{\mathrm{f}}, \widetilde{T}_{\mathrm{b}} \in M_2(\mathbb{C})$. Assuming that light reflection can usually be neglected in a PIP circuit [4, 17], we will consider that the *ideal* optical implementation of a gate is non-reflective. Hence, the scattering matrix of any optical implementation of a gate can ideally be assumed of the form:

$$S = \left(\begin{array}{c|c} 0 & \widetilde{T}_{\mathrm{b}} \\ \hline F & 0 \end{array} \right), \tag{43}$$

with $\widetilde{T}_{\mathrm{f}} \equiv F$. The form of the matrix $\widetilde{T}_{\mathrm{b}}$ directly depends on the specific optical architecture of the gate.

5. If the circuit of a gate is reciprocal, we know that $S = S^T$ [4]. Accordingly, $\widetilde{T}_{\mathrm{b}} \equiv F^T$ and the scattering matrix becomes:

$$S = \left(\begin{array}{c|c} 0 & F^T \\ \hline F & 0 \end{array} \right). \tag{44}$$

6. If the circuit of a gate is reciprocal and the gate satisfies the condition $F = F^T$, then the circuit preserves the FB symmetry ($\widetilde{T}_{\mathrm{f}} = \widetilde{T}_{\mathrm{b}} \equiv F$) and the scattering matrix is reduced to:

$$S = \left(\begin{array}{c|c} 0 & F \\ \hline F & 0 \end{array} \right). \tag{45}$$

Using the contrapositive statement, if the circuit of a gate breaks the FB symmetry ($\widetilde{T}_{\mathrm{f}} \neq \widetilde{T}_{\mathrm{b}}$), then it follows that the Lorentz reciprocity is broken *or* the gate is described by an asymmetric matrix ($F \neq F^T$). Both situations can take place simultaneously.

7. There is no logical implication between the concepts of circuital reciprocity and gate reversibility. As commented above, the reciprocity is a functional property of an optical implementation of a gate, while the reversibility is a mathematical property of the endomorphism defining the gate (discussed in the main text). In the same vein, there is no logical implication between the concepts of FB symmetry and gate reversibility.

2.2 Equivalent circuit architectures of single-anbit linear gates

U-gates. Equivalent optical implementations of a single-anbit U-gate can be proposed by selecting different rotation vectors in Euler's rotation theorem to factorize the 2×2 universal unitary matrix given by equation 2 of the paper [18]. For instance, instead of performing the factorization $U = e^{i\delta} R_{\hat{\mathbf{z}}}(\alpha_3) R_{\hat{\mathbf{x}}}(\alpha_2) R_{\hat{\mathbf{z}}}(\alpha_1)$, whose optical implementation is shown in Fig. 3b, we can select the unit vector $\hat{\mathbf{y}}$ in the second rotation:

$$U = e^{i\delta} R_{\hat{\mathbf{z}}}(\alpha_3) R_{\hat{\mathbf{y}}}(\alpha_2) R_{\hat{\mathbf{z}}}(\alpha_1) = e^{i\delta} \begin{pmatrix} \cos\frac{\alpha_2}{2} e^{-i\left(\frac{\alpha_3+\alpha_1}{2}\right)} & -\sin\frac{\alpha_2}{2} e^{-i\left(\frac{\alpha_3-\alpha_1}{2}\right)} \\ \sin\frac{\alpha_2}{2} e^{i\left(\frac{\alpha_3-\alpha_1}{2}\right)} & \cos\frac{\alpha_2}{2} e^{i\left(\frac{\alpha_3+\alpha_1}{2}\right)} \end{pmatrix}. \quad (46)$$

Supplementary Figure 5 shows the 2×2 optical system whose (reduced) forward transfer matrix $\widetilde{T}_{\mathrm{f}}$ is given by the above equation. In contrast to the architecture depicted in Fig. 3b, which requires a tunable symmetric directional coupler (DIC), this scheme is based on fixed couplers (50:50 beam splitters implemented via multi-mode interferometers (MMIs) or fixed symmetric DICs). Although the fabrication of a fixed coupler is simpler than that of a tunable coupler, the main drawback of this implementation of a U-gate is that it will approximately require the double footprint than that of the circuit of Fig. 3b because of a twice number of couplers must be integrated in this architecture.

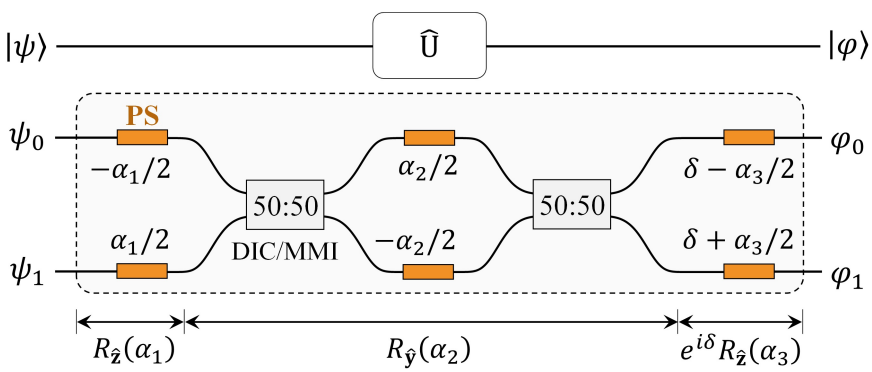

Supplementary Figure 5. Optical circuit of a U-gate implementing the universal unitary matrix of equation 2 of the paper via Euler's factorization given by Supplementary Equation 46.

On the other hand, it is natural to wonder about the possibility of building a more compact architecture of a U-gate (a 2×2 universal unitary system) than the scheme proposed in Fig. 3b by using a different factorization from Euler's rotation theorem. Remarkably, this question has been recently studied in ref. [18] within the context of unitary signal PIP processors. As reported in this reference, alternative 2×2 unitary factorization techniques can be found in the mathematical literature (e.g. the cosine-sine decomposition), but all of them lead to optical schemes of a 2×2 universal unitary system integrating a higher number of basic devices than in our proposal.

G-gates. An optical implementation of a single-anbit G-gate (different from but equivalent to the architecture depicted in Fig. 3c of the paper, based on the SVD) can be found by using *Mostow's decomposition* [19, 20]. This theorem establishes that a non-singular matrix G can be factorized as a function of a unitary matrix U, a real anti-symmetric matrix A ($A = -A^T$) and a real symmetric matrix B ($B = B^T$) following the expression:

$$G = U e^{iA} e^{B}. \tag{47}$$

The main handicap of Mostow's decomposition is that the exponential matrices cannot be directly implemented by employing mainstream PIP devices. In order to unveil the optical architecture of Supplementary Equation 47, it should be noted that $E_1 = e^{iA}$ and $E_2 = e^{B}$ are Hermitian (but non-unitary) matrices:

$$E_1^\dagger = \left(e^{iA}\right)^\dagger = e^{-iA^\dagger} = e^{-iA^T} = e^{iA} = E_1, \tag{48}$$

$$E_2^\dagger = \left(e^{B}\right)^\dagger = e^{B^\dagger} = e^{B^T} = e^{B} = E_2, \tag{49}$$

with $E_1^\dagger E_1 = E_1^2 = e^{i2A} \neq I$ and $E_2^\dagger E_2 = E_2^2 = e^{2B} \neq I$ ($\dagger$ denotes the conjugate transpose matrix). Therefore, E_1 and E_2 can be factorized by using the spectral decomposition as $E_1 = U_1 \Lambda_1 U_1^{-1}$ and $E_2 = U_2 \Lambda_2 U_2^{-1}$, where $U_{1,2}$ are matrices built from linearly independent eigenvectors of $E_{1,2}$ and $\Lambda_{1,2}$ are diagonal matrices whose entries are the corresponding (real) eigenvalues [9,12]. Moreover, since $\mathcal{B}_1 = \{|0\rangle, |1\rangle\}$ is an orthonormal basis, then it follows that $U_{1,2}$ are unitary matrices ($U_{1,2}^{-1} = U_{1,2}^\dagger$). Hence, Supplementary Equation 47 can be recast as:

$$G = \left(U U_1\right) \Lambda_1 \left(U_1^\dagger U_2\right) \Lambda_2 U_2^\dagger. \tag{50}$$

As seen, we have factorized G as a function of *three* unitary matrices UU_1, $U_1^\dagger U_2$, $U_2^\dagger$ and *two* diagonal matrices Λ_1, Λ_2. Interestingly, this factorization is implementable using basic PIP devices, see Supplementary Figure 6.

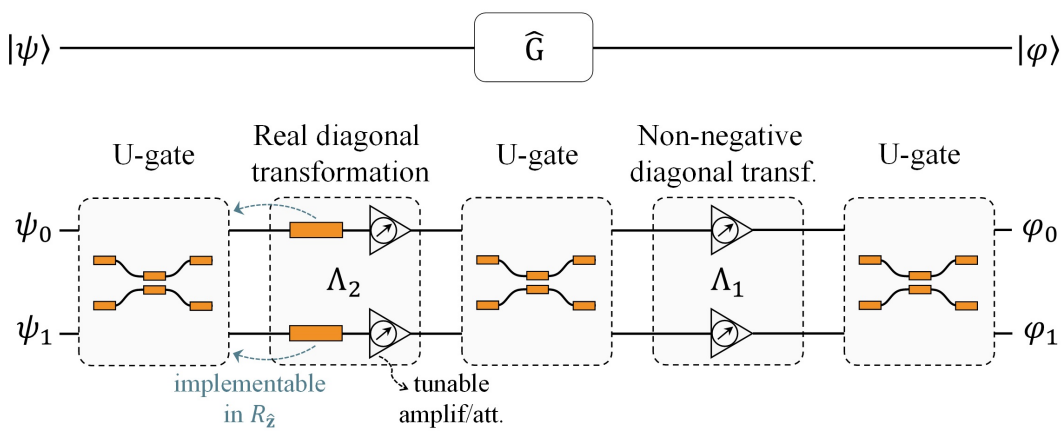

Supplementary Figure 6. Optical circuit of a G-gate based on Mostow's factorization.

An additional remark about this architecture should be discussed. While the first diagonal matrix of the circuit (Λ_2) may have positive and negative real entries (the negative sign is implemented by phase shifters (PSs) of π rad that can alternatively be implemented by the PSs of the final $R_{\hat{\mathbf{z}}}$ rotation in the first U-gate), the second diagonal matrix (Λ_1) has non-negative real entries.

For completeness, let us demonstrate the non-negative nature of the entries of Λ_1. Since A is real anti-symmetric, then it follows that A must be of the form:

$$A = \begin{pmatrix} 0 & a \\ -a & 0 \end{pmatrix}, \tag{51}$$

with $a \in \mathbb{R}$. The (non-degenerate) eigenvalues of A are found to be $\mu_{1,2} = \pm ia$. Here, since the geometric and algebraic multiplicity are the same, A is diagonalizable. This implies that A can be factorized by using the spectral decomposition. Hence, $A = U_1 D_1 U_1^{-1}$ with $D_1 = \mathrm{diag}\,(\mu_1, \mu_2)$ and:

$$e^{iA} = e^{iU_1 D_1 U_1^{-1}} = U_1 e^{iD_1} U_1^{-1} \equiv U_1 \Lambda_1 U_1^{-1}, \tag{52}$$

where the eigenvalues of e^{iA}, which are the entries of $\Lambda_1 = e^{iD_1}$, are found to be:

$$\lambda_{1,2} = e^{i\mu_{1,2}} = e^{\mp a} > 0. \tag{53}$$

M-gates. A single-anbit M-gate is described by a complex matrix belonging to $M_2\,(\mathbb{C})$:

$$M = \begin{pmatrix} m_{11} & m_{12} \\ m_{21} & m_{22} \end{pmatrix}. \tag{54}$$

Remarkably, $M_2\,(\mathbb{C})$ is the complex Lie algebra $\mathfrak{gl}\,(2, \mathbb{C})$ [7,21], with vector basis composed by the Pauli matrices $\{\sigma_k\}_{k=0}^{3}$:

$$\sigma_k := \begin{pmatrix} \delta_{k0} + \delta_{k3} & \delta_{k1} - i\delta_{k2} \\ \delta_{k1} + i\delta_{k2} & \delta_{k0} - \delta_{k3} \end{pmatrix}, \tag{55}$$

where δ_{kl} is the Kronecker delta ($\delta_{kl} = 1$ with $k = l$ and $\delta_{kl} = 0$ with $k \neq l$). This implies that any M-gate can be described as a linear combination of the Pauli matrices (see p. 427 of ref. [10]):

$$M = \sum_{k=0}^{3} \alpha_k \sigma_k, \tag{56}$$

where $\alpha_0 = (m_{11}+m_{22})/2$, $\alpha_1 = (m_{12}+m_{21})/2$, $\alpha_2 = i(m_{12}-m_{21})/2$ and $\alpha_3 = (m_{11}-m_{22})/2$. Consequently, an optical circuit implementing Supplementary Equation 56 will give rise to an equivalent scheme to the architecture of an M-gate depicted in Fig. 3c of the paper, based on the SVD.

To this end, let us express the Pauli matrices as a function of the rotation matrices of the Bloch sphere (which can be implemented via PIP technology because are unitary matrices [18]):

$$\sigma_0 = I, \quad \sigma_1 = iR_{\hat{\mathbf{x}}}\,(\pi)\,, \quad \sigma_2 = iR_{\hat{\mathbf{y}}}\,(\pi)\,, \quad \sigma_3 = iR_{\hat{\mathbf{z}}}\,(\pi)\,. \tag{57}$$

In this fashion, Supplementary Equation 56 becomes:

$$M = \alpha_0 I + i\alpha_1 R_{\hat{\mathbf{x}}}\,(\pi) + i\alpha_2 R_{\hat{\mathbf{y}}}\,(\pi) + i\alpha_3 R_{\hat{\mathbf{z}}}\,(\pi)\,. \tag{58}$$

The optical implementation of the above equation using PIP technology only requires (see Supplementary Figure 7): (i) the minimal circuit architecture (MCA) of the U-gates to generate the rotation matrices (see Fig. 3b of the paper), (ii) PSs and tunable optical attenuators and amplifiers to generate the terms α_0 and $i\alpha_{1,2,3}$, and (iii) fan-in and fan-out gates to obtain the linear combination of all terms (see Supplementary Note 3 for more details about these multi-anbit gates). As seen, this structure is more complex than the architecture of an M-gate based on the SVD (Fig. 3c) given that it involves a higher number of basic devices, requires ancilla anbits and generates gargabe anbits.

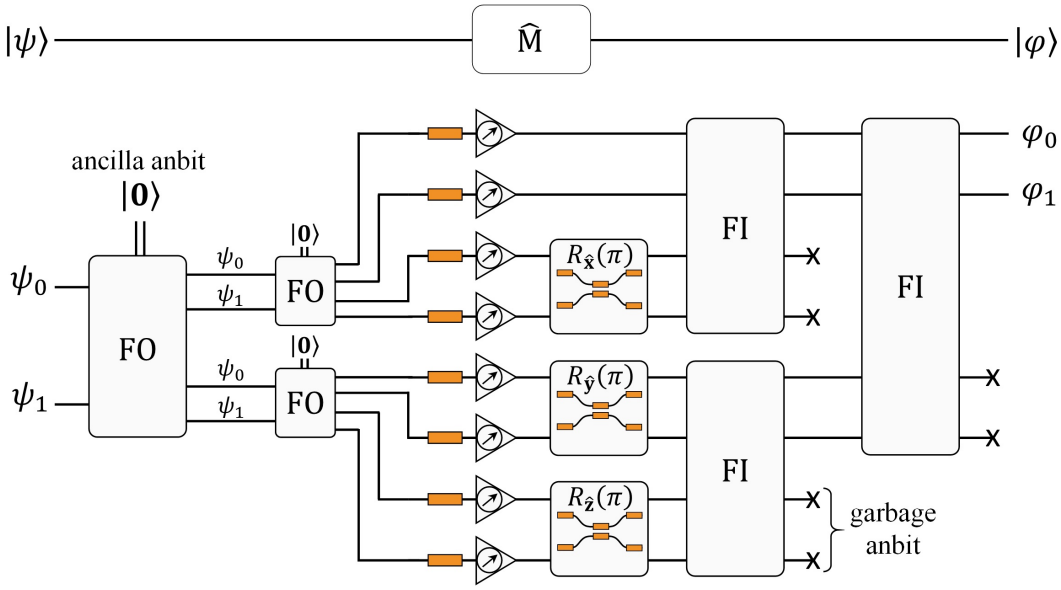

Supplementary Figure 7. Optical circuit of an M-gate based on the factorization described by Supplementary Equation 58. The gates fan-in (FI) and fan-out (FO) are described in Fig. 5a of the main text and in Supplementary Note 3, see p. 49.

2.3 Controlled gates

In any computation theory, a controlled gate is an operation of *multiple* units of information given that the goal is to perform a transformation on the target units of information (e.g. the target anbits, $|t\rangle$) depending on the value of the control units of information (e.g. the control anbits, $|c\rangle$).

In APC, the definition of a multi-anbit gate (in this case, a controlled gate) will depend on the kind of operation employed to describe the multiple input and output anbits. As commented in the main text, using the *tensor product* to describe $|t\rangle$ and $|c\rangle$, the mathematical framework of a controlled anbit gate can be directly extrapolated from a controlled quantum gate (but differing in some fundamental aspects).

Here, we develop in detail the theory of such a kind of gates within the context of APC highlighting the main differences with QC.

2.3.1 Single control anbit

Definition and formalism. Let us start by considering a single-anbit linear gate (a U-, G-, or M-gate) performing a transformation $\widehat{\mathrm{F}}$ on an input anbit $|t\rangle$: the target anbit. The controlled version of the $\widehat{\mathrm{F}}$-gate (termed as controlled-$\widehat{\mathrm{F}}$ gate) with a single control anbit $|c\rangle \in \{|0\rangle, |1\rangle\}$ is a linear operator $\widehat{\mathrm{F}}_{\mathrm{C}}$ defined via the tensor product as:

$$\widehat{\mathrm{F}}_{\mathrm{C}} := \widehat{1} \otimes \widehat{\mathrm{F}}^{c}, \tag{59}$$

which transforms the input $|c, t\rangle$ into the output:

$$\widehat{\mathrm{F}}_{\mathrm{C}}|c, t\rangle = \left(\widehat{1} \otimes \widehat{\mathrm{F}}^{c}\right)|c, t\rangle = |c\rangle \otimes \widehat{\mathrm{F}}^{c}|t\rangle. \tag{60}$$

The transformation $\widehat{\mathrm{F}}$ is applied to $|t\rangle$ when $|c\rangle = |1\rangle$ or, otherwise, $|t\rangle$ remains invariant at the output. Figure 4a of the paper shows the symbolic representation of $\widehat{\mathrm{F}}_{\mathrm{C}}$, the same as that of a controlled quantum gate for the sake of simplicity. However, in contrast to QC, $\widehat{\mathrm{F}}_{\mathrm{C}}$ will be a non-unitary operation when $\widehat{\mathrm{F}}\widehat{\mathrm{F}}^{\dagger} \neq \widehat{1}$, that is, when $\widehat{\mathrm{F}}$ is a G- or M-gate (see below the algebraic structure in properties).

In any case, the mathematical formalism of a controlled anbit gate is the same as that of a controlled quantum gate. Since we work with two input and output anbits, the underlying Hilbert space is $\mathscr{E}_2 = \mathscr{E}_1 \otimes \mathscr{E}_1$ and the canonical (orthonormal) basis is given by Supplementary Equation 24, reproduced here for clarity:

$$\mathcal{B}_2 = \left\{ |k\rangle \otimes |l\rangle \right\}_{k,l\in\{0,1\}} = \left\{ |0,0\rangle, |0,1\rangle, |1,0\rangle, |1,1\rangle \right\}. \tag{61}$$

Hence, the matrix representation of $\widehat{\mathrm{F}}_{\mathrm{C}}$ associated to $\mathcal{B}_2$ is:

$$F_{\mathrm{C}} = M_{\mathcal{B}_2}^{\mathcal{B}_2}(\widehat{\mathrm{F}}_{\mathrm{C}}) = \left(\begin{array}{ccc} \cdots & \left[\widehat{\mathrm{F}}_{\mathrm{C}}|k,l\rangle\right]_{\mathcal{B}_2} & \cdots \end{array} \right) = \left(\begin{array}{c|c} I & 0 \\ \hline 0 & F \end{array} \right), \tag{62}$$

where $F_{\mathrm{C}} \in M_4(\mathbb{C})$, I is the 2×2 identity matrix and $F \in M_2(\mathbb{C})$ is the matrix representation of $\widehat{\mathrm{F}}$ associated to the canonical basis $\mathcal{B}_1 = \{|0\rangle, |1\rangle\}$ of $\mathscr{E}_1$, see Supplementary Equation 36. Along this line, the ket-bra representation of $\widehat{\mathrm{F}}_{\mathrm{C}}$ can be calculated from the entries of F_{C} as follows (see previously p. 36, where the ket-bra representation of a gate is introduced):

$$\begin{aligned} \widehat{\mathrm{F}}_{\mathrm{C}} &= |0,0\rangle\langle 0,0| + |0,1\rangle\langle 0,1| \\ &\quad + F_{00}|1,0\rangle\langle 1,0| + F_{01}|1,0\rangle\langle 1,1| + F_{10}|1,1\rangle\langle 1,0| + F_{11}|1,1\rangle\langle 1,1| \\ &= |0\rangle\langle 0| \otimes \left(|0\rangle\langle 0| + |1\rangle\langle 1|\right) \\ &\quad + |1\rangle\langle 1| \otimes \left(F_{00}|0\rangle\langle 0| + F_{01}|0\rangle\langle 1| + F_{10}|1\rangle\langle 0| + F_{11}|1\rangle\langle 1|\right) \\ &= |0\rangle\langle 0| \otimes \widehat{1} + |1\rangle\langle 1| \otimes \widehat{\mathrm{F}}. \end{aligned} \tag{63}$$

In contrast to Supplementary Equation 59, the ket-bra representation of $\widehat{\mathrm{F}}_{\mathrm{C}}$ can be applied to an arbitrary control anbit $|c\rangle = c_0|0\rangle + c_1|1\rangle \notin \left\{|0\rangle, |1\rangle\right\}$. In such a scenario, using Supplementary Equation 63, $\widehat{\mathrm{F}}_{\mathrm{C}}$ generates the output:

$$\widehat{\mathrm{F}}_{\mathrm{C}}|c,t\rangle = \langle 0|c\rangle|0,t\rangle + \langle 1|c\rangle|1\rangle \otimes \widehat{\mathrm{F}}|t\rangle = c_0|0,t\rangle + c_1|1\rangle \otimes \widehat{\mathrm{F}}|t\rangle. \tag{64}$$

Note that this input-output relation is more general than Supplementary Equation 60.

On the other hand, although it is out of the scope of this work, it is worthy to note that a controlled anbit gate can alternatively be defined by using the *Cartesian product*. This possibility cannot be found in QC. Nevertheless, using the Cartesian product we cannot extrapolate the mathematical framework of the controlled quantum gates to the controlled anbit gates. In any case, for completeness, let us discuss this possibility. Here, the basic idea is to define a controlled anbit gate as follows: the transformation $\widehat{\mathrm{F}}$ is applied to $|t\rangle$ when $|c\rangle$ is the null anbit $|\mathbf{0}\rangle$ or, otherwise, $|t\rangle$ remains invariant at the output. In this way, using this definition and the canonical vector basis of $\mathscr{E}_2 = \mathscr{E}_1 \times \mathscr{E}_1$, given by Supplementary Equation 32, it is straightforward to demonstrate that we obtain the same matrix representation of $\widehat{\mathrm{F}}_{\mathrm{C}}$ as in Supplementary Equation 62.

Properties. The controlled anbit gate illustrated in Fig. 4a of the main text exhibits the following properties:

1. *Endomorphism.* The linear operator $\widehat{\mathrm{F}}_{\mathrm{C}}$ is an endomorphism of the Hilbert space $\mathscr{E}_2 = \mathscr{E}_1 \otimes \mathscr{E}_1$.

2. *EDF transformation.* If $\left|c\right\rangle = \left|1\right\rangle$, then $\widehat{\mathrm{F}}_{\mathrm{C}}$ modifies the EDFs of $\left|t\right\rangle$ according to $\widehat{\mathrm{F}}$ (a U-, G-, or M-gate). For instance, assuming a target anbit with 3 EDFs, if $\left|c\right\rangle = \left|1\right\rangle$ and $\widehat{\mathrm{F}}$ is a U-gate, then $\widehat{\mathrm{F}}_{\mathrm{C}}$ transforms these EDFs by rotating $\left|t\right\rangle$ in the GBS.

3. *Reversibility.* From Supplementary Equation 62, it is direct to verify that:

$$\det\left(F_{\mathrm{C}}\right) = \det\left(F\right). \tag{65}$$

   Consequently, the controlled-$\widehat{\mathrm{F}}$ gate is reversible if and only if the $\widehat{\mathrm{F}}$-gate is reversible ($\det\left(F\right) \neq 0$). In such a case, $\widehat{\mathrm{F}}_{\mathrm{C}}$ is an automorphism. The inverse controlled gate (inverse automorphism) is described by the linear operator $\widehat{\mathrm{F}}_{\mathrm{C}}^{-1}$, whose matrix representation associated to $\mathcal{B}_2$ is:

$$F_{\mathrm{C}}^{-1} = M_{\mathcal{B}_2}^{\mathcal{B}_2}\left(\widehat{\mathrm{F}}_{\mathrm{C}}^{-1}\right) = \left[M_{\mathcal{B}_2}^{\mathcal{B}_2}\left(\widehat{\mathrm{F}}_{\mathrm{C}}\right)\right]^{-1} = \left(\begin{array}{c|c} I & 0 \\ \hline 0 & F^{-1} \end{array}\right). \tag{66}$$

   In addition, if the controlled-$\widehat{\mathrm{F}}$ gate is reversible, then $\widehat{\mathrm{F}}_{\mathrm{C}}\left(\mathcal{B}_2\right) = \left\{\widehat{\mathrm{F}}_{\mathrm{C}}\left|k,l\right\rangle\right\}_{k,l\in\{0,1\}}$ is a vector basis of $\mathscr{E}_2$. Using the contrapositive statement, if $\widehat{\mathrm{F}}_{\mathrm{C}}\left(\mathcal{B}_2\right)$ is not a vector basis of $\mathscr{E}_2$, then it follows that the controlled-$\widehat{\mathrm{F}}$ gate is irreversible.

4. *Matrix factorizations.* Any matrix factorization of F can be directly applied to F_{C}:

$$F_{\mathrm{C}} = \left(\begin{array}{c|c} I & 0 \\ \hline 0 & F \end{array}\right) = \left(\begin{array}{c|c} I & 0 \\ \hline 0 & \prod_k F_k \end{array}\right) = \prod_k \left(\begin{array}{c|c} I & 0 \\ \hline 0 & F_k \end{array}\right). \tag{67}$$

   In other words, if the $\widehat{\mathrm{F}}$-gate is equivalent to a set of $\widehat{\mathrm{F}}_k$-gates connected in series, then the controlled-$\widehat{\mathrm{F}}$ gate is equivalent to a set of controlled-$\widehat{\mathrm{F}}_k$ gates connected in series.

5. *Algebraic structure.* The matrix F_{C} inherits the algebraic structure of F: if $F \in \mathrm{U}\left(2\right)$, then $F_{\mathrm{C}} \in \mathrm{U}\left(4\right)$; if $F \in \mathrm{GL}\left(2,\mathbb{C}\right)$, then $F_{\mathrm{C}} \in \mathrm{GL}\left(4,\mathbb{C}\right)$; if $F \in \mathfrak{gl}\left(2,\mathbb{C}\right)$, then $F_{\mathrm{C}} \in \mathfrak{gl}\left(4,\mathbb{C}\right)$ (the definition of the Lie groups $\mathrm{U}\left(n\right)$ and $\mathrm{GL}\left(n,\mathbb{C}\right)$, and the Lie algebra $\mathfrak{gl}\left(n,\mathbb{C}\right)$ is detailed in ref. [21]). Note that in QC, F_{C} can only belong to $\mathrm{U}\left(4\right)$.

6. *Universality.* A universal matrix of a controlled-$\widehat{\mathrm{F}}$ gate must be able to describe all the possible 4×4 matrix transformations of the form given by Supplementary Equation 62. Therefore, F_{C} is a universal matrix of a controlled-$\widehat{\mathrm{F}}$ gate if and only if F is a universal matrix of a U-, G-, or M-gate.

7. *PIP implementation.* In QC, the theoretical strategies to design controlled gates are focused on factorizing F_{C} as a function of single-qubit gates and the controlled-NOT (CNOT) gate [22]. Despite the fact that these schemes could be extrapolated to APC, the implementation of a controlled anbit gate using PIP technology does not require these intricate design strategies. Remarkably, *APC has its own design strategies and architectures*, as demonstrated in Figs. 4b, 4c and 4d of the paper.

2.3.2 Multiple control anbits

Definition and formalism. Consider a single-anbit $\widehat{\mathrm{F}}$-gate (a U-, G-, or M-gate) operating on a target anbit $\left|t\right\rangle$. The controlled-$\widehat{\mathrm{F}}$ gate with n control anbits $\left|c_{1,2,\ldots,n}\right\rangle \in \left\{\left|0\right\rangle, \left|1\right\rangle\right\}$ is a linear operator $\widehat{\mathrm{F}}_{\mathrm{C}}$ defined as:

$$\widehat{\mathrm{F}}_{\mathrm{C}} := \underbrace{\widehat{1} \otimes \ldots \otimes \widehat{1}}_{n-1 \text{ times}} \otimes \widehat{\mathrm{F}}^{c_1 c_2 \ldots c_n} = \widehat{1}^{\otimes(n-1)} \otimes \widehat{\mathrm{F}}^{c_1 c_2 \ldots c_n}, \tag{68}$$

which transforms the input $\left|c_1, c_2, \ldots, c_n\right\rangle \otimes \left|t\right\rangle$ into the output:

$$\widehat{\mathrm{F}}_{\mathrm{C}}\left(\left|c_1, c_2, \ldots, c_n\right\rangle \otimes \left|t\right\rangle\right) = \left|c_1, c_2, \ldots, c_n\right\rangle \otimes \widehat{\mathrm{F}}^{c_1 c_2 \ldots c_n}\left|t\right\rangle. \tag{69}$$

The transformation $\widehat{\mathrm{F}}$ is applied to $\left|t\right\rangle$ when $\left|c_1, c_2, \ldots, c_n\right\rangle = \left|1, 1, \ldots, 1\right\rangle$ or, otherwise, $\left|t\right\rangle$ remains invariant at the output. Supplementary Figure 8 depicts the symbolic representation of $\widehat{\mathrm{F}}_{\mathrm{C}}$, the same as that of a multi-controlled quantum gate for simplicity. Nevertheless, in contrast to QC, note that $\widehat{\mathrm{F}}_{\mathrm{C}}$ will be a non-unitary operation when $\widehat{\mathrm{F}}\widehat{\mathrm{F}}^{\dagger} \neq \widehat{1}$, that is, when $\widehat{\mathrm{F}}$ is a G- or M-gate.

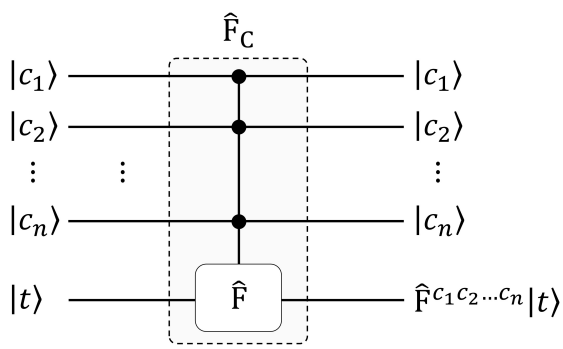

Supplementary Figure 8. Functional scheme and symbolic representation of a controlled-$\widehat{\mathrm{F}}$ gate with n control anbits $\left|c_{1,2,\ldots,n}\right\rangle \in \left\{\left|0\right\rangle, \left|1\right\rangle\right\}$ and a single target anbit $\left|t\right\rangle$. Inspired in a multi-controlled quantum gate, the single-anbit operation $\widehat{\mathrm{F}}$ (a U-, G-, or M-gate) is applied to $\left|t\right\rangle$ when $\left|c_1, c_2, \ldots, c_n\right\rangle = \left|1, 1, \ldots, 1\right\rangle$ or, otherwise, $\left|t\right\rangle$ remains invariant at the output.

Now, the Hilbert space is $\mathscr{E}_{n+1} = \mathscr{E}_1^{\otimes(n)}$ and the canonical (orthonormal) vector basis is found to be:

$$\mathcal{B}_{n+1} = \left\{\left|k_1\right\rangle \otimes \left|k_2\right\rangle \otimes \ldots \otimes \left|k_{n+1}\right\rangle\right\}_{k_{1,\ldots,n+1} \in \{0,1\}}. \tag{70}$$

Hence, the matrix representation of $\widehat{\mathrm{F}}_{\mathrm{C}}$ associated to $\mathcal{B}_{n+1}$ is:

$$F_{\mathrm{C}} = M_{\mathcal{B}_{n+1}}^{\mathcal{B}_{n+1}}\left(\widehat{\mathrm{F}}_{\mathrm{C}}\right) = \left(\begin{array}{c|c} I & 0 \\ \hline 0 & F \end{array}\right), \tag{71}$$

where $F_{\mathrm{C}} \in M_{2^{n+1}}(\mathbb{C})$, I is the identity matrix of size $\left(2^{n+1}-2\right) \times \left(2^{n+1}-2\right)$ and $F \in M_2(\mathbb{C})$ is the matrix representation of $\widehat{\mathrm{F}}$ associated to the canonical basis $\mathcal{B}_1 = \{\left|0\right\rangle, \left|1\right\rangle\}$ of $\mathscr{E}_1$ (see Supplementary Equation 38). Moreover, the ket-bra representation of $\widehat{\mathrm{F}}_{\mathrm{C}}$ can be calculated from the entries of F_{C} in the same way as in a controlled gate with a single control anbit (see p. 43).

Properties. A multi-controlled anbit gate has the same properties as a controlled gate with a single control anbit, see p. 44. Nonetheless, now we work with endomorphisms $\widehat{\mathrm{F}}_{\mathrm{C}}$ of the Hilbert space $\mathscr{E}_{n+1} = \mathscr{E}_1^{\otimes(n)}$ and matrices F_{C} belonging to $\mathrm{U}\big(2^{n+1}\big)$, $\mathrm{GL}\big(2^{n+1},\mathbb{C}\big)$ or $\mathfrak{gl}\big(2^{n+1},\mathbb{C}\big)$ when F is a U-, G-, or M-gate, respectively.

In addition, it should be noted that the PIP implementation of a multi-controlled gate can be designed as in a single-controlled gate: using an electro-optic or an all-optical architecture. In the former case, the amplitudes of the control anbits $\big|c_k\big\rangle = c_{k,0}\big|0\big\rangle + c_{k,1}\big|1\big\rangle$ $(k \in \{1,\ldots,n\})$ are encoded by the electrical control signals of the PIP platform and the amplitudes of the target anbit $\big|t\big\rangle = t_0\big|0\big\rangle + t_1\big|1\big\rangle$ are encoded by a 2D optical wave (Supplementary Figure 9a). In the latter case, the amplitudes of $\big|c_1, c_2, \ldots, c_n\big\rangle \otimes \big|t\big\rangle$ associated to the vector basis $\mathcal{B}_{n+1}$ are encoded by optical waves (Supplementary Figure 9b). Here, the reduced forward transfer matrix of the system must be F_{C}. Therefore, we require to use $2^{n+1} - 2$ waveguides to implement the submatrix I of F_{C} in combination with the MCA of the submatrix F (given by Fig. 3b if F is a U-gate or Fig. 3c if F is a G- or M-gate).

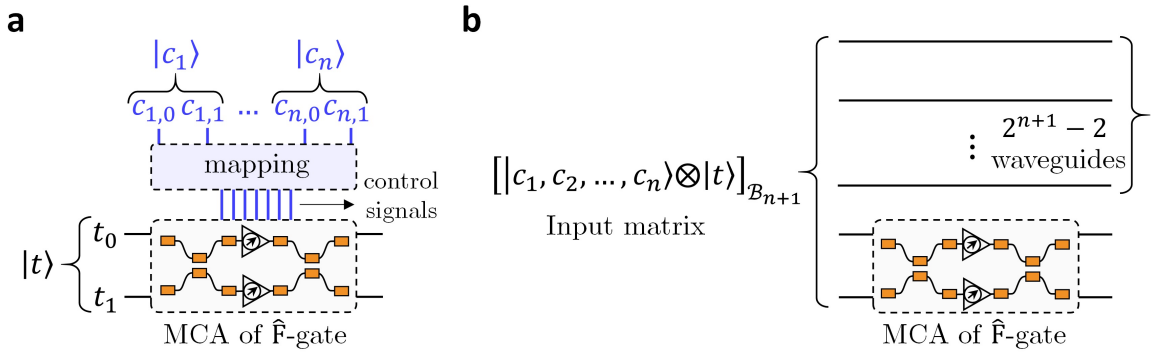

Supplementary Figure 9. PIP implementation of a multi-controlled gate with n control anbits $\big|c_1\big\rangle, \ldots, \big|c_n\big\rangle$ and a single target anbit $\big|t\big\rangle$, whose functionality is shown in Supplementary Figure 8. **a** Electro-optic design. The PIP circuit is the MCA of the single-anbit operation $\widehat{\mathrm{F}}$ associated to the target anbit (here we depict the MCA of an M-gate to cover the general case). The basic PIP devices are controlled by electrical signals (blue lines) mapped with the amplitudes of the control anbits $\big|c_k\big\rangle = c_{k,0}\big|0\big\rangle + c_{k,1}\big|1\big\rangle$ $(k \in \{1,\ldots,n\})$, e.g., via software [23]. The optical inputs encode the amplitudes of $\big|t\big\rangle = t_0\big|0\big\rangle + t_1\big|1\big\rangle$ (black lines). **b** All-optical design. The optical inputs encode the amplitudes of the tensor product $\big|c_1, c_2, \ldots, c_n\big\rangle \otimes \big|t\big\rangle$, given by the matrix $\big[\big|c_1, c_2, \ldots, c_n\big\rangle \otimes \big|t\big\rangle\big]_{\mathcal{B}_{n+1}}$, where $[\cdot]_{\mathcal{B}_{n+1}}$ is the component isomorphism (see p. 31). The whole structure implements the matrix F_{C} given by Supplementary Equation 71.

As seen, the all-optical architecture entails a higher footprint than that of the electro-optic design, which only requires to establish a mapping between the control anbits and the electrical control signals of the PIP circuit (e.g. via software [23]). In this fashion, the same MCAs as those of the U-, G-, and M-gates (depicted in Fig. 3 of the paper) may be employed to perform multi-controlled operations of each kind of gate via an electro-optic design.

A basic example. So far, we have developed the theory of the multi-controlled gates in abstract terms. To clarify these concepts, let us include an illustrative example: the Toffoli (or CCNOT) gate, a multi-controlled operation with 2 control anbits and 1 target anbit. Specifically, the matrix of this gate is found to be:

$$U_{\text{CCN}} := \left(\begin{array}{c|c} I_{6\times 6} & 0 \\ \hline 0 & \sigma_x \end{array}\right) = \begin{pmatrix} 1 & 0 & 0 & 0 & 0 & 0 & 0 & 0 \\ 0 & 1 & 0 & 0 & 0 & 0 & 0 & 0 \\ 0 & 0 & 1 & 0 & 0 & 0 & 0 & 0 \\ 0 & 0 & 0 & 1 & 0 & 0 & 0 & 0 \\ 0 & 0 & 0 & 0 & 1 & 0 & 0 & 0 \\ 0 & 0 & 0 & 0 & 0 & 1 & 0 & 0 \\ 0 & 0 & 0 & 0 & 0 & 0 & 0 & 1 \\ 0 & 0 & 0 & 0 & 0 & 0 & 1 & 0 \end{pmatrix}, \tag{72}$$

where:

$$\sigma_x := \begin{pmatrix} 0 & 1 \\ 1 & 0 \end{pmatrix}, \tag{73}$$

is a Pauli matrix, a single-anbit U-gate termed as the NOT gate within the literature of QC [22]. Therefore, the matrix F of Supplementary Equation 71 is the Pauli matrix σ_x in this example. Furthermore, the ket-bra representation can be calculated from U_{CCN} as:

$$\begin{aligned} \widehat{\mathrm{U}}_{\text{CCN}} &= |0,0,0\rangle\langle 0,0,0| + |0,0,1\rangle\langle 0,0,1| + |0,1,0\rangle\langle 0,1,0| + |0,1,1\rangle\langle 0,1,1| \\ &+ |1,0,0\rangle\langle 1,0,0| + |1,0,1\rangle\langle 1,0,1| + |1,1,0\rangle\langle 1,1,1| + |1,1,1\rangle\langle 1,1,0| \\ &= |0\rangle\langle 0| \otimes \widehat{1} \otimes \widehat{1} + |1\rangle\langle 1| \otimes |0\rangle\langle 0| \otimes \widehat{1} + |1\rangle\langle 1| \otimes |1\rangle\langle 1| \otimes \widehat{\sigma}_x, \end{aligned} \tag{74}$$

with $\widehat{\sigma}_x = |0\rangle\langle 1| + |1\rangle\langle 0|$.

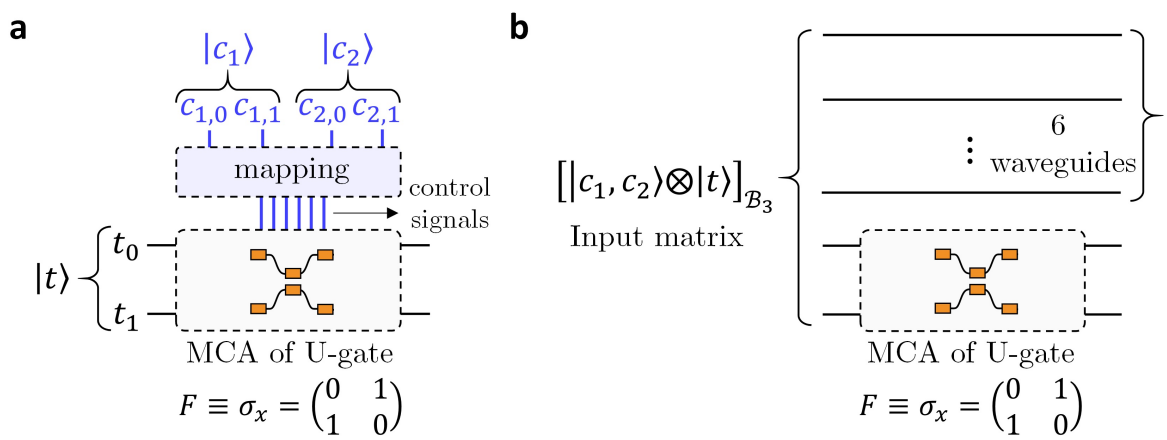

Supplementary Figure 10. PIP implementation of the Toffoli (or CCNOT) gate, a multi-controlled anbit gate with 2 control anbits $|c_1\rangle$, $|c_2\rangle$ and 1 target anbit $|t\rangle$. **a** Electro-optic design. The PIP circuit is the MCA of a U-gate since $F \equiv \sigma_x$ is a 2×2 unitary matrix. **b** All-optical design implementing the matrix U_{CCN} given by Supplementary Equation 72.

The PIP implementation of the CCNOT gate can be carried out via an electro-optic or an all-optical design, see Supplementary Figure 10. Both architectures are the same as those of Supplementary Figure 9, but restricted to the case of 2 control anbits and using the MCA of a U-gate to induce the σ_x-matrix transformation on the amplitudes of $|t\rangle$. It is worth mentioning that Supplementary Figure 10a is the same circuit as that of Fig. 4d of the paper, but including an additional control anbit $|c_2\rangle$ in the electrical domain. This result

demonstrates the possibility of *scaling* the controlled gates to the case of multiple control anbits without requiring extra PIP devices in the optical circuits, a fundamental feature of APC that cannot be found in optical QC.

Finally, in Supplementary Note 5, we report how to use the Toffoli gate to implement the Boolean logic of digital computation in APC, see p. 65.

Supplementary Note 3: sequential design

Here, we include additional information about the fundamental pieces required to construct sequential APC architectures: the fan-in (FI) and fan-out (FO) gates. Furthermore, the two sequential systems depicted in Fig. 5b and 5d of the main text are discussed in more detail. Both examples will allow us to establish the theoretical strategies to analyse and design sequential architectures in APC.

3.1 Fan-in and fan-out gates

In this subsection, we first study the definition and mathematical properties of the FI and FO gates and, subsequently, we propose a common PIP implementation for both multi-anbit operations.

3.1.1 Fan-in: anbit addition

Definition and formalism. Consider the single-anbit Hilbert space $\mathscr{E}_1$. Let us define the FI operation (anbit addition) as the linear mapping $\widehat{\mathrm{G}}_{\mathrm{FI}}$ of $\mathscr{E}_2 := \mathscr{E}_1 \times \mathscr{E}_1$ which transforms the input $\big(|\psi\rangle, |\varphi\rangle\big)$ into the output:

$$\widehat{\mathrm{G}}_{\mathrm{FI}}\left(|\psi\rangle, |\varphi\rangle; n, m\right) := \big(n\big(|\psi\rangle + |\varphi\rangle\big), m\big(|\psi\rangle - |\varphi\rangle\big)\big), \tag{75}$$

where $n, m \in \mathbb{C} - \{0\}$ are parameters of the operation ($n = m = 1$ will be assumed as the *default values* and, in such a case, the parameters can be omitted on the left-hand side of the above equation). Supplementary Figure 11 shows the functional scheme and symbolic representation of the FI gate. In most sequential APC architectures, the second output anbit $m\big(|\psi\rangle - |\varphi\rangle\big)$ will be considered as a *garbage* anbit and only the first output anbit $n\big(|\psi\rangle + |\varphi\rangle\big)$ will be utilised to build a feedback loop. Nevertheless, the aim of defining two output anbits is that, in this way, we will be able to describe the FI gate with a square matrix, see below.

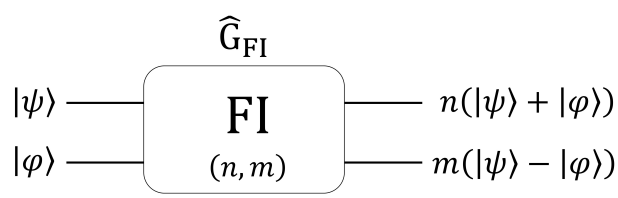

Supplementary Figure 11. Functional scheme and symbolic representation of the fan-in (FI) gate. The values of the (complex) parameters n, m should be indicate, except for the case $n = m = 1$, which are defined as the default values.

Taking into account that the FI gate is an operation of two input and output anbits, the underlying Hilbert space is $\mathscr{E}_2$ and the canonical (orthonormal) basis is given by Supplementary Equation 32, reproduced here for clarity:

$$\mathcal{B}_2 = \left\{ \big(|0\rangle, |\mathbf{0}\rangle\big), \big(|1\rangle, |\mathbf{0}\rangle\big), \big(|\mathbf{0}\rangle, |0\rangle\big), \big(|\mathbf{0}\rangle, |1\rangle\big) \right\}. \tag{76}$$

The matrix representation of $\widehat{\mathrm{G}}_{\mathrm{FI}}$ associated to $\mathcal{B}_2$ is:

$$\begin{aligned}
G_{\mathrm{FI}} &= M_{\mathcal{B}_2}^{\mathcal{B}_2}\big(\widehat{\mathrm{G}}_{\mathrm{FI}}\big) \\
&= \Big(\ \big[\widehat{\mathrm{G}}_{\mathrm{FI}}\left(|0\rangle, |\mathbf{0}\rangle\right)\big]_{\mathcal{B}_2} \quad \big[\widehat{\mathrm{G}}_{\mathrm{FI}}\left(|1\rangle, |\mathbf{0}\rangle\right)\big]_{\mathcal{B}_2} \quad \big[\widehat{\mathrm{G}}_{\mathrm{FI}}\left(|\mathbf{0}\rangle, |0\rangle\right)\big]_{\mathcal{B}_2} \quad \big[\widehat{\mathrm{G}}_{\mathrm{FI}}\left(|\mathbf{0}\rangle, |1\rangle\right)\big]_{\mathcal{B}_2} \ \Big) \\
&= \Big(\ \big[\big(n|0\rangle, m|0\rangle\big)\big]_{\mathcal{B}_2} \quad \big[\big(n|1\rangle, m|1\rangle\big)\big]_{\mathcal{B}_2} \quad \big[\big(n|0\rangle, -m|0\rangle\big)\big]_{\mathcal{B}_2} \quad \big[\big(n|1\rangle, -m|1\rangle\big)\big]_{\mathcal{B}_2} \ \Big) \\
&= \left(\begin{array}{c|c} nI & nI \\ \hline mI & -mI \end{array} \right). \qquad (77)
\end{aligned}$$

Thus, using the component isomorphism $[\cdot]_{\mathcal{B}_2}$, Supplementary Equation 75 can be recast as:

$$\big[\big(n\big(|\psi\rangle + |\varphi\rangle\big), m\big(|\psi\rangle - |\varphi\rangle\big)\big)\big]_{\mathcal{B}_2} = G_{\mathrm{FI}} \left[\big(|\psi\rangle, |\varphi\rangle\big)\right]_{\mathcal{B}_2}, \qquad (78)$$

leading to the following input-output matrix relation:

$$\begin{pmatrix} n\left(\psi_0 + \varphi_0\right) \\ n\left(\psi_1 + \varphi_1\right) \\ m\left(\psi_0 - \varphi_0\right) \\ m\left(\psi_1 - \varphi_1\right) \end{pmatrix} = \left(\begin{array}{cc|cc} n & 0 & n & 0 \\ 0 & n & 0 & n \\ \hline m & 0 & -m & 0 \\ 0 & m & 0 & -m \end{array} \right) \begin{pmatrix} \psi_0 \\ \psi_1 \\ \varphi_0 \\ \varphi_1 \end{pmatrix}. \qquad (79)$$

Setting $n = m = 1$, the above expression describes the computational system depicted in Fig. 5a of the paper.

As seen, defining the FI operation via the *Cartesian product*, we are able to: (i) work with (square) matrices providing a linear nature to this gate, (ii) independently transform the anbit amplitudes ψ_0, ψ_1, φ_0 and φ_1. Alternatively, we could define the FI gate via the *tensor product*. Nonetheless, in such a scenario, it is worthy to highlight that this version of the FI gate would have a nonlinear nature because we could not describe this multi-anbit operation via a matrix. The proof of this statement can be done in three steps. Firstly, note that the definition of the FI gate via the tensor product would be of the form:

$$\widehat{\mathrm{G}}_{\mathrm{FI}}|\psi, \varphi\rangle := |\psi + \varphi\rangle \otimes |\psi - \varphi\rangle = \sum_{k,l} \big(\psi_k + \varphi_k\big)\big(\psi_l - \varphi_l\big)|k, l\rangle. \qquad (80)$$

Secondly, we should derive the "apparent" matrix representation of $\widehat{\mathrm{G}}_{\mathrm{FI}}$ associated to the canonical basis $\mathcal{B}_2$ of $\mathscr{E}_1 \otimes \mathscr{E}_1$ (given by Supplementary Equation 24):

$$G_{\mathrm{FI}} = M_{\mathcal{B}_2}^{\mathcal{B}_2}\big(\widehat{\mathrm{G}}_{\mathrm{FI}}\big) = \big(\ \cdots \quad \big[\widehat{\mathrm{G}}_{\mathrm{FI}}|k, l\rangle\big]_{\mathcal{B}_2} \quad \cdots \ \big) = \begin{pmatrix} 0 & 0 & 0 & 0 \\ 0 & -1 & 0 & 0 \\ 0 & 0 & -1 & 0 \\ 0 & 0 & 0 & 0 \end{pmatrix}. \qquad (81)$$

Thirdly, we should compare the output generated by $\widehat{\mathrm{G}}_{\mathrm{FI}}$ with the output generated by G_{FI}. The operator $\widehat{\mathrm{G}}_{\mathrm{FI}}$ leads to the output described by Supplementary Equation 80, whose components associated to $\mathcal{B}_2$ are:

$$\big[\widehat{\mathrm{G}}_{\mathrm{FI}}|\psi, \varphi\rangle\big]_{\mathcal{B}_2} = \begin{pmatrix} \big(\psi_0 + \varphi_0\big)\big(\psi_0 - \varphi_0\big) \\ \big(\psi_0 + \varphi_0\big)\big(\psi_1 - \varphi_1\big) \\ \big(\psi_1 + \varphi_1\big)\big(\psi_0 - \varphi_0\big) \\ \big(\psi_1 + \varphi_1\big)\big(\psi_1 - \varphi_1\big) \end{pmatrix}. \qquad (82)$$

However, the matrix G_{FI} gives rise to a different output:

$$G_{\mathrm{FI}}\left[\left|\psi,\varphi\right\rangle\right]_{\mathcal{B}_2}=\begin{pmatrix}0&0&0&0\\0&-1&0&0\\0&0&-1&0\\0&0&0&0\end{pmatrix}\begin{pmatrix}\psi_0\varphi_0\\\psi_0\varphi_1\\\psi_1\varphi_0\\\psi_1\varphi_1\end{pmatrix}=\begin{pmatrix}0\\-\psi_0\varphi_1\\-\psi_1\varphi_0\\0\end{pmatrix}. \tag{83}$$

Consequently, $\widehat{\mathrm{G}}_{\mathrm{FI}}$ has no matrix representation. This implies that the global output (Supplementary Equation 82) is different from the linear superposition of the outputs generated by each vector of the basis $\mathcal{B}_2$ (Supplementary Equation 83). In other words, $\widehat{\mathrm{G}}_{\mathrm{FI}}$ is a nonlinear mapping of $\mathscr{E}_1\otimes\mathscr{E}_1$. For this reason, the FI gate is defined by using the Cartesian product as indicated by Supplementary Equation 75.

Properties. The FI gate illustrated in Supplementary Figure 11 exhibits the following properties:

1. *Automorphism.* The linear operator $\widehat{\mathrm{G}}_{\mathrm{FI}}$ is an automorphism of the Hilbert space $\mathscr{E}_2=\mathscr{E}_1\times\mathscr{E}_1$, i.e., a bijective endomorphism given that the FI gate is reversible, as demonstrated in property 2.

2. *Reversibility.* From Supplementary Equation 77, it follows that:

$$\det\big(G_{\mathrm{FI}}\big)=4n^2m^2\neq 0, \tag{84}$$

   that is, the FI gate is reversible.

3. *Commutativity.* The operation $\widehat{\mathrm{G}}_{\mathrm{FI}}$ holds the commutative property:

$$\widehat{\mathrm{G}}_{\mathrm{FI}}\left(\left|\psi\right\rangle,\left|\varphi\right\rangle;n,m\right)=\widehat{\mathrm{G}}_{\mathrm{FI}}\left(\left|\varphi\right\rangle,\left|\psi\right\rangle;n,-m\right). \tag{85}$$

   The order of the input anbits can be commuted preserving the state of the output anbits, provided that the sign of the second parameter is inverted.

4. *FI-FO connection.* The FO operation (defined below) of the anbit $\left|\psi\right\rangle$ can be performed by the FI gate setting $\left|\varphi\right\rangle=\left|\mathbf{0}\right\rangle$ and $n,m\in\mathbb{R}^+$ in Supplementary Equation 75. Moreover, a perfect cloning of $\left|\psi\right\rangle$ will be carried out taking $n=m=1$.

5. *Algebraic structure.* If $\left|n\right|^2=\left|m\right|^2=1/2$, then $G_{\mathrm{FI}}\in\mathrm{U}\left(4\right)$ and FI is a 2-anbit U-gate. Otherwise, $G_{\mathrm{FI}}\in\mathrm{GL}\left(4,\mathbb{C}\right)$ and FI is a 2-anbit G-gate.

6. *Universality and PIP implementation.* A universal matrix of the FI gate is of the form given by Supplementary Equation 77. A PIP implementation of such a matrix preserves the universality if the values of the parameters n and m may be optically tuned. Along this line, note that when $n=m$ then $G_{\mathrm{FI}}=G_{\mathrm{FI}}^T$ and, therefore, if the circuit preserves the Lorentz reciprocity, we may conclude that the circuit will also preserve the FB symmetry (as inferred from comment 6 on page 38). Remarkably, the PIP implementation of the FI gate depicted in Fig. 5a and Supplementary Figure 13 satisfies this property.

3.1.2 Fan-out: anbit cloning

Definition and formalism. Consider the single-anbit Hilbert space $\mathscr{E}_1$. Let us define the FO operation (anbit cloning) as the linear mapping $\widehat{\mathrm{M}}_{\mathrm{FO}}$ of $\mathscr{E}_2 := \mathscr{E}_1 \times \mathscr{E}_1$ which transforms the input $\big(|\psi\rangle, |\varphi\rangle\big)$ into the output:

$$\widehat{\mathrm{M}}_{\mathrm{FO}}\left(|\psi\rangle, |\varphi\rangle; n, m\right) := \big(n|\psi\rangle, m|\psi\rangle\big), \tag{86}$$

where $n, m \in \mathbb{R}^+$ are parameters of the operation ($n = m = 1$ will be assumed as the *default values* and, in such a case, the parameters can be omitted on the left-hand side of the above equation). Here, note that $|\varphi\rangle$ is an *ancilla* anbit since we are only interested in cloning a single input anbit ($|\psi\rangle$). Nonetheless, the aim of defining two input anbits is that, in this vein, we will be able to describe the FO operation via a square matrix, see below. Supplementary Figure 12 shows the functional scheme and symbolic representation of the FO gate.

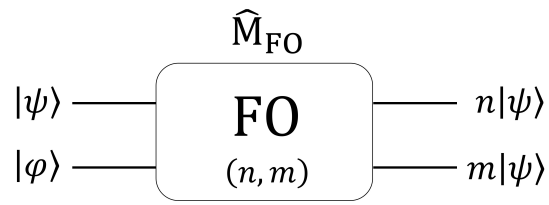

Supplementary Figure 12. Functional scheme and symbolic representation of the fan-out (FO) gate. The values of the (positive real) parameters n, m should be indicate, except for the case $n = m = 1$, which are defined as the default values and give rise to a perfect cloning of the input anbit $|\psi\rangle$.

The goal of the FO gate is to introduce an operation in APC that allows us to duplicate the state of an anbit with the same norm (perfect cloning, $n = m = 1$) or a different norm (imperfect cloning, $n \neq 1$ or $m \neq 1$), but without introducing an additional phase. To this end, the parameters n and m must be assumed positive real constants.

Bearing in mind that the FO gate is an operation of two input and output anbits, the underlying Hilbert space is $\mathscr{E}_2$ and the canonical (orthonormal) basis is $\mathcal{B}_2$, given by Supplementary Equation 76. In this scenario, the matrix representation of $\widehat{\mathrm{M}}_{\mathrm{FO}}$ associated to $\mathcal{B}_2$ is:

$$\begin{aligned}
M_{\mathrm{FO}} &= M_{\mathcal{B}_2}^{\mathcal{B}_2}\big(\widehat{\mathrm{M}}_{\mathrm{FO}}\big) \\
&= \Big(\left[\widehat{\mathrm{M}}_{\mathrm{FO}}\left(|0\rangle, |\mathbf{0}\rangle\right)\right]_{\mathcal{B}_2} \quad \left[\widehat{\mathrm{M}}_{\mathrm{FO}}\left(|1\rangle, |\mathbf{0}\rangle\right)\right]_{\mathcal{B}_2} \quad \left[\widehat{\mathrm{M}}_{\mathrm{FO}}\left(|\mathbf{0}\rangle, |0\rangle\right)\right]_{\mathcal{B}_2} \quad \left[\widehat{\mathrm{M}}_{\mathrm{FO}}\left(|\mathbf{0}\rangle, |1\rangle\right)\right]_{\mathcal{B}_2} \Big) \\
&= \Big(\left[(n|0\rangle, m|0\rangle)\right]_{\mathcal{B}_2} \quad \left[(n|1\rangle, m|1\rangle)\right]_{\mathcal{B}_2} \quad \left[(|\mathbf{0}\rangle, |\mathbf{0}\rangle)\right]_{\mathcal{B}_2} \quad \left[(|\mathbf{0}\rangle, |\mathbf{0}\rangle)\right]_{\mathcal{B}_2} \Big) \\
&= \left(\begin{array}{c|c} nI & 0 \\ \hline mI & 0 \end{array}\right).
\end{aligned} \tag{87}$$

Hence, applying the component isomorphism $[\cdot]_{\mathcal{B}_2}$ to Supplementary Equation 86, the input-output relation of the FO gate can be expressed by the matrix relation:

$$\begin{pmatrix} n\psi_0 \\ n\psi_1 \\ m\psi_0 \\ m\psi_1 \end{pmatrix} = \left(\begin{array}{cc|cc} n & 0 & 0 & 0 \\ 0 & n & 0 & 0 \\ \hline m & 0 & 0 & 0 \\ 0 & m & 0 & 0 \end{array}\right) \begin{pmatrix} \psi_0 \\ \psi_1 \\ \varphi_0 \\ \varphi_1 \end{pmatrix}. \tag{88}$$

It should be noted that the third and fourth columns of M_{FO} are found to be null as a direct consequence that the FO gate must clone $\big|\psi\big\rangle$ at the output for any ancilla anbit $\big|\varphi\big\rangle$ at the input. The main drawback of a matrix with two null columns is that its optical implementation will be restricted to a few number of PIP architectures.

In order to circumvent this technological limitation, let us take $\big|\varphi\big\rangle = \big|\mathbf{0}\big\rangle$. As a result, the entries of the third and fourth columns of M_{FO} can be regarded as degrees of freedom ($\alpha_{kl} \in \mathbb{C}$ with $k \in \{1,\ldots,4\}$ and $l \in \{3,4\}$):

$$\begin{pmatrix} n\psi_0 \\ n\psi_1 \\ m\psi_0 \\ m\psi_1 \end{pmatrix} = \left(\begin{array}{cc|cc} n & 0 & \alpha_{13} & \alpha_{14} \\ 0 & n & \alpha_{23} & \alpha_{24} \\ \hline m & 0 & \alpha_{33} & \alpha_{34} \\ 0 & m & \alpha_{43} & \alpha_{44} \end{array}\right) \begin{pmatrix} \psi_0 \\ \psi_1 \\ 0 \\ 0 \end{pmatrix}. \tag{89}$$

Remarkably, this new version of M_{FO} can be implemented by a larger gamut of PIP circuits than in Supplementary Equation 88. As a by-product, the same optical implementation of the FI gate could also be employed to implement M_{FO}, leading to a common PIP architecture for both operations (see below p. 54).

Finally, we should discuss the importance of defining the FO gate by using the *Cartesian product*. In the same way as in the FI operation, the Cartesian product provides a linear nature to the FO gate. Alternatively, we could define the FO gate via the *tensor product*. Nevertheless, in such a case, the FO gate would have a nonlinear nature. The proof of this statement may be performed in two steps. Firstly, note that the construction of the FO gate via the tensor product would be a mapping of $\mathscr{E}_1 \otimes \mathscr{E}_1$ defined as $\widehat{\mathrm{M}}_{\mathrm{FO}}\big|\psi,\varphi\big\rangle := \big|\psi,\psi\big\rangle$. Secondly, we can directly verify that this mapping has a nonlinear nature using *reductio ad absurdum* (i.e. we assume a linear behaviour to find an inconsistent conclusion):

$$\begin{aligned} \widehat{\mathrm{M}}_{\mathrm{FO}}\big|\psi,\varphi\big\rangle &= \widehat{\mathrm{M}}_{\mathrm{FO}}\big(\psi_0\big|0,\varphi\big\rangle + \psi_1\big|1,\varphi\big\rangle\big) \\ &= \psi_0\widehat{\mathrm{M}}_{\mathrm{FO}}\big|0,\varphi\big\rangle + \psi_1\widehat{\mathrm{M}}_{\mathrm{FO}}\big|1,\varphi\big\rangle \\ &= \psi_0\big|0,0\big\rangle + \psi_1\big|1,1\big\rangle \neq \big|\psi,\psi\big\rangle. \end{aligned} \tag{90}$$

The nonlinear behaviour of this version of the FO operation (defined via the tensor product) has extensively been discussed in QC within the context of the no-cloning theorem [24].

Properties. As commented above, any 4×4 matrix of the form:

$$M_{\mathrm{FO}} = \left(\begin{array}{c|c} nI & M_{12} \\ \hline mI & M_{22} \end{array}\right), \tag{91}$$

with M_{12} and M_{22} being 2×2 arbitrary submatrices, is able to carry out an FO operation of the input anbit $\big|\psi\big\rangle$ when the ancilla anbit is taken to be null $\big|\varphi\big\rangle = \big|\mathbf{0}\big\rangle$. Since this matrix is more general than Supplementary Equation 87, let us study its properties:

1. *Endomorphism family and FI-FO connection.* Specifically, M_{FO} describes a family of endomorphisms of $\mathscr{E}_2 = \mathscr{E}_1 \times \mathscr{E}_1$. In fact, note that the FI gate (see Supplementary Equation 77) is also described by M_{FO} taking $M_{12} \equiv nI$ and $M_{22} \equiv -mI$.

2. *Reversibility.* Given that $\det\big(M_{\mathrm{FO}}\big)$ depends on the value of the submatrices M_{12} and M_{22}, we conclude that the FO gate may be reversible ($\det\big(M_{\mathrm{FO}}\big) \neq 0$) or irreversible ($\det\big(M_{\mathrm{FO}}\big) = 0$).

3. *Non-commutativity.* In contrast to the FI operation, the order of the input anbits cannot be commuted in the FO gate.

4. *Algebraic structure.* From the expressions $M_{\mathrm{FO}}^{\dagger} M_{\mathrm{FO}} = I$ and $M_{\mathrm{FO}} M_{\mathrm{FO}}^{\dagger} = I$, we infer that $M_{\mathrm{FO}} \in \mathrm{U}(4)$ (a 2-anbit U-gate) if and only if the next necessary and sufficient conditions are fulfilled: (1) $n^2 + m^2 = 1$, (2) $nM_{12} + mM_{22} = 0$, (3) $M_{12}^{\dagger} M_{12} + M_{22}^{\dagger} M_{22} = I$, (4) $M_{12} M_{12}^{\dagger} = \left(1 - n^2\right) I$, (5) $M_{22} M_{12}^{\dagger} = -nmI$, (6) $M_{22} M_{22}^{\dagger} = \left(1 - m^2\right) I$. For instance, $n = m = 1/\sqrt{2}$ and $M_{12} = -M_{22} = \left(1/\sqrt{2}\right) I$ satisfy the above conditions. On the other hand, $M_{\mathrm{FO}} \in \mathrm{GL}(4, \mathbb{C})$ (a 2-anbit G-gate) by taking parameters n, m and submatrices M_{12} and M_{22} guaranteeing that $\det\left(M_{\mathrm{FO}}\right) \neq 0$. As an example, $n = m = 1$ and $M_{12} = -M_{22} = I$ satisfy these conditions. Finally, the cases where $\det\left(M_{\mathrm{FO}}\right) = 0$ correspond to an irreversible 2-anbit M-gate.

3.1.3 PIP implementation: a common architecture

From the study of the FI and FO gates, we know that both operations are connected via the equation:

$$\widehat{\mathrm{M}}_{\mathrm{FO}}\left(\left|\psi\right\rangle, \left|\varphi\right\rangle; n, m\right) = \widehat{\mathrm{G}}_{\mathrm{FI}}\left(\left|\psi\right\rangle, \left|\mathbf{0}\right\rangle; n, m\right). \tag{92}$$

Thus, the PIP circuit of the FI gate will also be able to perform the FO operation by taking $\left|\varphi\right\rangle = \left|\mathbf{0}\right\rangle$. Supplementary Figure 13 shows the optical circuit of the FI gate, whose (reduced) forward transfer matrix is G_{FI} (Supplementary Equation 77).

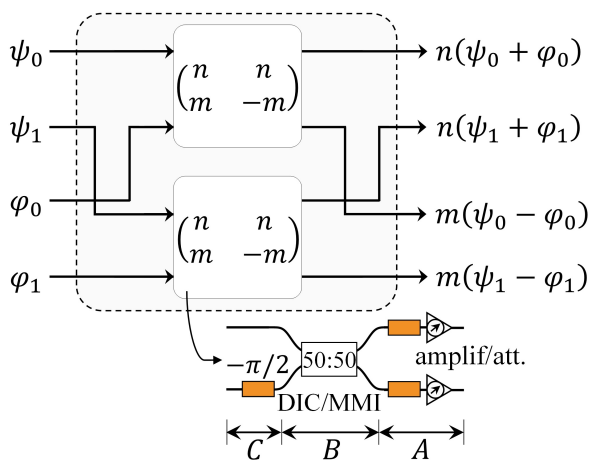

Supplementary Figure 13. PIP implementation of both fan-in (FI) and fan-out (FO) gates using an optical circuit whose (reduced) forward transfer matrix is given by G_{FI} (Supplementary Equation 77). The circuit carries out the FI operation by mapping the anbit amplitudes of $\left|\psi\right\rangle \times \left|\varphi\right\rangle$ into the anbit amplitudes of $n\left(\left|\psi\right\rangle + \left|\varphi\right\rangle\right) \times m\left(\left|\psi\right\rangle - \left|\varphi\right\rangle\right)$, with $n, m \in \mathbb{C} - \{0\}$. In addition, the FO operation of $\left|\psi\right\rangle$ can be performed by setting $\left|\varphi\right\rangle = \left|\mathbf{0}\right\rangle$ and using positive real parameters n, m.

This architecture is constructed from two identical 2×2 subsystems implementing the reduced forward transfer matrix depicted within the boxes, which may be factorised as:

$$\begin{pmatrix} n & n \\ m & -m \end{pmatrix} \equiv \underbrace{\begin{pmatrix} \sqrt{2}n & 0 \\ 0 & -i\sqrt{2}m \end{pmatrix}}_{A} \underbrace{\frac{1}{\sqrt{2}} \begin{pmatrix} 1 & i \\ i & 1 \end{pmatrix}}_{B} \underbrace{\begin{pmatrix} 1 & 0 \\ 0 & -i \end{pmatrix}}_{C}. \tag{93}$$

The matrices A, B, C can be implemented by PSs, tunable optical attenuators/amplifiers and a 50:50 beam splitter (the PIP implementation of each matrix is sketched in the figure for clarity). Along this line, it should be noted that Fig. 5a of the paper emerges from Supplementary Figure 13 by restricting the parameters to the default values $n = m = 1$.

Finally, let us conclude with a brief discussion about the reciprocity and FB symmetry of such a structure. Assuming reciprocal and FB-symmetric attenuators/amplifiers, the global system will preserve the Lorentz reciprocity by exhibiting a symmetric S matrix:

$$S = \left(\begin{array}{c|c} 0 & G_{\mathrm{FI}}^T \\ \hline G_{\mathrm{FI}} & 0 \end{array} \right), \tag{94}$$

and will preserve (break) the FB symmetry when $n = m$ ($n \neq m$). This can be easily verified by comparing the reduced forward and backward transfer matrices of the 2×2 subsystems integrating the whole structure, which are found to be:

$$\widetilde{T}_{\mathrm{f}} = \begin{pmatrix} n & n \\ m & -m \end{pmatrix}, \quad \widetilde{T}_{\mathrm{b}} = \begin{pmatrix} n & m \\ n & -m \end{pmatrix}. \tag{95}$$

As seen, $\widetilde{T}_{\mathrm{f}} = \widetilde{T}_{\mathrm{b}}$ when $n = m$. These conclusions are in line with property 6 of the FI gate (see p. 51).

3.2 First sequential system of the paper

In this subsection, we will analyse in detail the *first* sequential architecture reported in the main text (Fig. 5b). This scheme is the simplest sequential system that can be built in APC, composed by two FI/FO gates along with two M-gates that complete the feedback loop. While in the paper we use FI/FO gates with parameters fixed at the default value 1, let us consider here FI/FO operations with arbitrary parameters to carry out a complete and rigorous analysis of this first sequential scheme, see Supplementary Figure 14.

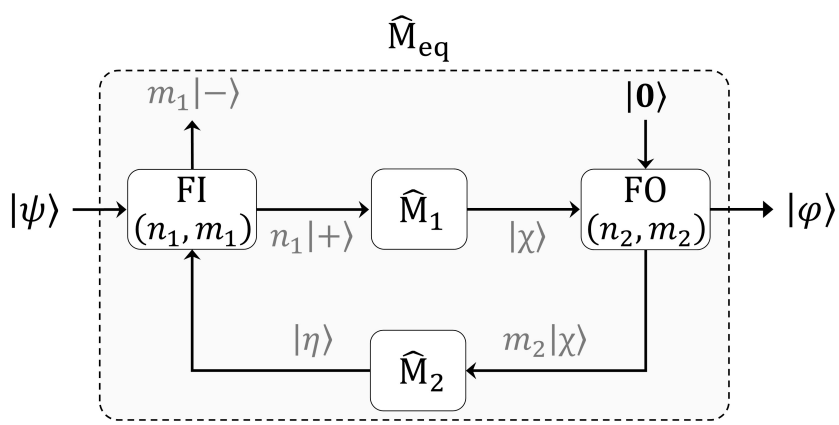

Supplementary Figure 14. Sequential computational system of a single anbit, composed by 2 single-anbit M-gates ($\widehat{\mathrm{M}}_1$ and $\widehat{\mathrm{M}}_2$), 1 FI gate and 1 FO gate. For the sake of completeness, we use here FI/FO operations with arbitrary parameters $n_1, m_1 \in \mathbb{C} - \{0\}$ and $n_2, m_2 \in \mathbb{R}^+$ (however, in the paper, these parameters are set to the default value 1 for simplicity).

Analysis. The strategy to analyse any sequential architecture in APC is the same as that of a combinational scheme: we must calculate the input-output relation, in this example $|\varphi\rangle = \widehat{\mathrm{M}}_{\mathrm{eq}}|\psi\rangle$. To this end, we should find the relation of $\widehat{\mathrm{M}}_{\mathrm{eq}}$ with the M-gates $\widehat{\mathrm{M}}_1$ and $\widehat{\mathrm{M}}_2$ following the anbit transformations that appear in the feedback loop. The simplest way is to start from the output anbit:

$$|\varphi\rangle = n_2|\chi\rangle = n_1 n_2 \widehat{\mathrm{M}}_1|+\rangle = n_1 n_2 \widehat{\mathrm{M}}_1\big(|\psi\rangle + |\eta\rangle\big). \tag{96}$$

Next, taking into account that $|\eta\rangle = m_2\widehat{\mathrm{M}}_2|\chi\rangle = \big(m_2/n_2\big)\widehat{\mathrm{M}}_2|\varphi\rangle$, the above equation becomes:

$$|\varphi\rangle = n_1 n_2 \widehat{\mathrm{M}}_1|\psi\rangle + n_1 m_2 \widehat{\mathrm{M}}_1\widehat{\mathrm{M}}_2|\varphi\rangle. \tag{97}$$

Therefore, the input-output relation of the system is found to be:

$$|\varphi\rangle = n_1 n_2\big(\widehat{1} - n_1 m_2 \widehat{\mathrm{M}}_1\widehat{\mathrm{M}}_2\big)^{-1}\widehat{\mathrm{M}}_1|\psi\rangle. \tag{98}$$

This implies that the sequential architecture is described by an *equivalent* linear operator of the form:

$$\widehat{\mathrm{M}}_{\mathrm{eq}} \equiv n_1 n_2\big(\widehat{1} - n_1 m_2 \widehat{\mathrm{M}}_1\widehat{\mathrm{M}}_2\big)^{-1}\widehat{\mathrm{M}}_1, \tag{99}$$

with $n_1 \in \mathbb{C} - \{0\}$ and $n_2, m_2 \in \mathbb{R}^+$.

Given that the system is an operation of a single anbit, the underlying Hilbert space is $\mathscr{E}_1$ (with canonical basis $\mathcal{B}_1 = \big\{|0\rangle, |1\rangle\big\}$). Hence, the matrix representation of $\widehat{\mathrm{M}}_{\mathrm{eq}}$ associated to $\mathcal{B}_1$ is:

$$M_{\mathrm{eq}} = M_{\mathcal{B}_1}^{\mathcal{B}_1}\big(\widehat{\mathrm{M}}_{\mathrm{eq}}\big) = n_1 n_2 \left(I - n_1 m_2 M_1 M_2\right)^{-1} M_1, \tag{100}$$

where M_1 and M_2 are the matrix representations of $\widehat{\mathrm{M}}_1$ and $\widehat{\mathrm{M}}_2$, respectively. Setting $n_1 = n_2 = m_2 \equiv 1$, Supplementary Equation 100 is reduced to the expression of M_{eq} reported in the main text.

Properties. The single-anbit sequential system of Supplementary Figure 14 has the next properties:

1. *Endomorphism.* The linear operator $\widehat{\mathrm{M}}_{\mathrm{eq}}$ is an endomorphism of the Hilbert space $\mathscr{E}_1$.

2. *Existence.* Let us rewrite Supplementary Equation 100 as $M_{\mathrm{eq}} = n_1 n_2 G^{-1} M_1$, with $G := I - n_1 m_2 M_1 M_2$. As can be seen, the existence of this sequential system (described by M_{eq}) directly depends on the existence of G^{-1}, that is:

$$\exists M_{\mathrm{eq}} \Leftrightarrow \exists G^{-1} \Leftrightarrow \det(G) \neq 0 \Leftrightarrow \det\big(I - n_1 m_2 M_1 M_2\big) \neq 0. \tag{101}$$

   Contrariwise, the sequential system could not be built because G would be singular.

3. *Reversibility.* The gate $\widehat{\mathrm{M}}_{\mathrm{eq}}$ is reversible (automorphism) if and only if $\det\big(G^{-1}\big) \neq 0$ and $\det\big(M_1\big) \neq 0$.

4. *Equivalent system.* Since $\widehat{\mathrm{M}}_{\mathrm{eq}}$ may be reversible or irreversible, then the anbit transformation can be regarded as a single-anbit combinational M-gate. In addition, it is interesting to highlight that the system is equivalent to two different single-anbit gates M_1 and $n_1 n_2 G^{-1}$ connected in series (Supplementary Figure 15). In this scenario, note that $n_1 n_2 G^{-1}$ actually describes a sequential system similar to that of Supplementary Figure 14, but with the M-gates being I and $M_1 M_2$. In particular, this system equivalence could be employed to simplify computational architectures that combine both combinational and sequential gates.

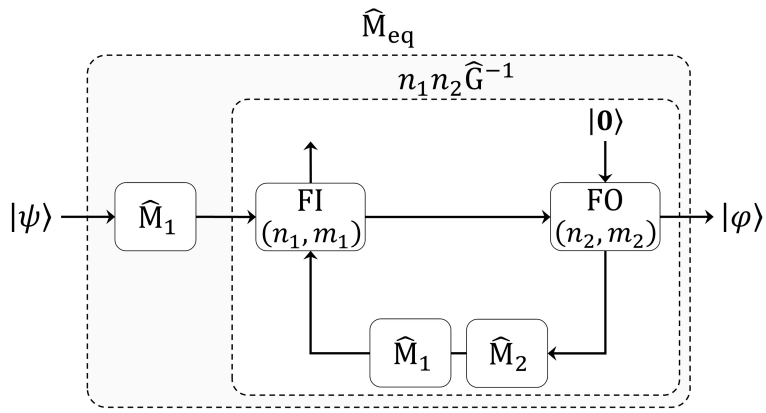

Supplementary Figure 15. Equivalent sequential system. The gate $\widehat{\mathrm{M}}_1$ can be extracted from the upper branch of the feedback loop following this scheme. The operator $\widehat{\mathrm{M}}_{\mathrm{eq}}$ is the same as that of the original system shown in Supplementary Figure 14.

5. *Algebraic structure.* The matrix M_{eq} belongs to $\mathrm{U}(2)$ (i.e. the system is equivalent to a U-gate) if M_1 and $n_1 n_2 G^{-1}$ are 2×2 unitary matrices. Here, $n_1 n_2 G^{-1} \in \mathrm{U}(2)$ if the following necessary and sufficient condition is satisfied:

$$A^{\dagger} A - \frac{1}{n_1^* n_2} A - \frac{1}{n_1 n_2} A^{\dagger} = \left(1 - \frac{1}{|n_1|^2 n_2^2}\right) I, \tag{102}$$

where $A := (m_2/n_2) M_1 M_2$ and $*$ denotes the complex conjugate. On the other hand, M_{eq} belongs to $\mathrm{GL}(2, \mathbb{C})$ (i.e. the system is equivalent to a G-gate) if M_1 is a general linear matrix (here, we implicitly assume that $G \in \mathrm{GL}(2, \mathbb{C})$ since it is a necessary and sufficient condition for the existence of M_{eq}, as discussed above). Finally, M_{eq} is an M-gate if M_1 is a singular matrix (irreversible operation).

6. *PIP implementation.* Using the circuits depicted in Figs. 3c and 5a of the paper to implement the gates of the feedback loop illustrated in Supplementary Figure 14, we will obtain an optical structure that breaks the Lorentz reciprocity and the FB symmetry.

3.3 Second sequential system of the paper

Finally, we will analyse the *second* sequential architecture reported in the main text (Fig. 5d). For clarity, we reproduce this scheme in Supplementary Figure 16 including the anbits employed in the mathematical discussions and considering FI/FO operations with arbitrary parameters to carry out a complete and rigorous analysis.

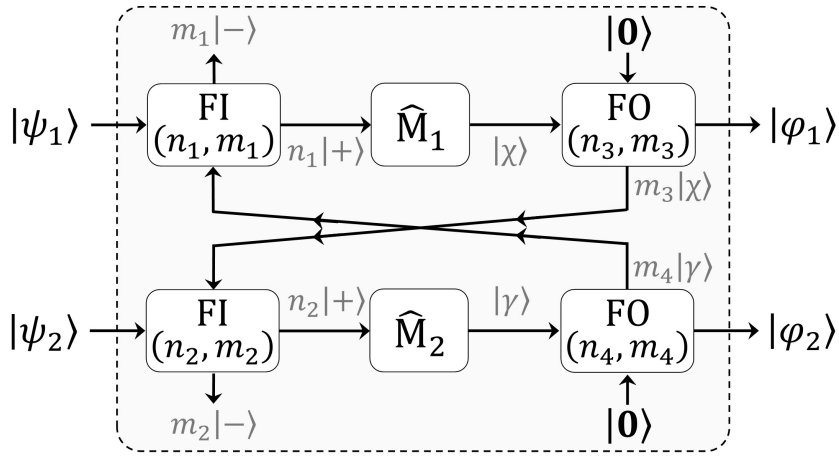

Supplementary Figure 16. Sequential computational system of two anbits, composed by 2 single-anbit M-gates ($\widehat{\mathrm{M}}_1$ and $\widehat{\mathrm{M}}_2$), 2 FI gates and 2 FO gates. For completeness, we use FI/FO operations with arbitrary parameters $n_{1,2}, m_{1,2} \in \mathbb{C} - \{0\}$ and $n_{3,4}, m_{3,4} \in \mathbb{R}^+$.

The goal is to find the input-output relation of the structure, as well as to demonstrate that such a mapping is equivalent to the input-output relation of the multi-anbit combinational architecture shown in Fig. 5c of the paper. With this approach in mind, we should start by calculating the output anbits $|\varphi_1\rangle$ and $|\varphi_2\rangle$ independently. The output anbit $|\varphi_1\rangle$ can be expressed as:

$$\begin{aligned}
|\varphi_1\rangle &= n_3|\chi\rangle \\
&= n_1 n_3 \widehat{\mathrm{M}}_1|+\rangle \\
&= n_1 n_3 \widehat{\mathrm{M}}_1\big(|\psi_1\rangle + m_4|\gamma\rangle\big) \\
&= n_1 n_3 \widehat{\mathrm{M}}_1|\psi_1\rangle + n_1 n_3 m_4 \widehat{\mathrm{M}}_1|\gamma\rangle \\
&= n_1 n_3 \widehat{\mathrm{M}}_1|\psi_1\rangle + n_1 n_2 n_3 m_4 \widehat{\mathrm{M}}_1\widehat{\mathrm{M}}_2|+\rangle \\
&= n_1 n_3 \widehat{\mathrm{M}}_1|\psi_1\rangle + n_1 n_2 n_3 m_4 \widehat{\mathrm{M}}_1\widehat{\mathrm{M}}_2\big(|\psi_2\rangle + m_3|\chi\rangle\big) \\
&= n_1 n_3 \widehat{\mathrm{M}}_1|\psi_1\rangle + n_1 n_2 n_3 m_4 \widehat{\mathrm{M}}_1\widehat{\mathrm{M}}_2\big(|\psi_2\rangle + \frac{m_3}{n_3}|\varphi_1\rangle\big) \\
&= n_1 n_3 \widehat{\mathrm{M}}_1|\psi_1\rangle + n_1 n_2 n_3 m_4 \widehat{\mathrm{M}}_1\widehat{\mathrm{M}}_2|\psi_2\rangle + n_1 n_2 m_3 m_4 \widehat{\mathrm{M}}_1\widehat{\mathrm{M}}_2|\varphi_1\rangle.
\end{aligned} \tag{103}$$

Hence, $|\varphi_1\rangle$ is found to be:

$$\begin{aligned}
|\varphi_1\rangle = {} & n_1 n_3 \big(\widehat{1} - n_1 n_2 m_3 m_4 \widehat{\mathrm{M}}_1\widehat{\mathrm{M}}_2\big)^{-1}\widehat{\mathrm{M}}_1|\psi_1\rangle \\
& + n_1 n_2 n_3 m_4 \big(\widehat{1} - n_1 n_2 m_3 m_4 \widehat{\mathrm{M}}_1\widehat{\mathrm{M}}_2\big)^{-1}\widehat{\mathrm{M}}_1\widehat{\mathrm{M}}_2|\psi_2\rangle.
\end{aligned} \tag{104}$$

Repeating the same procedure to calculate $|\varphi_2\rangle$, we obtain:

$$\begin{aligned}
|\varphi_2\rangle = {} & n_1 n_2 m_3 n_4 \big(\widehat{1} - n_1 n_2 m_3 m_4 \widehat{\mathrm{M}}_2\widehat{\mathrm{M}}_1\big)^{-1}\widehat{\mathrm{M}}_2\widehat{\mathrm{M}}_1|\psi_1\rangle \\
& + n_2 n_4 \big(\widehat{1} - n_1 n_2 m_3 m_4 \widehat{\mathrm{M}}_2\widehat{\mathrm{M}}_1\big)^{-1}\widehat{\mathrm{M}}_2|\psi_2\rangle.
\end{aligned} \tag{105}$$

For simplicity, let us compact the above expressions as:

$$\big|\varphi_1\big\rangle = \widehat{\mathrm{A}}_1\big|\psi_1\big\rangle + \widehat{\mathrm{A}}_2\big|\psi_2\big\rangle, \tag{106}$$

$$\big|\varphi_2\big\rangle = \widehat{\mathrm{B}}_1\big|\psi_1\big\rangle + \widehat{\mathrm{B}}_2\big|\psi_2\big\rangle, \tag{107}$$

where the operators $\widehat{\mathrm{A}}_{1,2}$ and $\widehat{\mathrm{B}}_{1,2}$ can be identified by comparing the corresponding equations. Using the *Cartesian product*, the input-output relation of the whole sequential structure is:

$$\begin{aligned}\big(\big|\varphi_1\big\rangle, \big|\varphi_2\big\rangle\big) &= \big(\widehat{\mathrm{A}}_1\big|\psi_1\big\rangle + \widehat{\mathrm{A}}_2\big|\psi_2\big\rangle, \widehat{\mathrm{B}}_1\big|\psi_1\big\rangle + \widehat{\mathrm{B}}_2\big|\psi_2\big\rangle\big)\\ &= \big(\widehat{\mathrm{A}}_1\big|\psi_1\big\rangle, \widehat{\mathrm{B}}_1\big|\psi_1\big\rangle\big) + \big(\widehat{\mathrm{A}}_2\big|\psi_2\big\rangle, \widehat{\mathrm{B}}_2\big|\psi_2\big\rangle\big)\\ &= \big(\widehat{\mathrm{A}}_1 \times \widehat{\mathrm{B}}_1\big)\,\big(\big|\psi_1\big\rangle, \big|\psi_1\big\rangle\big) + \big(\widehat{\mathrm{A}}_2 \times \widehat{\mathrm{B}}_2\big)\,\big(\big|\psi_2\big\rangle, \big|\psi_2\big\rangle\big).\end{aligned} \tag{108}$$

Furthermore, the input-output relation of the multi-anbit combinational architecture of Fig. 5c of the paper is:

$$\begin{aligned}\big(\big|\varphi_1\big\rangle, \big|\varphi_2\big\rangle\big) &= \big(\widehat{\mathrm{M}}_3\big|\psi_1\big\rangle + \widehat{\mathrm{M}}_5\big|\psi_2\big\rangle, \widehat{\mathrm{M}}_4\big|\psi_1\big\rangle + \widehat{\mathrm{M}}_6\big|\psi_2\big\rangle\big)\\ &= \big(\widehat{\mathrm{M}}_3\big|\psi_1\big\rangle, \widehat{\mathrm{M}}_4\big|\psi_1\big\rangle\big) + \big(\widehat{\mathrm{M}}_5\big|\psi_2\big\rangle, \widehat{\mathrm{M}}_6\big|\psi_2\big\rangle\big)\\ &= \big(\widehat{\mathrm{M}}_3 \times \widehat{\mathrm{M}}_4\big)\,\big(\big|\psi_1\big\rangle, \big|\psi_1\big\rangle\big) + \big(\widehat{\mathrm{M}}_5 \times \widehat{\mathrm{M}}_6\big)\,\big(\big|\psi_2\big\rangle, \big|\psi_2\big\rangle\big).\end{aligned} \tag{109}$$

As seen, Supplementary Equations 108 and 109 are equivalent mathematical expressions.

Supplementary Note 4: different versions of APC

The anbit is conceived as a vector function belonging to a two-dimensional (2D) Hilbert space. However, as commented in the main text, we have the possibility of defining the unit of information of APC in a Hilbert space with dimension $d \neq 2$, leading to different versions of APC, termed as d-APC. In this section, we discuss how to construct the computation theory (unit of information and basic gates) for the cases $d = 1$ and $d > 2$.

4.1 One-dimensional APC (1-APC)

4.1.1 Unit of information: the analog dit

Now, the unit of information is a 1D vector function $\left|\psi\left(t\right)\right\rangle = \psi_0\left(t\right)\left|0\right\rangle$ referred to as the *analog dit* (or *andit* for short), where ψ_0 is a scalar complex function termed as the andit amplitude and $\left|0\right\rangle$ is a constant unit vector. The user information is encoded in the module and phase of ψ_0.

In the same vein as an anbit, a 1D andit may be implementable in PIP via different modulation formats (see p. 25). For instance, using a SEM approach, ψ_0 can be encoded by an optical wave packet propagated by the fundamental mode $\left|0\right\rangle$ of a single-mode waveguide (Supplementary Figure 17). For coherence with the paper, the temporal shape of ψ_0 is assumed rectangular, although alternative physical implementations of a 1D andit can be proposed by exploring diverse temporal shapes of ψ_0. In addition, the following features of a 1D andit should be highlighted:

- *Hilbert space.* The single-andit vector space $\mathscr{E}_1 = \text{span}\left\{\left|0\right\rangle\right\}$ along with the standard complex inner product $\left\langle\cdot|\cdot\right\rangle$ lead to a 1D Hilbert space with canonical (normal) basis $\mathcal{B}_1 = \left\{\left|0\right\rangle\right\}$ and a finite norm $\|\cdot\|$. Specifically, $\|\psi\|^2$ describes the optical power ($\mathcal{P}$) propagated by the waveguide of Supplementary Figure 17: $\mathcal{P} = \|\psi\|^2 = \left\langle\psi|\psi\right\rangle = |\psi_0|^2$.

- *Andit period.* The andit period T_{ANDIT} is the time interval where $\psi_0\left(t\right)$ is defined.

- *Measurement and EDFs.* The number of EDFs that can be used to encode the user information depends solely on the kind of andit measurement employed at the receiver. A coherent measurement retrieves the module and phase of ψ_0 (2 EDFs), while a differential measurement only recovers $|\psi_0|^2$ (1 EDF).

- *Geometric representation.* A 1D andit can be geometrically represented by using a polar diagram illustrating the module and phase of ψ_0 in the complex plane (Supplementary Figure 17).

- *Multiple andits.* A computational system with n andits will require to operate in a Hilbert space $\mathscr{E}_n$ that can be constructed from $\mathscr{E}_1$ using the tensor or the Cartesian product. In the former case, we will obtain the Hilbert space $\mathscr{E}_n = \mathscr{E}_1^{\otimes(n-1)}$, with $\dim\left(\mathscr{E}_n\right) = \dim\left(\mathscr{E}_1\right)^n = 1$ and canonical basis $\mathcal{B}_n = \{|0,0,\ldots,0\rangle\}$. In the latter case, we will obtain the Hilbert space $\mathscr{E}_n = \mathscr{E}_1^{\times(n-1)}$, with $\dim\left(\mathscr{E}_n\right) = n\dim\left(\mathscr{E}_1\right) = n$ and canonical basis $\mathcal{B}_n = \left\{\left(\left|0\right\rangle,\left|\mathbf{0}\right\rangle,\ldots,\left|\mathbf{0}\right\rangle\right),\left(\left|\mathbf{0}\right\rangle,\left|0\right\rangle,\ldots,\left|\mathbf{0}\right\rangle\right),\ldots,\left(\left|\mathbf{0}\right\rangle,\left|\mathbf{0}\right\rangle,\ldots,\left|0\right\rangle\right)\right\}$. As we will see below, in 1-APC, it is more useful to work with the Cartesian product to define multi-andit operations.

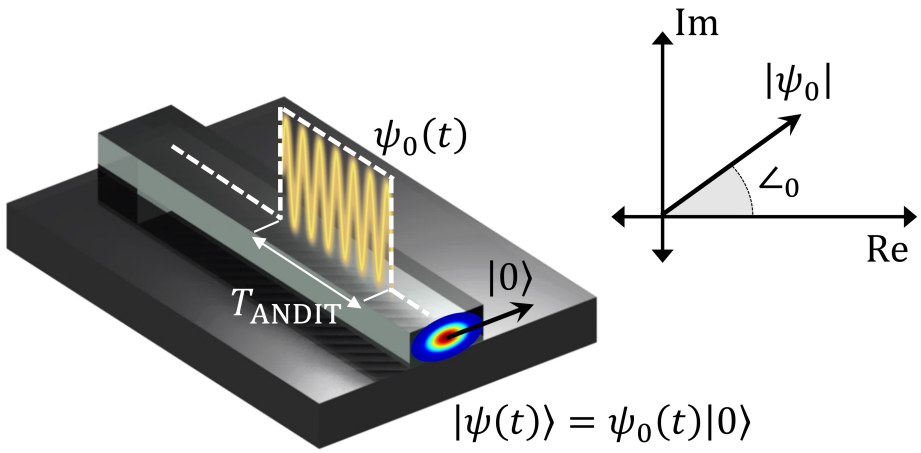

Supplementary Figure 17. Physical implementation of a one-dimensional andit $\left|\psi\left(t\right)\right\rangle = \psi_0\left(t\right)\left|0\right\rangle$ using PIP technology and a space-encoding modulation (SEM). The andit amplitude $\psi_0 = \left|\psi_0\right| e^{i\angle_0}$ is encoded by an optical wave packet (or complex envelope) propagated by the fundamental mode $\left|0\right\rangle$ of a single-mode waveguide. The andit is geometrically represented by using a polar diagram illustrating the module $|\psi_0|$ and phase $\angle_0$ in the complex plane.

4.1.2 Single-andit linear gates

Definition. In the same way as in 2-APC, a single-andit linear gate will be defined as a linear mapping $\widehat{\mathrm{F}}$ (or endomorphism) of $\mathscr{E}_1$. The operator $\widehat{\mathrm{F}}$ describes a transformation between an input andit $\left|\psi\right\rangle = \psi_0\left|0\right\rangle$ and an output andit $\left|\varphi\right\rangle = \varphi_0\left|0\right\rangle$.

General properties. The properties of a single-andit linear gate in 1-APC are the same as those of a single-anbit linear gate in 2-APC, but the following details should be highlighted:

- *Scalar representation.* Instead of using a matrix representation, the input-output relation $\left|\varphi\right\rangle = \widehat{\mathrm{F}}\left|\psi\right\rangle$ can equivalently be expressed via a scalar expression of the form $\varphi_0 = F\psi_0$, where $F = \left\langle 0\right|\widehat{\mathrm{F}}\left|0\right\rangle$. Utilising the component isomorphism $\left[\cdot\right]_{\mathcal{B}_1}$, it is direct to demonstrate the above equivalence:

$$\varphi_0 = \left[\left|\varphi\right\rangle\right]_{\mathcal{B}_1} = \left[\widehat{\mathrm{F}}\left|\psi\right\rangle\right]_{\mathcal{B}_1} = \psi_0\left[\widehat{\mathrm{F}}\left|0\right\rangle\right]_{\mathcal{B}_1} = \psi_0\left\langle 0\right|\widehat{\mathrm{F}}\left|0\right\rangle \equiv F\psi_0. \tag{110}$$

- *Reversibility.* By definition, the gate is reversible if and only if $|F| \neq 0$. The inverse gate is described by the inverse operator $\widehat{\mathrm{F}}^{-1}$, whose scalar representation is $F^{-1} = 1/F$.

- *Geometric representation.* A single-andit linear gate may be geometrically interpreted as a trajectory between two different points in the complex plane, from ψ_0 to φ_0.

- *Classes of linear gates.* We use the same classification as in 2-APC by considering U-, G-, and M-gates.

U-gates. Since a U-gate must preserve the norm of the input andit at the output andit ($|\varphi_0| = |\psi_0|$), this class of gates is associated to a unitary operator $\widehat{\mathrm{F}} = e^{i\delta}\left|0\right\rangle\left\langle 0\right|$ or scalar phase function $F = e^{i\delta}$. Hence, a U-gate only induces a global phase shifting and, consequently, the MCA is a PS.

G- and M-gates. The most general scalar complex function that can be defined is of the form $F = |F|\, e^{i\delta}$, with arbitrary module $|F|$ and arbitrary phase δ. Such a linear mapping will describe a G-gate when $|F| \neq 0$ (reversible operation) and will describe an M-gate when $|F| = 0$ (irreversible operation). The MCA is a PS connected in series with a tunable optical amplifier/attenuator accounting for the transformations $e^{i\delta}$ and $|F|$, respectively.

4.1.3 Dual-andit linear gates

Using the Cartesian product, we may define a Hilbert space $\mathscr{E}_2 = \mathscr{E}_1 \times \mathscr{E}_1$ with canonical basis $\mathcal{B}_2 = \big\{\big(|0\rangle, |\mathbf{0}\rangle\big), \big(|\mathbf{0}\rangle, |0\rangle\big)\big\}$ which is isomorphic to the Hilbert space of a single anbit in 2-APC ($\mathscr{E}_1^{(\text{2-APC})} = \text{span}\{|0\rangle, |1\rangle\}$). The isomorphism between both spaces is established by performing the identifications $\big(|0\rangle, |\mathbf{0}\rangle\big) \equiv |0\rangle$ and $\big(|\mathbf{0}\rangle, |0\rangle\big) \equiv |1\rangle$. In this way, any vector belonging to $\mathscr{E}_2$ in 1-APC of the form:

$$\big(|\alpha\rangle, |\beta\rangle\big) = \big(\alpha_0 |0\rangle, \beta_0 |0\rangle\big) = \alpha_0\big(|0\rangle, |\mathbf{0}\rangle\big) + \beta_0\big(|\mathbf{0}\rangle, |0\rangle\big), \tag{111}$$

has associated an anbit belonging to $\mathscr{E}_1^{(\text{2-APC})}$ of the form $|\psi\rangle = \alpha_0 |0\rangle + \beta_0 |1\rangle$. Using this isomorphism, we can directly extrapolate the theory and circuits of the single-anbit linear gates in 2-APC (see Fig. 3) to design and implement dual-andit linear gates in 1-APC. As seen, the Cartesian product paves the way to extrapolate the theory from 2-APC to 1-APC, a feature that cannot be found by using the tensor product.

On the other hand, the study of multi-andit linear gates in 1-APC will be investigated simultaneously along with the development of multi-anbit linear gates in 2-APC in future works. Here, the optical structures proposed by Reck and Clements in refs. [25, 26] could be of paramount importance to implement multi-andit U-gates in 1-APC.

4.1.4 Controlled gates

In 1-APC, a controlled gate should be defined in a different way from a controlled gate in 2-APC given that a control andit cannot commute between two different states. In this case, we may establish that a single-andit operation $\widehat{\mathrm{F}}$ is applied to a target andit $|t\rangle = t_0 |0\rangle$ when the amplitude of the control andit $|c\rangle = c_0 |0\rangle$ takes a specific complex value. In such a scenario, we can also propose an electro-optic design to implement a controlled gate, where the target and control andits are respectively encoded by 1D optical and electrical signals.

4.1.5 Sequential design

The fundamentals of sequential architectures in 1-APC can be directly extrapolated from 2-APC by restricting the analysis to 1D vectors. The FI and FO gates (the basic pieces to construct sequential schemes) can be implemented using similar circuits to those of proposed in Fig. 5a and Supplementary Figure 13. Concretely, in Fig. 5a, we should only work with the inputs ψ_0 and φ_0 and the outputs $\psi_0 + \varphi_0$ and $\psi_0 - \varphi_0$ to carry out FI/FO operations of 1D andits. Furthermore, note that the analysis and design of the sequential architectures shown in Figs. 5b and 5d are the same in 1-APC and 2-APC.

4.1.6 Nonlinear andit gates

The most general definition of a single-andit gate (including both linear and nonlinear contributions) is given by the expression $\widehat{\mathrm{F}}\big|\psi\big\rangle := f_0\big(\psi_0\big)\big|0\big\rangle$, with $f_0 \in \mathcal{F}\left(\mathbb{C},\mathbb{C}\right)$. Thus, $\widehat{\mathrm{F}}$ will induce a nonlinear transformation on the input andit $\big|\psi\big\rangle$ when the scalar function f_0 has a nonlinear behaviour. The theory of nonlinear gates in 1-APC is similar to that of nonlinear gates in 2-APC. Here, we should only restrict the mathematical formalism of equations 5 and 6 of the paper to 1D.

This kind of gates can be implemented in PIP, e.g., by exploiting the Pockels and Kerr effects in a *single-mode* waveguide to carry out second- and third-order nonlinear andit operations, respectively. As an example, stimulating the self-phase modulation effect in a single-mode waveguide (similar to that of depicted in Supplementary Figure 17), a nonlinear andit transformation of the form $\widehat{\mathrm{F}}\big|\psi\big\rangle = \psi_0 \exp\big(-i\gamma\big|\psi_0\big|^2 L_{\mathrm{eff}}\big)\big|0\big\rangle$ may be obtained (γ and L_{eff} are nonlinear parameters of the waveguide [27]).

4.2 Multi-dimensional APC (d-APC)

In d-APC with $d > 2$, the unit of information is a d-dimensional vector function:

$$\big|\psi\left(t\right)\big\rangle = \sum_{n=0}^{d-1} \psi_n\left(t\right)\big|n\big\rangle, \tag{112}$$

also termed as andit, where $\psi_0, \psi_1, \ldots, \psi_{d-1}$ are scalar complex functions termed as the andit amplitudes and $\big|0\big\rangle, \big|1\big\rangle, \ldots, \big|d-1\big\rangle$ are constant orthonormal vectors. The user information is encoded in the moduli and phases of the andit amplitudes.

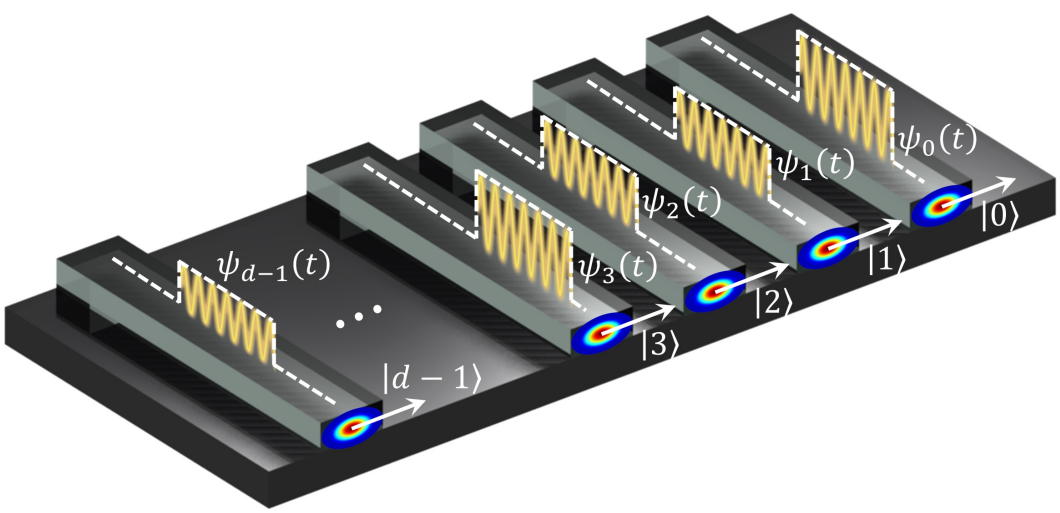

Supplementary Figure 18. Physical implementation of a d-dimensional andit using PIP technology and a space-encoding modulation (SEM). The andit amplitudes $\psi_0, \psi_1, \psi_2, \psi_3, \ldots, \psi_{d-1}$ are encoded by d different optical wave packets (or complex envelopes) propagated by the fundamental modes $\big|0\big\rangle, \big|1\big\rangle, \big|2\big\rangle, \big|3\big\rangle, \ldots, \big|d-1\big\rangle$ of d different single-mode waveguides.

A d-dimensional andit can be implemented in PIP via different modulation formats that make use of the space, mode, frequency and time domain of light. These modulation formats are similar to those proposed for the anbit in Supplementary Note 1 (p. 25), but generalised for a d-dimensional vector. As an example, in a SEM technique, we can associate $|0\rangle, |1\rangle, \ldots, |d-1\rangle$ to the fundamental modes of d different single-mode waveguides and the andit amplitudes can be encoded by d different optical wave packets propagated by these fundamental modes, see Supplementary Figure 18. Moreover, although the temporal shape of the andit amplitudes is assumed rectangular (for coherence with the main text), diverse options may be explored in forthcoming works by employing optical wave packets with different shapes.

The properties of a d-dimensional andit are similar to those of an anbit. In particular, now, we will have $2d$ or $2d-1$ EDFs when using coherent or differential measurement, respectively. In the latter case, the global phase of the andit amplitudes cannot be recovered.

Once we have defined the unit of information of d-APC, the subsequent steps to construct this version of the computation theory are to study single-andit linear gates, controlled gates, FI/FO gates, sequential architectures and nonlinear andit gates. Despite the fact that the theoretical details of these points are out of the scope of this work, the following considerations are in order:

- From a theoretical perspective, the fundamentals of combinational and sequential computing systems in d-APC are the same as those of 2-APC. The main difference appears in the mathematical formalism of nonlinear gates, that will require the use of multi-dimensional multi-variable Taylor series in d-APC.

- From a technological perspective, the PIP implementation of single-andit gates would require basic devices with d inputs and d outputs. Since the mainstream PIP devices are 1×1 and 2×2 optical systems [4], a possible difficulty might arise to implement these gates. Nonetheless, a suitable PIP implementation of d-APC could be proposed using the approaches reported in refs. [25, 26, 28], based on reconfigurable PSs, beam splitters (combiners) and micro-ring resonators that allow to integrate the desired number of inputs and outputs within the same optical system. As an example, the results of ref. [28] can be directly applied to implement single-andit U-gates in 3-APC.

- In QC, the optical implementation of universal quantum gates may be simplified by combining the use of qubits and qudits [29]. In the same vein, d-APC might be envisioned as a theoretical tool that could allow us to simplify the PIP implementation of the analog logic of 2-APC by utilising anbits and andits within the same circuit.

Supplementary Note 5: implementing other computing theories

In this section, we will discuss how to describe the unit of information and basic operations of digital computation (DC), neuromorphic computation (NC) and quantum computation (QC) using the mathematical framework of APC.

5.1 Digital computation

The implementation of DC with APC architectures requires to describe the digital bit and the Boolean logic using the anbit and its basic gates. Remarkably, an anbit $|\psi\rangle = \psi_0|0\rangle + \psi_1|1\rangle$ is able to describe the digital bit by taking $\psi_0 \in \{0,1\}$ and $\psi_1 = 1 - \psi_0$. Here, the state of the anbit is $|0\rangle$ or $|1\rangle$, but the possibility of having a linear combination of both states is discarded.

Furthermore, the description of the Boolean logic can be carried out in APC keeping in mind that any Boolean function can be decomposed in terms of NAND gates [30]. Thus, implementing the NAND operation of DC utilising basic anbit gates, we will be able to perform any Boolean function in APC.

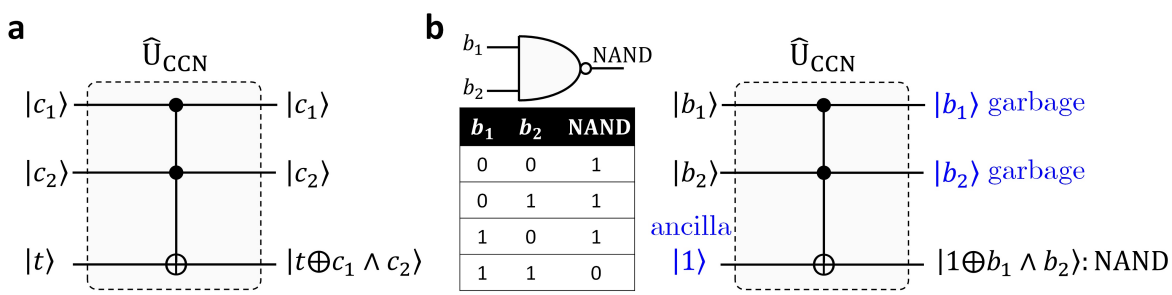

b_1	b_2	NAND
0	0	1
0	1	1
1	0	1
1	1	0

Supplementary Figure 19. Implementation of Boolean logic in APC. **a** Functional scheme of the Toffoli (or CCNOT) gate, described by Supplementary Equation 113, a multi-anbit controlled gate with 2 control anbits $|c_1\rangle$, $|c_2\rangle$ and 1 target anbit $|t\rangle$. **b** NAND operation of DC (defined via its truth table) implemented by the Toffoli gate in APC.

In this scenario, note that the linear unitary mapping of the Toffoli (or CCNOT) gate given by Supplementary Equation 74 can be recast of the form [22, 31]:

$$|c_1, c_2, t\rangle \xrightarrow{\text{CCNOT}} \widehat{U}_{\text{CCN}}|c_1, c_2, t\rangle = |c_1, c_2, t \oplus c_1 \wedge c_2\rangle, \tag{113}$$

where $\oplus$ is the modulo-2 addition and $\wedge$ is the AND operation (Supplementary Figure 19a). This expression allows us to infer that the Toffoli gate may be employed to implement the NAND gate:

$$\text{NAND}(b_1, b_2) := \neg(b_1 \wedge b_2) = 1 \oplus b_1 \wedge b_2, \tag{114}$$

by performing the following identification:

$$|b_1, b_2, \text{NAND}(b_1, b_2)\rangle = |b_1, b_2, 1 \oplus b_1 \wedge b_2\rangle \equiv \widehat{U}_{\text{CCN}}|b_1, b_2, 1\rangle, \tag{115}$$

where b_1 and b_2 are digital bits (i.e., $b_{1,2} \in \{0,1\}$) playing the role of the control anbits in the Toffoli gate. Moreover, the target anbit is set to $|t\rangle = |1\rangle$ at the input (Supplementary Figure 19b). As seen, the use of the Toffoli gate in APC to implement the NAND gate of DC requires

1 ancilla anbit and 2 garbage anbits (the same remark is found in QC to implement DC via the quantum Toffoli gate [22, 31]). Likewise, let us remember that the PIP implementation of the Toffoli gate is shown in Supplementary Figure 10 (see p. 47).

On the other hand, a complete implementation of DC in APC requires the ability to build sequential digital circuits (e.g., digital memories). To this end, latches and flip-flops (the basic building blocks of most sequential digital systems [30]) could be mimicked in APC by employing sequential anbit computational schemes. This point should be further investigated in forthcoming works.

5.2 Neuromorphic computation

NC is a computational model inspired by signal processing in the brain using the so-called artificial neural networks (ANNs) [32, 33]. The functional principle of an ANN is sketched in Supplementary Figure 20. Specifically, an ANN is arranged in several layers, which are composed by small processing units known as *neurons*. Each neuron processes a 1D complex signal (the unit of information in NC). In this example, we observe 3 layers with 3 neurons per layer. Mathematically, the communication between two adjacent layers can be modelled in two steps [33]:

1. Firstly, it is performed a matrix transformation of a 3D input vector $\mathbf{x} = (x_1, x_2, x_3)$, composed by 3 different units of information $x_{1,2,3}$. The output is also a 3D vector $\mathbf{y} = (y_1, y_2, y_3)$ (the dimension of $\mathbf{x}$ and $\mathbf{y}$ depends on the number of neurons per layer). Hence, this first step is a multi-linear mapping described by a matrix equation of the form $\mathbf{y} = M\mathbf{x}$, where M is a 3×3 matrix with complex entries.

2. Secondly, a nonlinear function $f \in \mathcal{F}(\mathbb{C}, \mathbb{C})$ is applied on each component y_k of the vector $\mathbf{y}$. The output of this second step is a 3D vector $\mathbf{z} = (z_1, z_2, z_3)$ with $z_k = f(y_k)$, $\forall k \in \{1, 2, 3\}$.

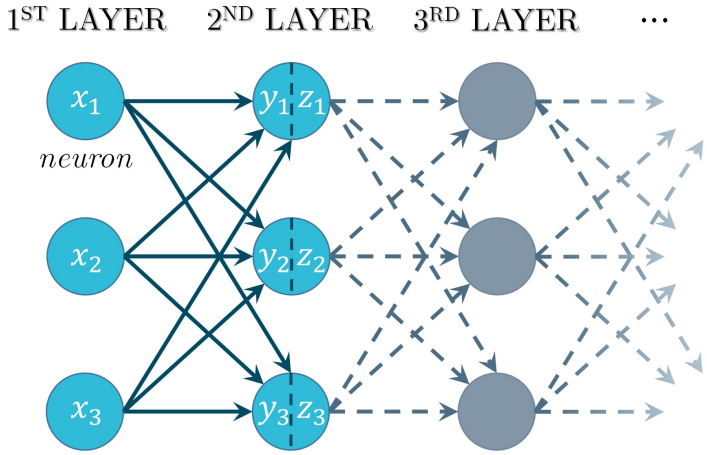

Supplementary Figure 20. Artificial neural network (ANN) with 3 neurons per layer [33].

Therefore, the description of NC is straightforward by using 1-APC (see Supplementary Note 4, on p. 60). In order to explain the connection between NC and 1-APC as simple as possible, let us describe the ANN depicted in Supplementary Figure 20 via 1-APC. In such a scenario, the following considerations are in order:

- Firstly, we should note that the unit of information of NC may be described by a 1D andit. For instance, the unit of information x_1 can be described by a 1D andit of the form $\left|x_1\right\rangle = x_1\left|0\right\rangle$.

- Secondly, the 3D input vector $\mathbf{x} = (x_1, x_2, x_3)$ should be written as a function of 3 different 1D andits $\left|x_1\right\rangle = x_1\left|0\right\rangle$, $\left|x_2\right\rangle = x_2\left|0\right\rangle$ and $\left|x_3\right\rangle = x_3\left|0\right\rangle$ connected via the Cartesian product. Hence, the vector $\mathbf{x}$ may be described by a ket of the form $\left|X\right\rangle = \left|x_1\right\rangle \times \left|x_2\right\rangle \times \left|x_3\right\rangle$. In the same vein, the vectors $\mathbf{y} = (y_1, y_2, y_3)$ and $\mathbf{z} = (z_1, z_2, z_3)$ can respectively be described by the kets $\left|Y\right\rangle = \left|y_1\right\rangle \times \left|y_2\right\rangle \times \left|y_3\right\rangle$ and $\left|Z\right\rangle = \left|z_1\right\rangle \times \left|z_2\right\rangle \times \left|z_3\right\rangle$, where $\left|y_k\right\rangle = y_k\left|0\right\rangle$ and $\left|z_k\right\rangle = z_k\left|0\right\rangle$, $\forall k \in \{1, 2, 3\}$.

- Thirdly, the linear and nonlinear mappings of the ANN can respectively be described in 1-APC by a linear operator $\widehat{\mathrm{M}}$ (whose matrix representation must be the M-matrix used to transform $\mathbf{x}$ into $\mathbf{y}$) and a nonlinear operator $\widehat{\mathrm{F}}$ connecting the kets $\left|X\right\rangle$, $\left|Y\right\rangle$, $\left|Z\right\rangle$ via the expressions $\left|Y\right\rangle = \widehat{\mathrm{M}}\left|X\right\rangle$ and $\left|Z\right\rangle = \widehat{\mathrm{F}}\left|Y\right\rangle = f\left(y_1\right)\left|0\right\rangle \times f\left(y_2\right)\left|0\right\rangle \times f\left(y_3\right)\left|0\right\rangle$.

5.3 Quantum computation

As expected, APC is also able to describe the mathematical model of QC, but only partially. It is worth mentioning that there are some fundamental concepts of the qubit and its basic operations that cannot be modelled with APC since it is a computing theory whose unit of information is implemented by classical waves. In order to clarify these concepts, let us take a closer look at the unit of information and basic operations of QC.

Unit of information: the qubit. An arbitrary state of a qubit is described by a ket of the form [22]:

$$\left|\psi\right\rangle = \cos\frac{\theta}{2}\left|0\right\rangle + e^{i\varphi}\sin\frac{\theta}{2}\left|1\right\rangle, \tag{116}$$

with 2 EDFs (θ and φ) and a constant norm $\left\|\psi\right\|^2 = \left\langle\psi|\psi\right\rangle = 1$. Given that an anbit has more EDFs than a qubit, we can use the former to describe the latter by setting a constant norm equal to 1 and using quantum waves to implement the anbit amplitudes.

As commented in the paper, the main differences between both units of information are associated to the measurement, the description of multiple units of information and the entanglement of units of information:

- *Measurement.* In quantum mechanics, the wave function collapse makes an ideal quantum measurement a *non-reversible* operation in QC [10, 22]. It is impossible to reconstruct the information encoded by the EDFs of a pre-measurement qubit from the state of a post-measurement qubit. In contrast, in APC, a measurement is always a *reversible* operation because the number of EDFs is preserved, see Supplementary Note 1 on p. 28. The information encoded by the EDFs of a pre-measurement anbit may be retrieved from the state of the post-measurement anbit, regardless of whether a coherent or differential measurement strategy is employed. Therefore, an ideal quantum measurement cannot be described by the mathematical framework of APC.

- *Multiple units of information.* While the description of multiple anbits can be carried out using the tensor product or the Cartesian product in APC, the description of multiple qubits must be exclusively performed via the tensor product in QC. This composition rule is derived from the state postulate and the measurement postulate of quantum mechanics [34]. However, it is direct to infer that this remark does not impose any limitation on APC to describe multiple qubits.

- *Entanglement.* The entanglement of different qubits is possible thanks to the non-local nature of quantum mechanics [22]. Unfortunately, this instantaneous non-locality cannot be found in a deterministic physical theory, e.g., in classical electromagnetism [35]. Although electromagnetic non-local media are supported by Maxwell's equations, the time response is causal, that is, there is a time delay between the incident electric field strength ($\boldsymbol{\mathcal{E}} = \sum_l \mathcal{E}_l \hat{\mathbf{u}}_l$) and the electric displacement ($\boldsymbol{\mathcal{D}} = \sum_k \mathcal{D}_k \hat{\mathbf{u}}_k$). Here, it should be noted that the most general non-local linear constitutive relation between $\boldsymbol{\mathcal{E}}$ and $\boldsymbol{\mathcal{D}}$ is given by the expression (Einstein's summation convention) [36]:

$$\mathcal{D}_k\left(\mathbf{r}, t\right) = \int_{-\infty}^{\infty} \int_{-\infty}^{t} \varepsilon_{kl}\left(\mathbf{r}, \mathbf{r}', t, t'\right) \mathcal{E}_l\left(\mathbf{r}', t'\right) \mathrm{d}t' \mathrm{d}^3 r', \tag{117}$$

  where ε_{kl} is the electric permittivity tensor. Specifically, the time integral precludes instantaneous non-local effects in classical electromagnetism. Consequently, the quantum entanglement cannot be described by APC given that its technological PIP implementation is based on classical electromagnetic waves.

Basic qubit operations. The basic operations of QC are single-qubit gates and controlled qubit gates. Interestingly, the mathematical framework of APC is able to describe all these operations. A single-qubit gate is mathematically equivalent to a single-anbit U-gate and the theoretical formalism of a controlled anbit gate is the same as that of a controlled qubit gate (as commented on p. 43). In addition, taking into account that any qubit logic gate may be composed from single-qubit gates and controlled qubit gates [22], we infer that a multi-qubit operation can also be described by APC. Nonetheless, any quantum operation exploiting the non-local nature of quantum mechanics cannot be emulated with APC.

Conclusion. APC is able to *partially* describe the mathematical (and physical) model of QC given that the ideal quantum measurement and the quantum entanglement have no classical analogy in our computation theory, as discussed above. Nevertheless, APC might be regarded as a potential theoretical and didactic toolbox (implementable with current technology) that could improve our comprehension about the subtle (but essential) differences between quantum and classical systems.

References

[1] Okamoto, K. *Fundamentals of Optical Waveguides*. 2nd ed. (Elsevier, London, 2006).

[2] Winzer, P. J. & Essiambre, R.-J. Advanced modulation formats for high-capacity optical transport networks. *J. Lightwave Technology* **24**, 4711 (2006).

[3] Chen, X., Macho, A. & Horche, P. R. Performance evaluation of 100 and 200-Gb/s WDM PM-QPSK transmission systems: tolerance analysis to the optical link impairments according to the optical carrier shape. *Optical Review* **25**, 663 (2018).

[4] Capmany, J. & Pérez, D. *Programmable Integrated Photonics*. (Oxford University Press, Oxford, 2020).

[5] Slepian, D. & Pollak, H. O. Prolate spheroidal wave functions, Fourier analysis and uncertainty-I. *Bell System Technical Journal* **40**, 43 (1961).

[6] Ho, K.-P. *Phase-Modulated Optical Communications Systems*. (Springer, New York, 2005).

[7] Kirillov, A. *An Introduction to Lie Groups and Lie Algebras*. (Cambridge University Press, Cambridge, 2008).

[8] Frankel, T. *The Geometry of Physics*. (Cambridge University Press, Cambridge, 2011).

[9] Landi, G. & Zampini, A. *Linear Algebra and Analytic Geometry for Physical Sciences*. (Springer, Cham, 2018).

[10] Cohen-Tannoudji, C., Diu, B. & Laloë, F. *Quantum Mechanics, Volume I: Basic Concepts, Tools, and Applications*. (Wiley, Weinheim, 2020).

[11] Rieffel, E. & Polak, W. *Quantum Computing: A Gentle Introduction, Ch. 3*. (The MIT Press, Massachusetts, 2011).

[12] Roman, S. *Advanced Linear Algebra*. (Springer, New York, 2005).

[13] Golub, G. H. & Van Loan, C. F. *Matrix Computations*. (The Johns Hopkins University Press, Baltimore, 2013).

[14] Jalas, D. *et al.* What is - and what is not - an optical isolator. *Nature Photonics* **7**, 579 (2013).

[15] Caloz, C. *et al.* Electromagnetic nonreciprocity. *Physical Review Applied* **10**, 047001 (2018).

[16] Pérez, D., Gasulla, I., DasMahapatra, P. & Capmany, J. Principles, fundamentals and applications of programmable integrated photonics. *Advances in Optics and Photonics* **12**, 709 (2020).

[17] Pérez, D. & Capmany, J. Scalable analysis for arbitrary photonic integrated waveguide meshes. *Optica* **6**, 19 (2019).

[18] Macho, A., Pérez, D. & Capmany, J. Optical implementation of 2×2 universal unitary matrix transformations. *Laser & Photonics Reviews* **15**, 2000473 (2021).

[19] Mostow, G. D. Some new decomposition theorems for semi-simple groups. *Memoirs of the American Mathematical Society* **14**, 31 (1955).

[20] Nielsen, F. & Bhatia, R. *Matrix Information Geometry*. (Springer, Berlin, 2012).

[21] Hall, B. C. *Lie Groups, Lie Algebras, and Representations*. (Springer, New York, 2003).

[22] Nielsen, M. A. & Chuang, I. L. *Quantum Computation and Quantum Information*. (Cambridge University Press, Cambridge, 2016).

[23] Pérez, D., López, A., Dasmahapatra, P. & Capmany, J. Multipurpose self-configuration of programmable photonic circuits. *Nature Communications* **11**, 6359 (2020).

[24] Scarani, V., Iblisdir, S., Gisin, N. & Acín, A. Quantum cloning. *Reviews of Modern Physics* **77**, 1225 (2005).

[25] Reck, M., Zeilinger, A., Bernstein, H. J. & Bertani, P. Experimental realization of any discrete unitary operator. *Physical Review Letters* **73**, 58 (1994).

[26] Clements, W. R., Humphreys, P. C., Metcalf, B. J., Kolthammer, W. S. & Walmsley, I. A. Optimal design for universal multiport interferometers. *Optica* **3**, 1460 (2016).

[27] Agrawal, G. P. *Nonlinear Fiber Optics*. (Elsevier, Oxford, 2013).

[28] Sato, T. & Enokihara, A. Ultrasmall design of a universal linear circuit based on microring resonators. *Optics Express* **27**, 33005 (2019).

[29] Lanyon, B. P. *et al.* Simplifying quantum logic using higher-dimensional Hilbert spaces. *Nature Physics* **5**, 134 (2009).

[30] Wakerly, J. F. *Digital Design: Principles and Practices*. (Pearson, New Jersey, 2006).

[31] Desurvire, E. *Classical and Quantum Information Theory: An Introduction for the Telecom Scientist*. (Cambridge University Press, Cambridge, 2009).

[32] Mohamed, K. S. *Neuromorphic Computing and Beyond*. (Springer, Cham, 2020).

[33] Cartlidge, E. Optical neural networks. *Optics & Photonics News* **6**, 34 (2020).

[34] Carcassi, G., Maccone, L. & Aidala, C. A. Four postulates of quantum mechanics are three. *Physical Review Letters* **126**, 110402 (2021).

[35] Popescu, S. Nonlocality beyond quantum mechanics. *Nature Physics* **10**, 264 (2014).

[36] Mikki, S. M. & Kishk, A. A. Nonlocal Electromagnetic Media: A Paradigm for Material Engineering. In *Passive Microwave Components and Antennas* (ed. Zhurbenko, V.) 73-94 (InTech, Rijeka, 2010).